

Aus dem Institut für Prophylaxe und Epidemiologie der Kreislaufkrankheiten

der Ludwig-Maximilians-Universität München

Direktor: Univ.-Prof. Dr. med. Christian Weber

Role of *Dicer* in smooth muscle cells during neointima formation



Dissertation

Zum Erwerb des Doktorgrades des Naturwissenschaften

an der Medizinischen Fakultät

der Ludwig-Maximilians-Universität zu München

vorgelegt von

Farima Zahedi, M.Sc.

aus Teheran, Iran

2016

Mit Genehmigung der Medizinischen Fakultät der Universität München

Betreuerin: Prof. Dr. rer. nat. Sabine Steffens

Zweitgutachterin: Prof. Dr. Johanna Scheuermann

Dekan: Prof. Dr. med. dent. Reinhard Hickel

Tag der mündlichen Prüfung: 09.05.2017

The result of this work was in part published in:

Zahedi F*, Nazari-Jahantigh M*, Zhou Z, Subramanian P, Wei Y, Grommes J, Offermanns S, Steffens S, Weber C, and Schober A. Dicer generates a regulatory microRNA network in smooth muscle cells that limits neointima formation during vascular repair. *Cell Mol Life Sci.* 2016, doi:10.1007/s00018-016-2349-0, 1-14. *Equal contribution.

Table of contents

Role of <i>Dicer</i> in smooth muscle cells during neointima formation	I
Table of contents.....	IV
Abbreviations.....	VII
1 Introduction.....	1
1.1 Neointima formation	1
1.1.1 SMC proliferation during neointima formation.....	3
1.2 MiRNAs in arterial pathologies.....	4
1.2.1 MiRNA processing enzyme Dicer.....	5
1.2.2 MiRNAs in SMC phenotypic switch during neointima formation.....	9
1.3 Aims of the study	10
2 Materials and methods	12
2.1 General equipment	12
2.2 Chemicals	13
2.3 Antibodies	14
2.3.1 Primary antibodies.....	14
2.3.2 Secondary antibodies.....	14
2.4 Buffers	14
2.5 Mouse husbandry	15
2.6 Mouse strains.....	15
2.6.1 Endothelial denudation injury to the carotid artery	16
2.6.1 <i>In situ</i> perfusion of the vasculature	17
2.7 MiRNA expression profile	17
2.8 MiRNA real-time PCR array.....	18
2.9 Global gene expression analysis.....	20
2.9.1 Prediction of miRNAs target genes.....	20
2.10 Quantitative real-time polymerase chain reaction (qRT-PCR)	20
2.11 Histochemistry.....	24
2.11.1 Paraffin embedding, sectioning, and deparaffinization	24
2.11.1 EVG staining	25
2.11.2 <i>In vivo</i> immunostaining	27
2.11.3 Combined <i>in situ</i> PCR and immunostaining	27

2.12	Laser-Capture Microdissection system (LCM)	28
2.12.1	Human carotid lesion samples	29
2.13	Cell culture	30
2.14	<i>In vitro</i> immunostaining	30
2.15	MiRNA target identification and quantification system (MirTrap)	31
2.16	Luciferase reporter assay	31
2.17	Western blot analysis	32
2.18	Statistics	32
3	Results	33
3.1	Expression pattern of <i>Dicer</i> and miRNAs during neointima formation	33
3.1.1	MiRNAs expression patterns during neointima formation	33
3.1.2	Expression of <i>Dicer</i> during neointima formation	35
3.2	The effect of <i>Dicer</i> knockout in SMCs on neointima formation	35
	<i>-/-</i>	35
3.2.1	Effect of SMC-specific- <i>Dicer</i> knockout on neointima formation	36
3.2.1	SMC-specific deletion of <i>Dicer</i> in ApoE ^{-/-} mice	
3.2.2	Effect of <i>Dicer</i> deficiency on neointimal SMC proliferation and apoptosis	41
3.2.3	Effect of SM- <i>Dicer</i> deficiency on endothelial recovery	44
3.2.4	Effect of <i>Dicer</i> deletion on SMC differentiation	45
3.3	Effect of SM- <i>Dicer</i> deficiency on the miRNA expression profiles	46
3.4	Effect of SM- <i>Dicer</i> deficiency on the mRNA expression profiles	51
3.4.1	MiRNA-mRNA interactions involved in neointima formation	52
3.5	Expression of miR-27a-3p in medial and neointimal SMCs	54
3.6	Identification of miR-27a-3p targets in SMCs	56
3.6.1	Effect of miR-27a-3p on the expression of predicted targets in SMCs	56
3.6.2	MRNA targets of miR-27a-3p in SMCs	57
3.6.3	Binding site of miR-27a-3p in the <i>ARHGEF26</i> 3'-UTR	57
3.7	Effect of miR-27a-3p targeting <i>ARHGEF26</i> on SMC proliferation	58
3.8	Effect of IL-1 α on the expression of miR-27a-3p and <i>ARHGEF26</i>	61
3.9	MiR-27a-3p and <i>ARHGEF26</i> expression in SMCs of mouse and human lesions	62
3.9.1	Arhgef26 protein expression in mouse neointimal SMCs	62
3.9.2	MiR-27a-3p and <i>ARHGEF26</i> expression in human atherosclerotic lesions	62
4	Discussion	64
4.1	MiRNAs are differentially expressed after vascular injury	64
4.2	<i>Dicer</i> limits neointima formation by reducing SMC proliferation	64

4.3	Dicer generates anti-proliferative miRNAs in SMCs.....	66
4.4	MiR-27a-3p reduced SMC proliferation	68
4.5	MiR-27a-3p inhibits SMC proliferation by targeting <i>ARHGEF26</i>	68
5	Summary.....	71
6	Zusammenfassung	73
7	References.....	75
8	Acknowledgment.....	83
9	Curriculum vitae.....	84

Abbreviations

Ab	Antibody
Ago2	Argonaute 2
AKT	AKT Serine/threonine protein kinase 1
<i>Apoe</i>	Apolipoprotein E
<i>ARHGEF26</i>	Rho guanine nucleotide exchange factor 26
α -SMA	Smooth muscle actin
BSA	Bovine serum albumin
CAD	Coronary artery disease
CALMK	Calmodulin K
CCA	Common carotid artery
CDKN1A	Cyclin-dependent kinase inhibitor 1A (p21)
CDKN1B	Cyclin-dependent kinase inhibitor 1B (p27)
CDKN1C	Cyclin-dependent kinase inhibitor 1C (p57)
<i>CHST1</i>	Carbohydrate (keratan sulfate Gal-6) sulfotransferase 1
C-kit	V-kit Hardy-Zuckerman 4 feline sarcoma viral oncogene homolog
CVD	Cardiovascular diseases
Cy3	Cyanine 3
d	Day
DAPI	4',6-Diamidino-2-phenylindol
DGCR8	DiGeorge syndrome chromosomal region 8
DH	Dbl homology
DIG	Digoxigenin
<i>DLL4</i>	Delta like 4
DMEM	Dulbecco's modified eagle medium
dsRNA	Double-stranded RNA
EC	Endothelial cell
ECA	External carotid artery
EDTA	Ethylenediaminetetraacetic acid
ELK-1	ETS domain-containing protein

ER	Endoplasmic reticulum
ERK1/2	Extracellular signal-regulated kinase 1/2
EVG	Elastic van Gieson
EXP5	Exportin 5
FITC	Fluorescein isothiocyanate
FRA-1	Fos related antigene-1
GAPDH	Glyceraldehyde-3-phosphate dehydrogenase
GEF	Guanine nucleotide exchange factor
GLuc	Gaussia luciferase
GTP	Guanosine triphosphate
HASMC	Human aortic smooth muscle cell
HEK293	Human embryonic kidney 293 cell
HFD	High-fed diet
Hsa	Homo sapiens
ICA	Internal carotid artery
IEL	Internal elastic lamina
<i>IGFBP3</i>	Insulin-like growth factor binding protein 3
IL-1	Interleukin 1
IL-6	Interleukin 6
IP	Immunoprecipitation
i.p.	Intraperitoneal
IPA	Ingenuity pathway analysis
KLF4/5	Krüppel-like factor 4/5
L	Lumen
LATS2	Large tumour suppressor homolog 2
LCM	Laser-capture microdissection system
LNA	Locked nucleic acid
MAPK	mitogen-activated protein kinase
Min	Minute
MiR, MiRNA	MicroRNA
MiRISC	MiRNA induced silencing complex

Mmu	Mus musculus
MRTF-B	Myocardin-related transcription factor-B
mTOR	Mammalian target of rapamycin
MYH11	SM myosin heavy chains
Myoc	Myocardin
NF- κ B	Nuclear factor kappa B
ON	Overnight
<i>OIT3</i>	oncoprotein induced transcript 3
PAZ	PIWI, Argonaute and Zwillie
PBS	Phosphate buffered saline
PCI	Percutaneous coronary intervention
PDCD4	Programmed cell death 4
PDGF	Platelet-derived growth factor
PFA	Paraformaldehyde
PSGL-1	P-selectin glycoprotein ligand 1 binding
PI3K	Phosphatidylinositide 3-kinase
PIM-1	Proviral integration site 1
PTEN	Phosphatase and tensin homolog
qRT-PCR	Quantitative real-time polymerase chain reaction
RHOG	Ras homolog family member G
RIIDs	RNase III domains
RNU44	Small nucleolar RNA, C/D box 44
RQ	Relative quantification
RT	Reverse transcription
SEAP	secreted alkaline phosphatase
Sec	Second
<i>SH2D5</i>	SH2 domain containing 5
<i>SH3BGRL2</i>	SH3 domain binding glutamate-rich protein like
SMC	Smooth muscle cell
SMMHC	SM myosin heavy chain
<i>SnoRNA135</i>	small nucleolar RNA, C/D box 65

Abbreviations

Sp-1	Sp1 transcription factor
<i>TAGLN2</i>	Transgelin 2
TGF- β	Transforming growth factor beta
TNF- α	Tumor necrosis factor- α
TRB3	Tribbles-like protein-3
TRBP	Tar RNA binding protein
TSA	Tyramide-based amplification
TSB	Target site blocker
UP	Ultra-pure
UTR	Untranslated region

1 Introduction

1.1 Neointima formation

Cardiovascular diseases (CVD) are the main cause of mortality worldwide¹. One of the most common types of CVD is coronary artery disease (CAD) which is mainly caused by atherosclerosis². A main way to treat CAD is to open the stenotic atherosclerotic artery by percutaneous coronary intervention (PCI), such as balloon angioplasty and stent implantation, to mechanically widen the arterial lumen³⁻⁵. This procedure causes mechanical injury of the artery and induces a vascular healing response that can lead to re-narrowing of the target vessel, called restenosis, in which the tunica intima of an artery thickens due to accumulation of vascular smooth muscle cells (SMCs) and extracellular matrix⁶. Restenosis occurs in up to 12% of patients with coronary or peripheral artery disease within 6 to 12 months after the PCI^{5, 7, 8}. The pathology and mechanisms of neointima formation differ from those of atherosclerotic plaque formation⁹. During the initial phase, balloon angioplasty-induced vascular injury results in endothelial denudation and apoptosis of medial SMCs due to stretching of the artery. Platelets attach to the subendothelial matrix of the denuded vessel wall via glycoprotein Ib platelet alpha subunit-von Willebrand factor and glycoprotein VI-collagen interactions^{10, 11}. Circulating leukocytes, such as neutrophils and monocytes, start rolling on the adherent platelets and firmly adhere through P-selectin glycoprotein ligand 1 binding to platelet P-selectin¹⁰⁻¹³. Subsequently, adherent leukocytes migrate into the vessel wall guided by chemokines secreted from activated SMCs¹⁴. Moreover, platelets, leukocytes, and apoptotic SMCs serve as a scaffold for initial recruitment of monocytes, which differentiate into macrophages and contribute to the neointimal size, and activate SMCs by releasing growth factors and cytokines, such as platelet-derived growth factor (PDGF), interleukin 1 (IL-1), interleukin 6 (IL-6), and tumor necrosis factor α (TNF- α)¹⁵⁻¹⁷. Activation changes SMCs into proliferating and extracellular matrix-producing phenotype, which primarily promotes neointimal growth (Figure 1)^{18, 19}. Complete re-endothelialization terminates SMC proliferation and neointima formation^{18, 20}. Taken together intimal SMC proliferation represents an important mechanism of vascular healing but is also a common cause for vascular narrowing following injury.

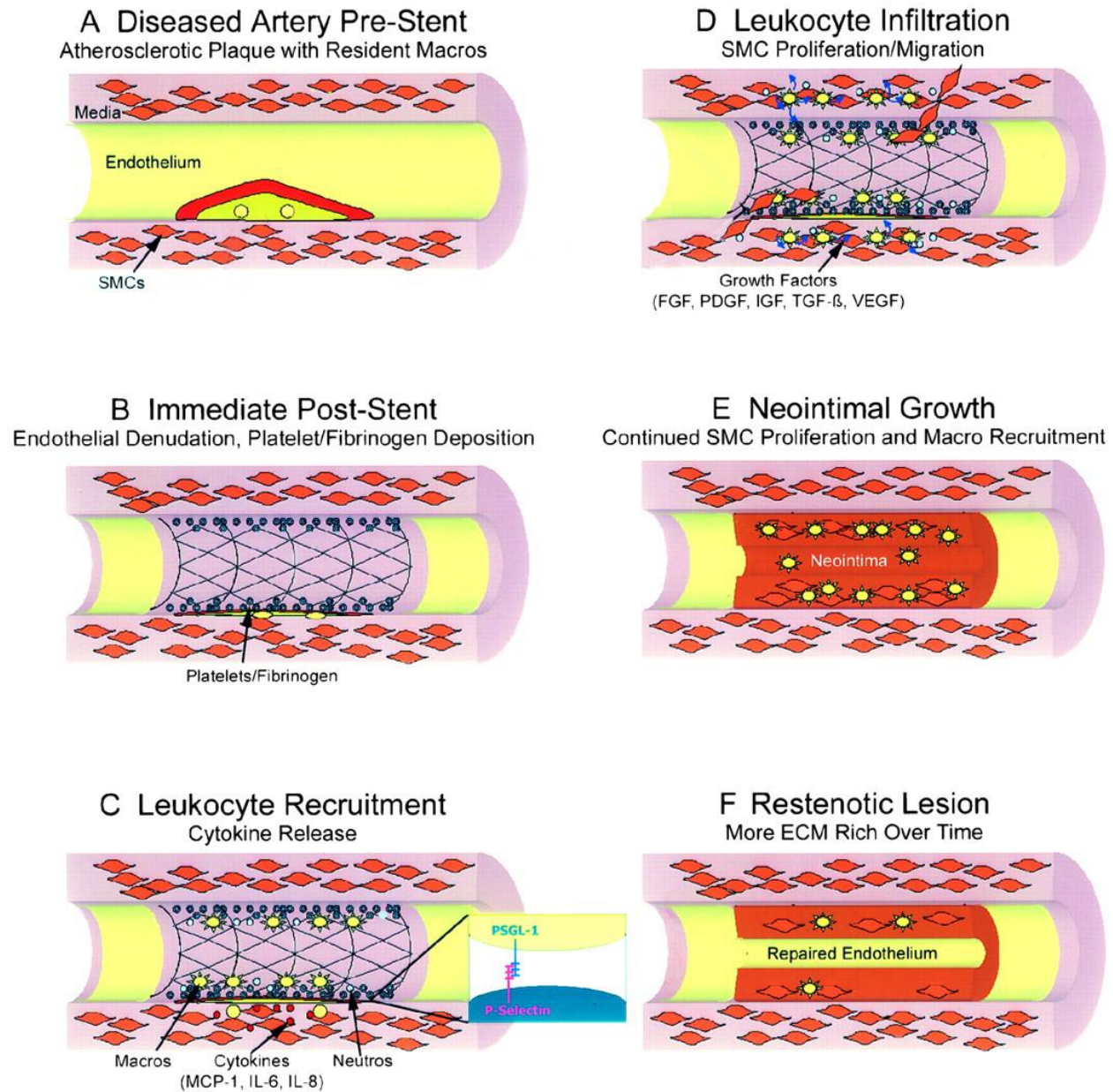


Figure 1. Neointimal hyperplasia after mechanical injury. (A) An atherosclerotic plaque before intervention. (B) The immediate effects of mechanical vascular injury are endothelial denudation, adhesion of platelets to the subendothelial matrix, and apoptosis of medial SMCs. (C) Circulating leukocytes start rolling on the adherent platelets and firmly adhere through P-selectin glycoprotein ligand 1 binding (PSGL-1) to platelet P-selectin. (D) and (E) Subsequently, SMCs accumulate in the neointima and surface adherent platelets mediate the recruitment of monocytes, which differentiate into macrophages and contribute to the neointimal size. (E) Finally, the neointimal growth terminates with the repair of the endothelium. Macros, macrophages; Neutros, neutrophils; MCP-1, monocyte chemoattractant protein-1; IL, interleukin; FGF, fibroblast growth factor; PDGF, platelet-derived growth factor; IGF, insulin-like growth factor; TGF- β , transforming growth factor β ; VEGF, vascular endothelial growth factor; ECM, extra cellular matrix²¹.

SMCs are a unique cell type that can switch between a quiescent, differentiated, and "contractile" phenotype and the proliferative, dedifferentiated and "synthetic" state depending on the environmental cues²². Contractile SMCs are spindle-shaped with a central nucleus oriented along the axis of proliferation (Figure 2). The orientation of SMCs in the tunica media of the blood vessels is spiral, which improves regulation of the vascular tone and the luminal diameter during contraction or relaxation of the SMCs, and thereby contributes to blood pressure control²². Contractile SMCs contain a functional contractile apparatus consisting of SM α -actin, SM myosin heavy chains (*Myh11*), calponin (*Cnn1*), SM-22 α , and smoothelin. Small molecule signals, such as norepinephrine and acetylcholine, induce the contraction and relaxation of SMCs, respectively²²⁻²⁵. In contrast to contractile SMCs, synthetic SMCs are characterized by a higher growth rate and increased migratory activity, by their epithelioid-shape and by their high content of rough endoplasmic reticulum (ER), Golgi organelles, and ribosomes in the cytoplasm, which are necessary for synthetic capacity (Figure 2)²⁵⁻²⁸.

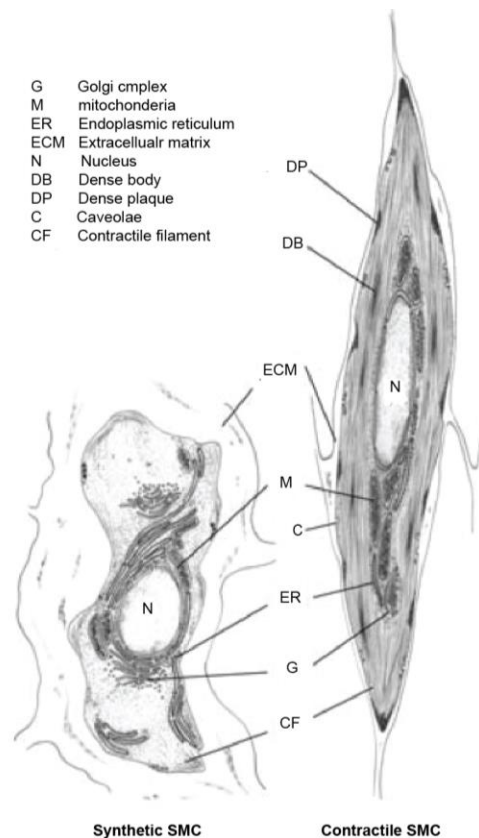


Figure 2. Ultrastructural characteristics of SMC contractile and synthetic phenotypes. Contractile SMCs are elongated, spindle shaped cells, whereas synthetic SMCs are less elongated and have cobblestone morphology²⁶.

Extracellular signaling factors, such as transforming growth factor beta 1 (TGF- β 1) and heparin, promote a SMC contractile phenotype through inhibition of mitogen-activated protein kinase (MAPK) activation^{26, 29}. However, several signaling factors including PDGF, insulin-like growth factors (IGFs), epidermal growth factor (EGF), and basic fibroblast growth factor (bFGF) mediate the phenotypic switch from contractile into synthetic SMCs^{16, 29, 30}. These growth factors induce proliferation of SMC following vascular injury by activating mutually crosslinked mitogenic signaling modules, such as phosphatidylinositol-3-kinase (PI3K)/Akt/mammalian target of rapamycin (mTOR) and the Ras/RAF/extracellular signal-regulated kinase 1/2 (ERK1/2)^{16, 30-35}. Drug-eluting stents coated with several anti-proliferative drugs like sirolimus and its derivatives (including biolimus, everolimus, and zotarolimus) minimize SMC proliferation and reduce restenosis by inhibiting the PI3K/Akt/mTOR signaling pathway³¹⁻³⁸. PI3K/Akt signaling module is linked to the nuclear factor kappa B (NF- κ B) pathway, a crucial inflammatory signaling cascade in synthetic SMCs, via its negative regulator phosphatase and tensin homolog (PTEN)^{36, 37, 39}. NF- κ B-mediated upregulation of chemokines, such as CX₃CL1 and CCL2, in SMCs can, in turn, perpetuate and enhance the activation of NF- κ B and PI3K/Akt in a positive autoregulatory loop³⁹. Taken together, the combined activation of PI3K/Akt/mTOR, Ras/RAF/ERK1/2, and NF- κ B signaling pathways appears to be essential for initiation of SMC proliferation.

1.2 MiRNAs in arterial pathologies

A new class of gene expression regulators called microRNAs (miRNAs) first discovered in 1993 on the *lin-4* gene, which control the timing of *Caenorhabditis elegans* larval development^{40, 41}. MiRNAs are small non-coding RNAs (~22nt) that regulate post-transcriptional gene expression through mRNA cleavage or translational repression⁴². The miRNAs discovery also revealed a new class of regulators that play a key role in the fine regulation of several CVD processes including restenosis and atherosclerosis⁴³⁻⁴⁶. Moreover, miRNAs are involved in numerous pathophysiological CVD processes, such as inflammation, cell proliferation, apoptosis and lipid metabolism^{47, 48}. Therefore, miRNAs as natural products that are released by almost all cell types can represent promising targets for the efficient therapeutic strategies to treat restenosis and atherosclerosis.

RNA polymerase II transcribes the majority of primary miRNA transcript (pri-miRNA) which has embedded the mature miRNA sequences in their double-stranded stem structure⁴⁹. In the miRNA biogenesis process Drosha and Dicer (RNase III enzymes) are two major enzymes which are located processing enzyme in the nucleus and cytoplasm, respectively⁵⁰. To date, approximately 1000 different miRNAs have been predicted in humans of which most of them have not yet been verified experimentally⁵¹. In mammals, miRNAs regulate the expression of 50% of all protein-coding genes⁴⁹.

The long pri-miRNA is cleaved by a microprocessor complex in the nucleus that contains Drosha and double-stranded RNA binding protein, DiGeorge syndrome chromosomal region 8 (DGCR8), to precursor miRNA (pre-miRNA)⁵². The 60–90-nt pre-miRNAs form stem and loop structures that contain terminal and internal loops, bulges, and a two- nucleotide-long 3' overhang end. Pre-miRNA is then exported from the nucleus to the cytoplasm by a transport complex containing the protein exportin 5 (EXP5) and guanosine triphosphate (GTP)-binding nuclear protein RAN·GTP^{53, 54}. During translocation GTP is hydrolysed, which results in the disassembly of the transport complex and the pre-miRNA release into the cytosol (Figure 3). Subsequently, in the cytoplasm the pre-miRNA is processed by a second enzyme, Dicer, to form a mature miRNA^{55, 56}.

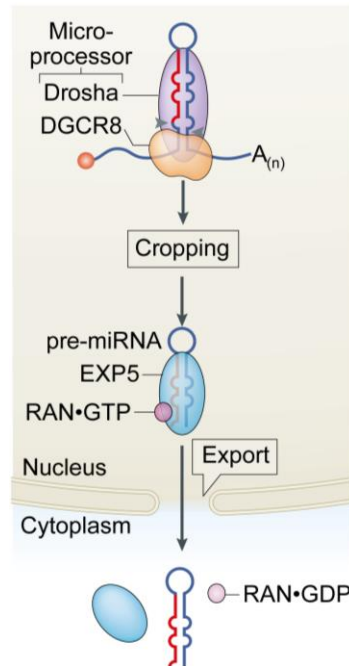


Figure 3. Translocation of pre-miRNA from the nucleus and release into the cytoplasm. The protein EXP5 and GTP-binding nuclear protein RAN•GTP form a complex with pre-miRNA to transport pre-miRNA from cytoplasm to the nucleus⁵⁴.

The ribonuclease III Dicer is a ~200 kDa multidomain enzyme, which cleaves double-stranded RNA (dsRNA) that contains a two-nucleotide overhang, plays a pivotal role in the biogenesis of miRNAs⁵⁷.

The Dicer enzyme is composed of a putative helicase domain, the domain of unknown function (DUF) 283, the platform structure, and PIWI, Argonaute and Zwiille (PAZ) domain at the N terminus and RNase III domains (RIIIDs) and a dsRNA binding domain (dsRBD) at the C terminus (Figure 4)^{50, 57}. In the cytosol, Dicer together with an RNA binding protein called tar RNA binding protein (TRBP), cleaves a pre-miRNA hairpin into a short (~22 nt) miRNA duplex⁵⁸. The N-terminal helicase of Dicer interacts with the terminal loop of the pre-miRNA whereas the PAZ domain anchors the ends of the pre-miRNA⁵⁹. The PAZ domain has two basic pockets that can bind to the both 5' and 3' ends of the pre-miRNA, but usually binds at the 3' end to the two-nucleotide overhang of the dsRNA substrate^{59, 60}. However, the 5' end binding occurs when the end is thermodynamically unstable, but not when the end is strongly paired (such as through G•C base pairs)⁶¹.

A connector helix, so-called ruler, separates the PAZ domain from the RIIIDs tandem at a distance of approximately 22 nt, and thereby controls the accurate cutting of the pre-miRNA⁵⁴. The RIIIDs of the Dicer form an internal dimer to build the catalytic core of the enzyme that

cleaves 22 nt away from the 3' end (the 3'-counting rule) or from the thermodynamically unstable 5' end (the 5'-counting rule) of pre-miRNAs (Figure 4)⁶². The large helicase acts as an autoinhibitory module for the production of certain classes of small RNAs, contacts precursor miRNA substrates, and contributes to the processing activity of the enzyme⁶². Following the helicase domain is the small DUF283 domain that can bind to single-stranded nucleic acids and act as an annealer that facilitates hybridization between complementary RNA or DNA molecules (Figure 4)^{60, 62-64}. The full structure of Dicer is required for specificity and efficiency of Dicer function. Functional disruption of Dicer for example by deletion of RIIIDs provides a tool for studying the global role of miRNAs in various diseases. For instance, mutations in RIIIDs of Dicer may affect the expression levels of miRNAs in which dysfunctional RIIIDa and RIIIDb impair production of miRNAs from the 3'- and 5'-arm of pre-miRNA hairpins, respectively⁶⁵⁻⁶⁹.

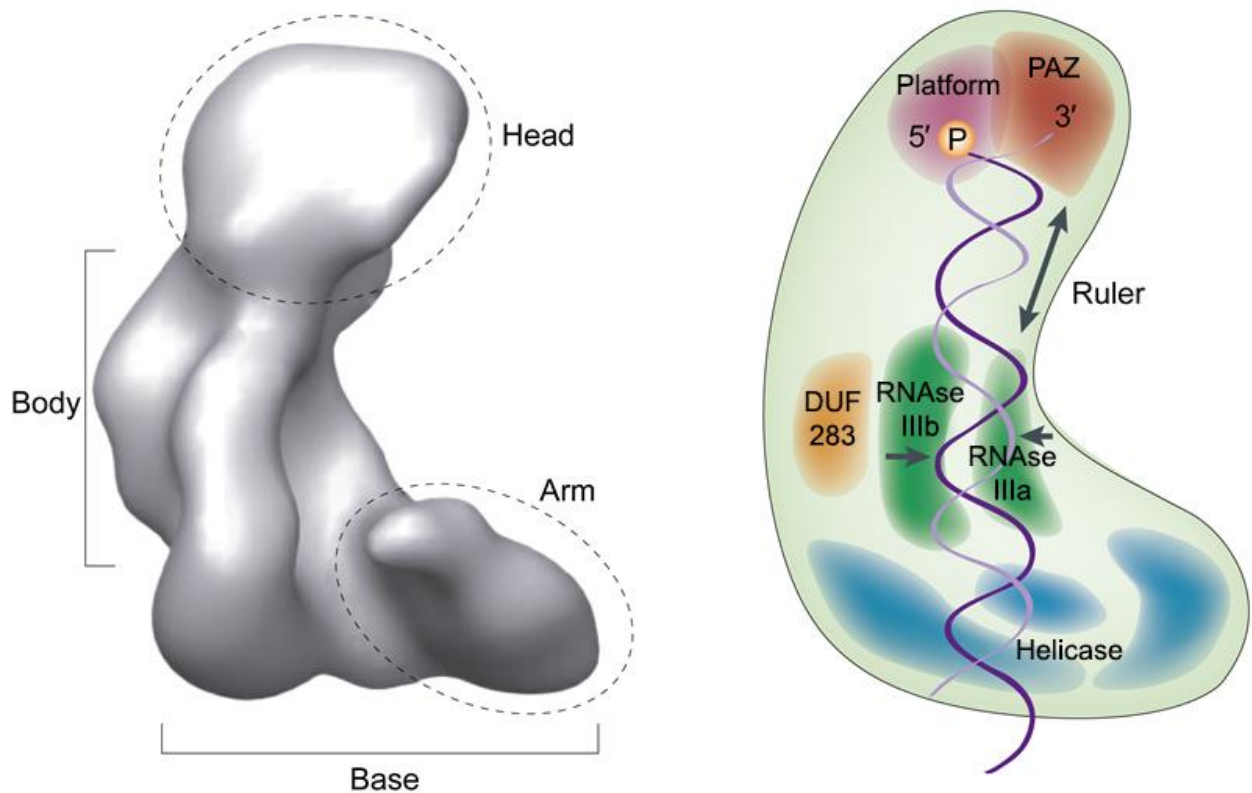
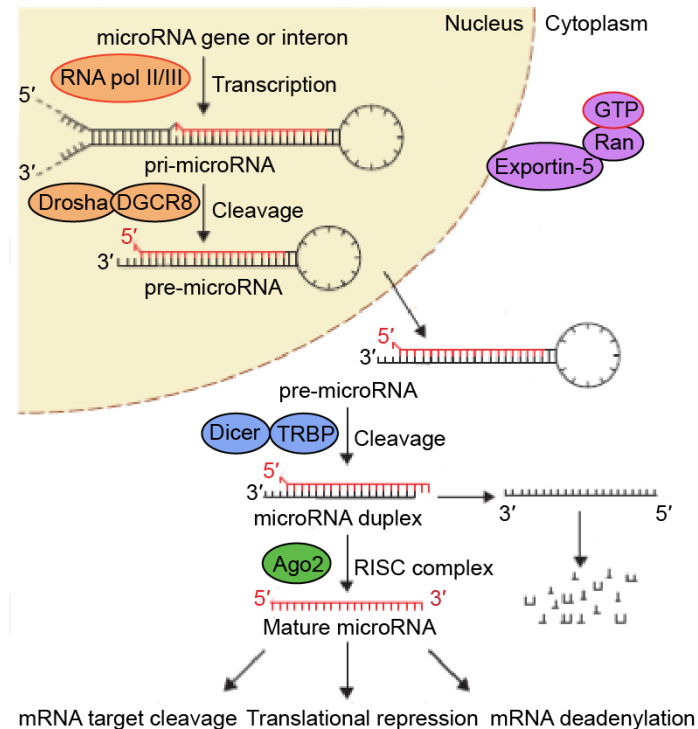


Figure 4. Human Dicer domain architecture. Schematic representation of human Dicer domains⁶⁹.

In the following processing step, the miRNA duplex then is loaded onto a complex called miRNA-induced silencing complex (miRISC) that composed of Argonaute (AGO) proteins^{69, 70}. Two steps are predicted in the miRISC assembly. The first step is unwinding of the miRNA duplex within the AGO protein and the second step is the retention of the guide strand, while the

passenger strand or miRNA* is discarded^{70, 71}. The mature miRISCs is now containing the single-stranded miRNA which is ready to bind target mRNA. MiRNAs bind through the “seed” sequence at the 5' end of miRNAs, more precisely nucleotides 2 to 8, to the complementary sequences located at the 3'-untranslated region (UTR) of the target mRNAs and thereby mediate



transcriptional repression via cleavage of mRNA molecules (Figure 5)^{70, 72-75}.

Figure 5. Current model of miRNA biogenesis. MiRNA processing includes: primary miRNA transcript (pri-miRNA) production by RNA polymerase II or III. Pri-miRNA is cleaved by Drosha–DGCR8 (Pasha) complex in the nucleus and processed into the precursor hairpin, pre-miR. The pre-miRNA is exported from the nucleus to the cytoplasm by Exportin-5–Ran-GTP; the complex of RNase Dicer/TRBP cleaves the pre-miRNA hairpin to miRNA duplex. The mature miRNA together with argonaute (Ago2) proteins is loaded into the miRNA-induced silencing complex (miRISC), where silencing of target mRNAs happens through mRNA decay, translational inhibition or deadenylation, whereas the passenger strand (in black) is degraded⁷³.

Dicer is a central regulator of gene expression by producing miRNAs that post-transcriptionally regulate mRNA expression⁷⁶. The accurate regulation of Dicer activity is the critical step in the functioning of all eukaryotic organisms^{50, 77, 78}. Many cell-, tissue- or stage-specific factors can regulate the Dicer gene transcription⁷⁹. For example transcription factor SOX4 and microphthalmia-associated transcription factor induce Dicer expression in cancer cells and

melanocytes, respectively^{80, 81}. Multiple transcript variants of Dicer produced by starting transcription from alternative promoters and splicing from one Dicer gene. Shorter Dicer mRNA variants are produced in cancer cell lines and differentiated epithelial cells^{79, 82}. The protein level and activity of human Dicer can be also regulated by its post-translational modification; for example phosphorylation induces nuclear localization of Dicer and inhibits its function, SUMOylation following cigarette smoke exposure decreases Dicer activity, and glycosylation by ER maintains Dicer protein levels⁷³. Due to the profound effect on miRNAs processing and therefore on cellular post transcriptional activity, Dicer plays an important role in various processes from embryologic cell development to various disease such as CVD.

Since disruption of Dicer leads to global loss of miRNAs, deficiency of this enzyme has been used as an approach to study the biological effect of miRNAs in various cell types^{73, 83-88}. Deletion of Dicer in SMCs during embryonic development causes late embryonic lethality and skin hemorrhage⁸³. These effects are associated with thin blood vessel wall formation due to a diminished proliferation and differentiation of SMC⁸³. However, loss of Dicer in adult mice is not lethal but dramatically decreases blood pressure owing to the loss of SMC contractile functions^{83, 89}.

MiRNAs are involved in all cellular events under normal condition as well as pathological process of arterial remodeling, including platelet and leukocyte activation, SMC migration and proliferation, as well as EC recovery⁸⁹⁻⁹³. Notably, miRNAs play key role in phenotypic switch of SMCs. For instance, the miR-143/145 cluster, encoding the most abundant miRNAs in normal vascular walls, is required for SMC contractile phenotype (Figure 6)⁹⁰⁻⁹⁶. SMC differentiation is promoted by miR-145-5p in part by increasing myocardin d (Myocd) protein and functioning in a feed-forward loop to reinforce its own expression by the serum response factor -Myocd complex⁹⁴⁻⁹⁷. Moreover, miR-145-5p overexpression increases SMC contractile marker genes expression, such as SM α -actin, Cnn1, and SM-MHC^{95, 98}. Furthermore, miR-143-3p inhibition increases the proliferation rate of SMCs in vitro, demonstrating the miR-143-3p as a negative regulator of SMC proliferation by targeting Myocd's competitor, ETS domain-containing protein^{95, 98}.

Moreover, miR-221, miR-222, and miR-21 are up-regulated following vascular injury and increase SMC proliferation and thereby neointima formation^{99, 100}. MiR-221 and -222 are induced

in response to vascular injury and increase neointima formation and SMCs proliferation by targeting p27(Kip1) and p57(Kip2)^{95, 99, 100}. Moreover, miR-21 is the first miRNA in SMCs describe to have a pro-proliferative and antiapoptotic effect in a carotid injury model in rats^{99, 100}. The NF- κ B-regulated miR-21 mediates SMC proliferation following vascular injury most likely by suppressing PTEN and increasing expression of B-cell leukemia/lymphoma 2 (Figure 6)¹⁰⁰. Accordingly, stents coated with inhibitors of miRNAs, such as miR-21, can effectively reduce in-stent-restenosis without affecting re-endothelialization¹⁰¹. Thus, an emerging theme in miRNA research from SMCs demonstrates miRNAs as potential targets to fine tune phenotypic switch of SMCs and to use miRNA-based therapy for cardiovascular disease.

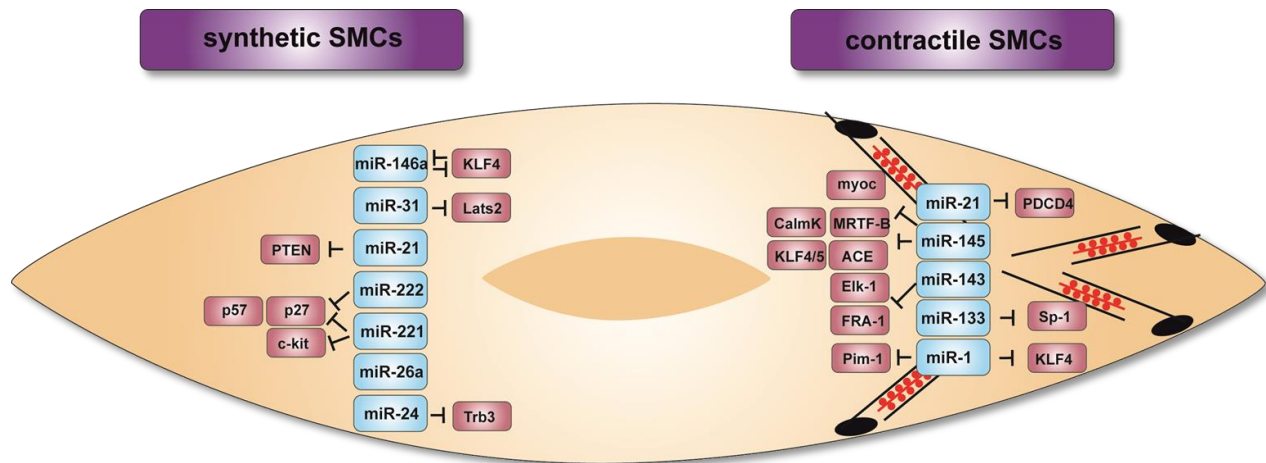


Figure 6. Phenotype-specific gene expression in SMCs is mediated by miRNAs. Synthetic and contractile SMCs are characterized by increased expression of a specific set (network) of miRNAs that either inhibit or promote the proliferation and/or expression of contractile proteins. Lats2, large tumour suppressor homolog 2; Trb3, Tribbles-like protein-3; myoc, myocardin; CalmK, calmodulin K; MRTF-B, myocardin-related transcription factor-B; KLF4/5, Krüppel-like factor 4/5; FRA-1, Fos related antigene-1; PDCD4, programmed cell death 4; Sp-1, Sp1 transcription factor; ACE, angiotensin-converting enzyme; PTEN, phosphatase and tensin homolog; p57, cyclin-dependent kinase inhibitor 1C (CDKN1C); p27, cyclin-dependent kinase inhibitor 1B (CDKN1B); c-kit, v-kit Hardy-Zuckerman 4 feline sarcoma viral oncogene homolog; ELK-1, ELK1 member of ETS oncogene family; PIM-1, proviral integration site 1⁴⁷.

1.3 Aims of the study

Stent implantation into arteries with atherosclerotic plaque cause injury that frequently results in excessive neointima formation because of SMC proliferation, which causes re-narrowing of the arterial lumen (known as restenosis)^{5, 7, 47}. Current approaches to reduce the rate of neointima formation have successfully applied new stent platforms that elute anti-proliferative drugs such as sirolimus to reduce SMC proliferation^{5, 7, 102}. However, the anti-proliferative effect of drugs is

unspecific and also affects endothelial recovery. This may cause late stent thrombosis and atherosclerosis. Therefore, development of new drug-eluting stents that specifically target SMC proliferation can be a promising approach to overcome restenosis without increasing the risk of in-stent thrombosis in the future.

There is growing experimental evidence that miRNAs regulate the transition of SMCs from a contractile to a proliferating phenotype^{5, 47, 103-105}. MiRNAs are essential for embryonic development by controlling protein expression variability against intrinsic noise of transcriptional changes during cell fate switches^{47, 103, 106-108}. Moreover, individual miRNAs have beneficial or detrimental effect in arterial repair, for instance some miRNAs inhibit (e.g., miR-143-3p and -145-5p) or promote (e.g., miR-21-5p) neointima formation, indicating that miRNAs play different roles in SMCs during vascular development and remodeling^{96, 98, 100, 106-109}. The current study aimed at identifying the expression profile of miRNAs during neointima formation in *Apoe*^{-/-} mice.

All mature miRNAs are reduced by the RNase III endonuclease Dicer, which cleaves precursor miRNAs. In SMCs, Dicer is essential for development and maintenance of the contractile phenotype^{83, 89}. Despite numerous studies on the impact of miRNA expression on neointima formation and atherosclerosis, the role of SMC specific Dicer deletion on arterial repair remains unclear. The second aim of the study was to determine the role of miRNA biogenesis by Dicer in SMC phenotypic switch and proliferation during neointima formation using SMC-specific Dicer knockout mice.

Single miRNA can bind hundreds of target mRNAs, and conversely, one mRNA can be targeted by multiple miRNAs, indicating that large and diverse miRNA-mRNA interaction networks can regulate gene expression in a cell type-specific manner^{110, 111}. Therefore, the third aim was to investigate the mRNA-miRNA interaction that contributes mostly in observed effect of Dicer deletion in SMC after vascular injury. In particular, we focused on miR-27a-3p during SMC proliferation, because several studies suggest that the miR-27 family has important roles in atherosclerosis and more recently it has been shown that miR-27a-3p and miR-27b-3p are among those miRNAs which affect SMC proliferation *in vitro*^{103, 112}. However, the role of miR-27a-3p in SMCs proliferation remains unclear. Therefore, the functional mechanism of miR-27a-3p during SMC proliferation was studied.

2 Materials and methods

All solutions were prepared with ultra-pure (UP) water (Milli-Q Plus ultrapure purification, Millipore, Billerica, USA). The reagents were purchased from Sigma-Aldrich (Steinheim, Germany), Carl Roth (Karlsruhe, Germany), Merck (Darmstadt, Germany) and Fluka (Buchs, Switzerland) unless stated otherwise in the text.

2.1 General equipment

Balance -	Precisa 92SM-202A (Sartorius mechatronics, Göttingen, Germany)
Centrifuge -	Heraeus Pico 17 (Thermoscientific, Massachusetts, USA), Heraeus Megafuge 1.0R (Thermoscientific, Massachusetts, USA), Eppendorf 5430R and Eppendorf 5415D (Eppendorf AG, Hamburg, Germany)
Microscopes -	Olympus SZX10 (Olympus optical, Hamburg, Germany)
Laminar flow hood -	HeraSafe (Heraeus, Osterode, Germany) MaxiSafe (Thermoscientific, Massachusetts, USA)
pH-meter -	WTW pH 526 (Weilheim, Germany)
Spectrophotometer -	Nanodrop 1000 (PiqLab, Erlangen, Germany)
PCR thermocyclers -	MasterCycler Nexus (Eppendorf AG, Hamburg, Germany) Thermal Cycler 2720 and 7900HT fast real-time PCR system (Applied Biosystems, Darmstadt, Germany)
Tissue homogenizer -	TissueLyserLT (Qiagen, Hilden, Germany)
Autoclave -	systec VX-95 (systec, Wetzlar, Germany)
Microtome -	Leica RM2235 (Leica Biosystems, Nussloch, Germany)
Plate reader -	SpectraFluor Plus (Tecan, Crailsheim, Germany)
Imaging software -	Leica-DM6000B (Leica Biosystems, Nussloch, Germany)
Thermoblocks-	Thermostat Plus (Eppendorf AG, Hamburg, Germany)
Embedding station-	Leica EG1160 (Leica-Microsystems)
CO2 Incubator-	Galaxy S (RS Biotech, Irvine, UK)
Laser-Capture Microdissection system (LCM)	LMD7000 (Leica Microsystem, Wetzlar, Germany)

2.2 Chemicals

β-Mercaptoethanol (Sigma-Aldrich, Steinheim, Germany)
Dimethyl sulfoxide (DMSO) (Carl Roth, Karlsruhe, Germany)
Dithiothreitol (DTT) (Carl Roth, Karlsruhe, Germany)
Horse serum (Vector Laboratories, Burlingame, California, USA)
Ketamin (Pfizer, Berlin, Germany)
Xylazine (Serumwerk, Bernburg, Germany)
Lipofectamin 2000 (Thermo Scientific, California, USA)
Mounting medium with DAPI (Vector Laboratories, California, USA)
NP-40 alternative (Merck, Darmstadt, Germany)
Paraformaldehyde (PFA) (Carl Roth, Karlsruhe, Germany)
Paxgene tissue container (PreAnalytiX, Hombrechtikon, Switzerland)
Phosphate-buffered saline, PBS Dulbecco (Thermo Scientific, California, USA)
RNaseZap decontamination solution (Thermo Scientific, California, USA)
RNAlater (Thermo Scientific, California, USA)
Triton X-100 (Sigma-Aldrich, Steinheim, Germany)
Tween® 20 (Merck, Darmstadt, Germany)
Vitro Clud (R. Langenbrinck, Emmendingen, Germany)
Borgal solution 24% (Virac, Carros, France)
Ethanol absolute (Sigma-Aldrich, Steinheim, Germany)
Neutral oil (Miglyol, Sasol, Hamburg, Germany)
BSA (SERVA Electrophoresis GmbH, Heidelberg, Germany)
Acid-Phenol: Chloroform (Applied Biosystems, Darmstadt, Germany)
Xylol (Honeywell, Stuttgart, Germany)

2.3 Antibodies

Antigen	Clone	Host	Catalogue #	Company
α -SMA	1A4	mouse	M0851	Dako, Hamburg, Germany
Mac-2	M3/38	rat	CL8942AP	Cedarlane, Burlington, Canada
2.3.1 ARHGEF26	polyclonal	rabbit	ab129265	Abcam, Cambridge, UK
CD31	polyclonal	goat	sc-1506	Santa Cruz Biotechnology, Santa Cruz, CA, USA
Ki67	polyclonal	rabbit	ab15580	Abcam
Caspase3	polyclonal	rabbit	9662S	Cell Signaling, Danvers, MA, USA
Nonspecific primary antibody (Ab)	monoclonal	mouse	sc-2025	Santa Cruz Biotechnology
Nonspecific primary Ab	monoclonal	rat	sc-2026	Santa Cruz Biotechnology
Nonspecific primary Ab	polyclonal	rabbit	ab27472	Abcam
Nonspecific primary Ab	polyclonal	goat	sc-2028	Santa Cruz Biotechnology

Antigen	Secondary antibody	Conjugated	Host	Catalogue #	Company
2.3.2 anti-rabbit IgG	Dylight549-conjugated		goat	042-04-15-06	KPL, Gaithersburg, MD, USA
anti-mouse IgG	FITC-conjugated		donkey	715-096-150	Jackson immunoResearch, Pennsylvania, USA
anti-rat IgG	FITC-conjugated		donkey	712-095-153	Jackson immunoResearch
anti-rabbit IgG	FITC-conjugated		donkey	711-095-152	Jackson immunoResearch
anti-mouse IgG	Cy3-conjugated		donkey	715-165-151	Jackson immunoResearch

2.4 Buffers

20× SSC buffer: 3 M NaCl, 0.3 M Na citrate (pH 7.0).

Tris/EDTA buffer: 100 mM Tris (pH 7.4), 10 mM EDTA (pH 8.0).

Citrate buffer: 630 ml UP water, 12.6 ml solution A (2.101 g citric acid in 100 ml UP water), 57.4ml solution B (14.70 g nitrium citrate in 500 ml of UP water), 320 μ l Tween 20, (pH 6.0).

Elastic Van Gieson (EVG) staining solutions:

Solution A: 10 g of hematoxylin was dissolved in 100 ml of 96% ethanol

Solution B: 29% Iron (III)-Chloride solution (145 g of Iron (III)-Chloride was dissolved in 500 ml of UP water) and 7.5 ml of 37% HCL was added to 950 ml of UP water.

TBS (1X):

25 mM Tris-HCL, pH 7.4, 2.7 mM KCl, 137 mM NaCl

4% PFA:

16 g of PFA was added to 184 ml of UP water and dissolved by adding 5 ml of 10 M NaOH during heating at 100°C. The pH was decreased to 7.4-8 by adding 25% HCl. Subsequently, an equal volume of 2×PBS was added and the solution was filtered through a filter paper.

Immunofluorescence staining:

Blocking solution A: 5.4 ml PBS, 600 µl 10% BSA, 3 drops 2.5% normal horse serum.

Oil Red O stock solution:

1 g Oil Red O powder (Sigma-Aldrich) was dissolved in 200 ml 99% isopropanol

Oil Red O working solution:

160 ml Oil Red O stock solution was mixed with 120 ml UP water and stored at room temperature for 1 h. The solution was filtered through a filter paper.

2.5 Mouse husbandry

Mice were housed 4 per cage in a barrier facility and maintained on a 12 hour light-dark schedule within the animal laboratory facility of the University, the Zentrale Versuchstierhaltung (ZVH), Klinikum Universität München. Mice had free access to water and chow. All animal experiments were reviewed and approved by the local authorities (District Government of Upper Bavaria) in accordance with the German animal protection laws.

2.6 Mouse strains

Apolipoprotein E^{-/-} (*Apoe*^{-/-}) mice were purchased from the Jackson Laboratory (Bar Harbor, ME, USA) and used for some experiments. Male smooth muscle myosin heavy chain (SMMHC)-*Cre*⁺ mice (kindly provided by Dr. Stefan Offermanns, Max Planck Institute for Heart and Lung Research, Bad Nauheim, Germany) were crossed with *Dicer*^{+/+} *Apoe*^{-/-} and *Dicer*^{flox/flox}/*Apoe*^{-/-} mice (The Jackson Laboratory) to obtain SMMHC-*Cre*⁺*Dicer*^{+/+} *Apoe*^{-/-} (SM-*Dicer*^{+/+}) mice (as control group) and SMMHC-*Cre*⁺*Dicer*^{flox/flox} *Apoe*^{-/-} (SM-*Dicer*^{-/-}) mice^{113, 114}. *Dicer* floxed

mutant mice possess loxP sites flanking exon 23 of the *Dicer1* gene. Cre-mediated recombination after tamoxifen injection results in the loss RIIIDb function due to the deletion of 90 amino acids in this domain¹¹³.

SM-*Dicer*^{+/+}, SM-*Dicer*^{-/-} male mice, and *Apoe*^{-/-} mice (6-8 weeks old) were used for experiments. To induce cre recombinase activity the SM-*Dicer*^{+/+} and SM-*Dicer*^{-/-} mice were injected intraperitoneal (i.p.) with tamoxifen (2 mg per 20 g body weight; Sigma-Aldrich) dissolved in neutral oil for 5 consecutive days and 7 days after the last tamoxifen injection they fed a high-fat diet (HFD) comprising 0.15% cholesterol, 21% crude fat and 19.5% casein (ssniff Spezialdiäten GmbH, Soest, Germany or Altromin GmbH, Lage, Germany) for 7 days¹¹³. *Apoe*^{-/-} mice were also fed a HFD for 7 days. Animals were anesthetized with ketamin (80 mg/kg, i.p., Pfizer, Berlin, Germany) and xylazine (5 mg/kg, i.p., Serumwerk, Bernburg, Germany). Wire-induced endothelial denudation was performed in the left carotid artery using a flexible angioplasty guide wire (0.36 mm diameter). The common, internal, and external carotid arteries were transiently ligated to interrupt the blood flow. After a transverse arteriotomy made in the external carotid artery (ECA), the angioplasty guide wire was inserted into the common carotid artery (CCA). The wire was rotated and moved 3 times back and forth the CCA resulting in endothelial denudation. After removal of the wire, the ECA was completely ligated and the blood flow restored through the common and the internal carotid arteries (ICA) (Figure 7)¹¹⁵.

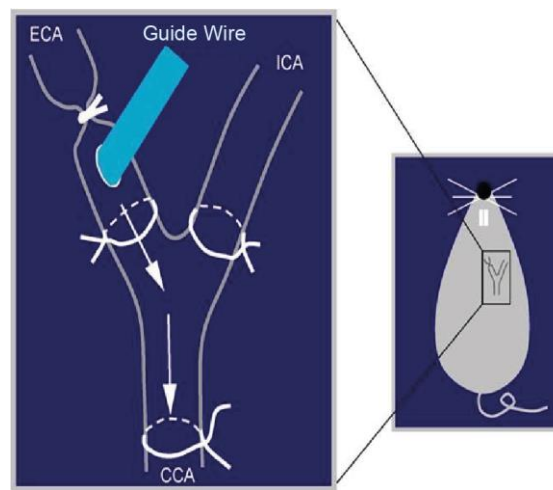


Figure 7. Wire-induced endothelial denudation of murine carotid arteries. Blood flow was transiently obstructed by ligating the CCA, the ECA and the ICA. Endothelial denudation of the CCA was achieved by 3 rotational passes using an angioplasty guide wire inserted into the ECA. The blood flow through the CCA and the ICA was restored by removing the ligation, whereas the ECA was occluded.

Mice were anesthetized with ketamine hydrochloride and xylazine (as described in chapter 2.6.1) blood was taken by cardiac puncture for serum lipid measurements, the chest was opened, and a catheter was inserted into the left ventricle through an incision in the apex. Mice were then perfused ~~with PAXgene Tissue Fix (PAXgene Tissue Fix Containers; Qiagen)~~ with PAXgene Tissue Fix (PAXgene Tissue Fix Containers; Qiagen) or PAXgene Tissue Fix (PAXgene Tissue Fix Containers; Qiagen) before harvesting of the tissues.

To perfuse the animal with Paxgene Tissue Fix or RNA later, the right atrium was cut and a needle connected to a 1 ml syringe was inserted into the left ventricle. The vascular system was first perfused with 1 ml ice-cold PBS to remove blood and subsequently with 1 ml PAXgene Tissue Fix solution or RNAlater.

After the perfusion with PAXgene, tissues were harvested and placed in PAXgene Tissue Fix solution for 2 h. Following fixation, tissues were removed from the PAXgene Tissue Fix solution and transferred to the PAXgene Tissue Stabilizer solution. Stabilized samples were embedded in paraffin for histological studies (see section 2.11.1). It includes 2 solutions PAXgene Tissue Fix, which rapidly enters and fixes the tissue, and PAXgene Tissue Stabilizer which protects nucleic acids and morphology of the tissue for up to 7 days at room temperature and at 2-8°C or -20°C for longer periods.

To stabilize RNA, the vascular tree was flushed with 0.5-1 ml RNAlater solution. After this perfusion, tissues were dissected and placed in RNAlater solution. Samples were stored in RNAlater solution up to 21 days at 4°C before the RNA was isolated for qRT-PCR analysis. All instruments used during organ dissection were first treated with RNaseZap according to the manufacturer's instructions.

2.7 MiRNA expression profile

Carotid arteries from *Apoe*^{-/-} mice were perfused with RNAlater and harvested before (0 day) and 1, 7, 14, and 28 days after wire injury. Of note, animal experiment for miRNA microarrays including surgical wire injury procedure and carotid harvest was performed by Maliheh Nazari-Jahantigh. Total RNA was isolated from the carotid arteries using the mirVana miRNA isolation kit (Thermo Scientific) according to the manufacturer's protocol. Briefly, the samples were disrupted with tissue homogenizer (Qiagen) and lysed in a denaturing lysis buffer, which stabilizes RNA and inactivates RNases. Next, the lysate was subjected to acid-phenol: chloroform extraction, which removes most of the DNA and the other cellular components. The

semi-pure RNA extracts were further purified over a glass-fiber filter to obtain total RNA. The RNA integrity number (RIN) of each sample was determined by capillary electrophoresis (Bioanalyzer Agilent 2100) using RNA 6000 Nano LabChip Kits (Agilent Technologies). The RNA was separated according to fragment size, and the fragments are detected and depicted as electropherograms and virtual gel images. The RIN was derived from the electrophoretic profile of the 28S and 18S-rRNAs (indicating massive degradation) to 10 (indicating no degradation). In addition to the 28S and 18S-rRNA peaks, the RIN calculation also takes into account the entire electrophoretic profile (e.g., the fraction of short degraded RNA species). RNA samples with a $RIN \geq 7.5$ were used for further downstream analysis. A one-color-based hybridization protocol (DNAvision, Gosselies, Belgium) was applied using SurePrint mouse miRNA microarrays (Sanger miRBase v12) (Agilent Technologies). The microarray data were analyzed using Genespring GX13 software (Agilent Technologies).

2.8 MiRNA real-time PCR array

Total RNA from carotid arteries of *SM-Dicer^{+/+}* and *SM-Dicer^{-/-}* mice was isolated using mirVana kit according to the standard protocol of kit. The RNA quality of the samples was determined using an Agilent 2100 Bioanalyzer. RNA samples with $RIN \geq 7.5$ were used for the array. Reverse transcription and pre-amplification were performed using the Megaplex reverse transcription (RT) & Preamp Rodent Pool Set (Thermo Scientific) according to the manufacturer's instructions. To synthesize single-stranded cDNA, TaqMan microRNA reverse transcription kit (Thermo Scientific) and the Megaplex rodent RT primers (Thermo Scientific) were used. To perform reverse transcription, 3 μ L (1 to 350 ng) total RNA were added to the 4.5 μ L of RT reaction mix. The RT reaction was carried out in the thermal cycler (Table 1).

Table 1. Thermal cycling conditions

Stage	Temperature	Time
Stage 1-40	16°C	2 min
	42°C	1 min
	50°C	1 sec
Stage 41	85°C	5 min
Hold	4°C	∞

Next, the cDNA samples were preamplified using Megaplex rodent preamplification primers and TaqMan preamplification master mix (both from Thermo Scientific). To prepare the

preamplification reaction 2.5 μ L RT products were added to 22.5 μ L preamplification reaction mix (Table 2).

Table 2. Preamplification reaction

Stage	Temperature	Time
Stage 1	95°C	10 min
Stage 2	55°C	2 min
Stage 3	72°C	2 min
Stage 4-16 (12 Cycles)	95°C	15 sec
	60°C	4 min
Stage 17‡	99.9°C	10 min
Hold	4°C	∞

‡ Required for enzyme inactivation.

Preamplified products were diluted using 75 μ L of tris-EDTA buffer pH 8.0. The PCR reaction mix for one array plate was prepared as follows in the Table 3.

Table 3. PCR reaction

Component	Volume
TaqMan universal PCR master mix, no ampErase UNG, 2x	450 μ l
Diluted preamplified product	9 μ l
Nuclease-free water	441 μ l
Total	900 μ l

Finally, the samples were loaded into preconfigured 384-well microfluidic cards (TaqMan Array MicroRNA Cards, Thermo Scientific) and real-time analysis of 518 mouse miRNAs (Sanger miRBase v10) using the 7900HT real-time-PCR System was used (Table 4).

Table 4. Real-time PCR program

Stage	Temperature	Time
Stage 1	50°C	2 min
Stage 2	94.5°C	10 min
Stage 3-43 (40 Cycles)	97°C	30 sec
	59.7°C	1 min

Data were analyzed using StatMiner software (Integromics, Granada, Spain) according to the $\Delta\Delta$ Ct method using multiple internal control genes. The most stable combination of internal controls was determined using the Genorm algorithm. The fold change compared with the control group was calculated and logarithmically transformed (log10).

2.9 Global gene expression analysis

Carotid arteries of SM-*Dicer*^{+/+} and SM-*Dicer*^{-/-} mice were harvested 14 days after vascular injury, following *in situ* perfusion with RNAlater (see also section 2.6.1). Animal experiments for gene expression the microarray were performed by Zhe Zhou. Total RNA was isolated using RNeasy micro Kit (Qiagen). The quality of the RNA samples was checked by 2100 Bioanalyzer and only the samples with RIN ≥ 7.5 were used for the array. A one-color based hybridization protocol was applied (IMGH Laboratories, Munich, Germany) using SurePrint G3 Mouse GE Microarrays (8x 60K format, Agilent). The microarray data were analyzed by GeneSpring GX13 software. Data were analyzed by Ingenuity Pathway Analysis (IPA, Qiagen) to predict upstream regulators of the differentially expressed genes.

Integrative target prediction analysis of 66 downregulated miRNAs ($P < 0.05$; fold change ≥ 2) and 217 upregulated miRNAs (fold change ≥ 2) were compared between SM-*Dicer*^{-/-} mice and SM-*Dicer*^{+/+} mice using the web tool Magia² (<http://gencomp.bio.unipd.it/magia2/start/>) with the miRanda prediction algorithm (<http://www.microrna.org/microrna/home.do>) including the top 50% predictions (prediction score cut-off = -0.3)¹¹⁶. First, a meta-analysis approach based on a P value calculation according to linear models for microarray data was applied separately for miRNAs and genes in the 2 groups and combined with the inverse chi square distribution to identify oppositely regulated miRNA-gene pairs. In addition, false positive discovery rates for each mRNA-miRNA interaction were calculated following the Benjamini and Hochberg estimation method and interactions with an adjusted P value < 0.05 were selected. The network of the top 70 interactions was graphically depicted using Cytoscape software (<http://www.cytoscape.org/>). The conservation of miRNA binding sites in the mRNA targets between human and mouse was analyzed with TargetScan (<http://www.targetscan.org>). Potential target genes of miRNAs were identified among the up-regulated genes (> 2 -fold) 14 days after injury in carotid arteries of SM-*Dicer*^{+/+} and SM-*Dicer*^{-/-} mice.

2.10 Quantitative real-time polymerase chain reaction (qRT-PCR)

The differential regulation of the miRNAs and mRNAs was studied by qRT-PCR which runs on a 7900HT thermocycler. TaqMan gene or SYBR green expression assays were used in all the

experiments. SYBR green is a DNA binding dye that binds to all double stranded DNA during PCR and results in fluorescence which can be measured. It is important to have well-designed SYBR green primers that do not amplify non-target sequences. In this technique, the amplified cDNA is measured as the reaction progresses. During PCR, an increase in the DNA product leads to an increase in fluorescence intensity which can be measured at each cycle and hence the DNA concentration is quantified. This in turn can be used to calculate the expression of a target gene. The TaqMan gene expression assay consists of primers and probes. The purpose of these designed probes is to increase the specificity of quantitative PCR. The TaqMan probe contains a reporter dye at the 5' end and a nonfluorescent quencher at the 3' end. During the PCR reaction, the probe is cleaved, thereby separating the reporter dye and the quencher dye resulting in a fluorescent signal. The accumulation of the PCR products is detected by monitoring the increase in fluorescence of the reporter dye.

Total RNA was isolated from paraffin embedded sections or from cultured SMCs using mirVana miRNA isolation kit (Thermo Scientific), PAXgene RNA MinElute kit (Qiagen), or RNeasy Mini Kit (Qiagen). The RNA concentration was determined by measuring the absorbance at 260 nm (A260) using spectrophotometer. The absorbance at 280 nm was also measured to determine the RNA purity. RNA with an A260/A280 ratio of 1.8-2.0 was used. For both SYBR green and TaqMan gene expression assays, RNA was reverse transcribed with the reverse transcription master mix (High capacity cDNA reverse transcription kit, Applied Biosystems, Foster city, CA) according to the manufacturer's protocol (Table 5). The RT reaction consists of the following four steps: 25°C for 10 min, 37°C for 120 min, 85°C for 5 min and 4°C.

The cDNA was subjected to PCR amplification with specific set of SYBR green primers (Sigma-Aldrich, Table 6). PCR was performed in a 7900HT fast real-time PCR system (Applied Biosystems, Darmstadt, Germany) (Table 7).

Table 5. Reverse transcription

Solution	Volume
RT buffer, 10x	2 μ l
dNTP mix (100 mM), 25x	0.8 μ l
RT random primers, 10x	2 μ l
multiscribe reverse transcriptase	1 μ l
RNase inhibitor	1 μ l
Nuclease-free water	3.2 μ l
RNA (up to 500 ng)	10 μ l

Table 6. Real-time PCR

Solution	Volume
SYBR green master mix	12.5 μ l
nuclease-free water	9.5 μ l
each forward and reverse primer	0.5 μ l
cDNA (25 ng)	2 μ l

Table 7. Real-time PCR program

Steps	Temperature	Time
Initial denaturation	95° C	10 min
Denaturation	95° C	15 sec
Annealing	63° C	30 sec
Extension	72° C	30 sec

40

To check the expression of genes using TaqMan gene expression assays, cDNA was subjected to PCR amplification with TaqMan premixed primers and probes (Thermo scientific, Table 8). PCR was performed in a 7900HT fast real-time PCR system (Table 9).

Table 8. Real-time PCR

Solution	Volume
TaqMan universal PCR master mix	5 μ l
TaqMan gene expression assay mix, 20x	0.5 μ l
cDNA diluted in nuclease-free water (25 ng)	4.5 μ l

Table 9. Real-time PCR program

Stage	Temperature	Time
UNG activation	50° C	2 min
	95° C	10 min
Denaturation	95° C	15 sec
Annealing/extension	60° C	1 min

40

The relative expression levels were calculated using multiple internal control genes, adjusted for differences in PCR efficiency (Qbase, Biogazelle, Zwijnaarde, Belgium) and logarithmically transformed. Expression of the housekeeping genes such as *Gapdh* and *Actb* which is used to normalize the target gene expression should not vary among different samples used in the study¹¹⁷. However, previous studies show that housekeeping gene expression can vary in different tissues; therefore the use of one housekeeping gene to normalize gene expression may lead to errors. In order to obtain accurate measurement of gene expression, multiple internal control genes were used and the analysis was performed using the Qbase software. This software calculates the expression stability of the housekeeping genes in different samples. This is based on the principle that the ratio of two housekeeping gene expression is identical among all the samples¹¹⁷. An increasing variation in the ratio corresponds to decreasing expression stability of the housekeeping genes. The relative expression levels were normalized to the reference genes and logarithmically transformed (\log_{10}) (Qbase, Biogazelle).

The mRNA expression levels of Rho guanine nucleotide exchange factor 26 (*Arhgef26*), SH3 domain binding glutamate-rich protein like (*Sh3bgrl2*), SH2 domain containing 5 (*Sh2d5*), Delta like 4 (*Dll4*), carbohydrate (keratan sulfate Gal-6) sulfotransferase 1 (*Chst1*), Insulin-like growth factor binding protein 3 (*Igfbp3*) and oncoprotein induced transcript 3 (*Oit3*) were quantified using either self-designed primers (Sigma-Aldrich) (Table 10) or TaqMan gene expression assays (Thermo scientific).

Table 10. PCR primer sequences

Gene	Primer sequence
<i>CDKN1A</i>	5'-GTGAAAACAGAGCGAGAGAGATG-3' 5'-CAGGGGTACAGTGCTAAAGGC-3'
<i>CDKN1B</i>	5'-TAATTGGGGCTCCGGCTAACT-3' 5'-TGCAGGTCGCTTCCTTATTCC-3'
<i>MYH11</i>	5'-TGGAACCTTCATCGACTTTGGG-3' 5'-ACAGCTTCTCCACGAAAGAC-3'
<i>DLL4</i>	5'-CACGGAGGTATAAGGCAGGAG-3' 5'-TCACAGTCTGTCCGGTTCCT-3'
<i>OIT3</i>	5'-GTACAGTGGTCGATGTGGTGA-3' 5'-GCTTGCTGGTTCGGATGATG-3'
<i>TAGLN</i>	5'-TCCAGACTGTTGACCTCTTG-3' 5'-CAGTTGGGATCTCCACGGTAG-3'
<i>GAPDH</i>	5'-AGGGCTGCTTTTAACTCTGGT-3' 5'-CCCCACTTGATTTTGGAGGGA-3'
<i>Arhgef26</i>	5'-CATGCTACTAGGCGCTGAGAC-3' 5'-GTCAGGGTGGTTCTGTCTGGT-3'
<i>Chst1</i>	5'-TCTTGAAGGCTGTCCTCCT-3' 5'-CCAGGGCAAGTGTGGAAAGA-3'
<i>Sh3bgrl2</i>	5'-AATGGCACTGTCTGGGCATC-3' 5'-AGCAGCTTTCAGGCCATAGT-3'
<i>Dicer1</i>	5'-GAATAAGGCTTATCTTCTGCAGG-3' 5'-CATAAAGGTGCTTGGTTATGAGG-3'
<i>Dll4</i>	5'-GAACAGAGGTCCAAGCCGAA-3' 5'-CAGGCCCATCTCCAGATCG-3'
<i>Tagln2</i>	5'-CCAAGCAGACTTCCATGGGC-3' 5'-TGTTGAGGCAGAGAAGGCTTG-3'
<i>B2m</i>	5'-TCGGTGACCCTGGTCTTTCT-3' 5'-TTTGAGGGGTTTTCTGGATAGCA-3'

2.11 Histochemistry

2.11.1 Paraffin embedding, sectioning, and deparaffinization

To quantify the lesion size, samples (arteries) were harvested from mice following *in situ* perfusion and fixation. Next, tissues were dehydrated using tissue processor and embedded in liquid paraffin (approximate temperature 60°C) according to the following protocol:

- Ethanol 70% for 30 min at 20°C
- Ethanol 70% for 30 min at 20°C
- Ethanol 96% for 30 min at 20°C
- Ethanol 96% for 30 min at 20°C
- Ethanol 100% for 30 min at 20°C

- Ethanol 100% for 30 min at 20°C
- Ethanol 100% for 30 min at 20°C
- Xylol for 30 min at 45°C
- Xylol for 30 min at 45°C
- Xylol for 30 min at 45°C
- Paraffin I for 30 min at 62°C
- Paraffin II for 30 min at 62°C
- Paraffin III overnight at 62°C

The paraffin blocks were allowed to harden at -20°C (Leica EG1160) before sectioning using a microtome. Serial sections (5 µm thick) of the common carotid artery were collected on glass slides (Superfrost plus glass slides, Thermo Scientific) within 1 mm of the bifurcation area. After sectioning, the slides were incubated in a 37°C incubator for 5-6 h or at room temperature overnight to reduce detachment of the tissue during staining.

To measure lesion size in paraffin embedded tissues EVG staining was performed. Cross sections
2.11.1 **EVG staining** of the carotid artery (3-5 per mouse) obtained at a standard distance (50 µm) starting from the bifurcation was used for staining. In order to stain the sections, deparaffinization and rehydration was performed according to the following protocol:

Incubate in Xylol for 10 min

Incubate in Xylol for 10 min

Incubate in 100% ethanol for 5 min

Incubate in 100% ethanol for 5 min

Incubate in 96% ethanol for 5 min

Incubate in 70% ethanol for 5 min

Incubate in UP water for 5 min

Incubate in PBS for 5 min

EVG staining was performed using the following protocol:

- 1) The sections were deparaffinized and rehydrated by the following procedure:
- 2) Stained in resorcin-fuchsin solution (Roth, X877.1) for 15 min at 56°C followed by slowly dipping in tap water 1-2 times.
- 3) Differentiated in 80% ethanol followed by dipping in tap water and UP water

- 4) Incubated in solution A+B (100ml solution A and 100 ml solution B, freshly prepared, see also section 2.4) for 5 min
- 5) Differentiated with 0.5% HCL-alcohol by dipping in the solution a few times
- 6) Washed in tap water until the color of the nucleus turned blue
- 7) Incubated in pikrofuchsin (Merck, 1.15974/4) for 1 min and washed in tap water shortly
- 8) Dipped shortly in 70% ethanol followed by 96% ethanol
- 9) Incubated in 100% ethanol for 3 min followed by 5 min in xylol and then the cover slip was placed using Vitro-Clud

Images were obtained under a bright-field microscope (Leica DM6000B) connected to a camera (Leica DFC295) and using LAS software (Leica Microsystems). To measure the neointima area, images were opened with the image analysis software (ImageJ) available for free download <http://rsb.info.nih.gov/ij/download.html>. Next, the straight line draws along with the scale bar of the image to set up the accurate measurement by the software. To define the neointima area, a line was drawn manually around the neointima area and the software calculates the area automatically (Figure 8).

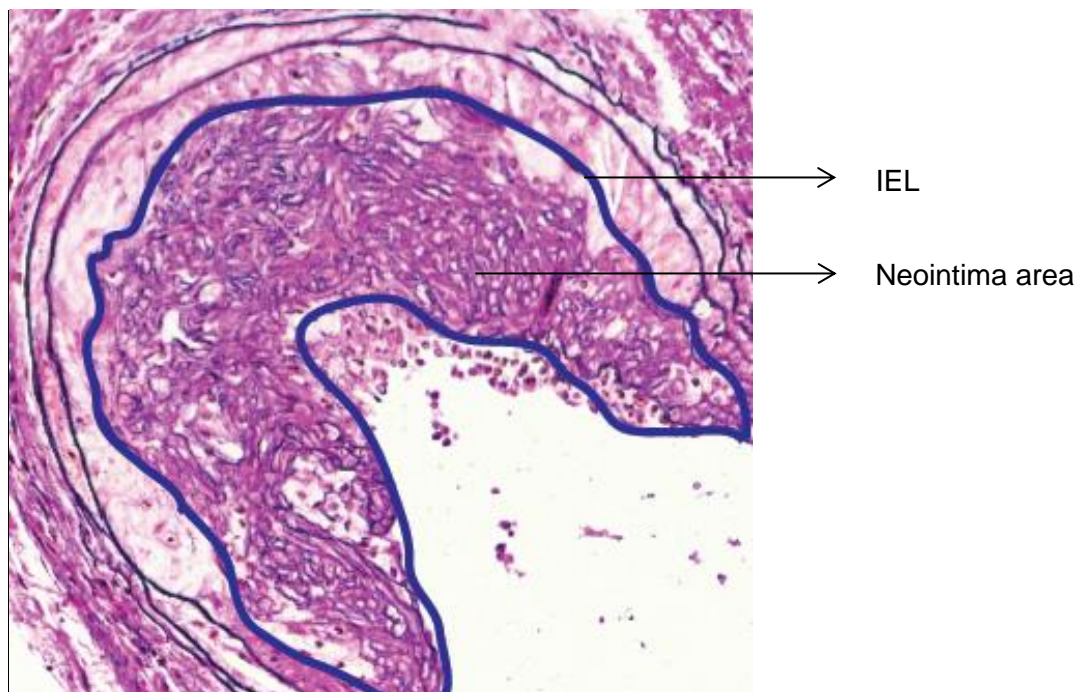


Figure 8. Morphometric analysis of the CCA. IEL- internal elastic lamina.

To determine the composition of the neointimal area following wire injury, quantitative immunostaining in carotid artery sections (5 μm thick) was performed using primary antibodies for α -smooth muscle actin (SMA; 1:200), macrophage specific (Mac2, 1:200), Ki67 (1:1500), 2.1ARHGEF26 (1:20), activatedgCaspase 3 (1:400), and CD31 (1:75) (Table 8, see also section 2.3.1). To detect the primary antibody, fluorescently conjugated secondary antibodies (FITC, Cy3, Dylight488, or Dylight549) were used (Table 11, see also section 2.3.2). The nuclei were counterstained with 4', 6-Diamidino-2-phenylindol (DAPI, Vector Laboratories). Fluorescence microscope (Leica-DM6000B) connected to a charge coupled device camera (Leica DFC365FX) was used to acquired digital images. The percentage of the cell number or positively stained area (2–3 sections/mouse, 50 μm distance between sections) was quantified using ImageJ software. To adjust the threshold, the background of negative control staining was used. In addition, the number of immunostained cells in the plaques was determined by counting DAPI positive nuclei within the immunostained area. The number of the immunostained cells was expressed as the percentage of total plaque cells.

Table 11. Immunostaining protocols: Ab details are given in sections 2.3.1 – 2.3.2

Antigen	Antigen retrieval	Blocking	Primary Ab	Detection system
SMA	Citrate buffer, 20 min (100°C)	Blocking solution A (see section 2.4), 30 min	1:200, clone 1A4, 4°C, overnight (ON)	anti-mouse Cy3 1:300, 30 min
Mac-2	Citrate buffer, 20 min (100°C)	Blocking solution A (see section 2.4), 30 min	1:200, clone M3/38, 4°C, ON	anti-rat FITC, 1:100, 30 min
CD31	Citrate buffer, 20 min (100°C)	Blocking solution A (see section 2.4), 30 min	1:75, goat polyclonal, 4°C, ON	anti-goat-Cy3, 1:300, 30 min
Activated Caspase 3	Citrate buffer, 20 min (100°C)	Blocking solution A (see section 2.4), 30 min	1:400, rabbit polyclonal, 4°C, ON	anti-rabbit-FITC, 1:100, 30 min
Ki67	Citrate buffer, 20 min (100°C)	Blocking solution A (see section 2.4), 30 min	1:1500, rabbit polyclonal, 4°C, ON	anti-rabbit-FITC, 1:100, 30 min

2.4.1.3 Combined *in situ* PCR and immunostaining

In situ PCR is a method for the miRNAs detection in formalin fixed, or paraffin-embedded tissues. This method involves the extension of the labeled miRNA hybridized to a template with

100-nucleotide-long ultramer that contains the complementary sequence of the miRNA 3'-UTR. The extension method results in visualizing the miRNA signal in specific cells and tissues with using RT-PCR¹¹⁸.

PAXgene-fixed carotid artery sections (5 µm thick) were deparaffinized in absolute ethanol, 96% ethanol, 70% ethanol, each 5 min; and absolute ethanol for 5-8 sec. Sections were incubated with DNase (Roche, Basel, Switzerland) ON at 37°C. One-step reverse transcriptase *in situ* PCR was performed in MasterCycler equipped with an adjustable slide container using gene-specific PCR *in situ* primers (Sigma-Aldrich, Table 12), SuperScript One-Step RT-PCR with PlatinumTaq (Thermo Scientific) and digoxigenin-11-dUTPs (Roche)^{118, 119}. After washing with SSC buffer and blocking the nonspecific binding sites using nitroblue tetrazolium chloride (PerkinElmer, MA, USA) and biotin/avidin binding sites by using a blocking kit (Vector Laboratories), sections were incubated for 1 h at 37°C with a peroxidase-conjugated anti-digoxigenin sheep F'ab fragments (Fab fragments from sheep, 1:100 dilution; Roche). To visualize the probe a tyramide-based amplification system (TSA Plus Biotin, PerkinElmer) and Dylight 549-conjugated streptavidin (1:200) were used. Sections were subsequently stained with SMA antibody (1:200) followed by a FITC-conjugated secondary antibody (Jackson ImmunoResearch).

Table 12. *In situ* PCR primer sequences

Gene	Primer sequence	Company
Taq- <i>in situ</i> -miR-27a RT	5'-GTATTCGCATGGATACGACGCGGA GTCGTATCCAGTGCAGGGTCCGAG-3'	Sigma-Aldrich
Taq- <i>in situ</i> -miR-27a	5'-GCCCTTCACAGTGGCTAAGT-3'	Sigma-Aldrich

2.12 Laser-Capture Microdissection system (LCM)

Laser-Capture Microdissection system (LCM) is used to isolate specific cells of interest from microscopic regions of cells, tissue, and organisms. The area around the sample was cut by laser and collects it in the microfuge tube cap containing a buffer to adhere the tissue inside the cap (Figure 9).

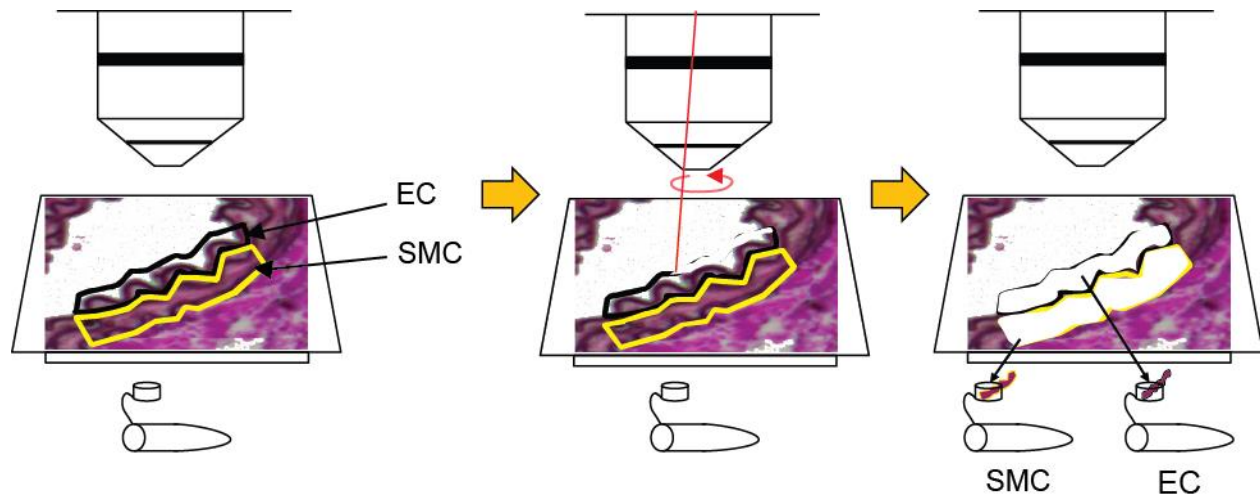


Figure 9. Laser-Capture Microdissection system (LCM). By using this method, the area around EC and SMC layers of an artery is cut by laser and collected in the microfuge tube cap containing a buffer.

PAXgen-fixed serial sections (4 μm thick) of the uninjured (right) carotid arteries from SM-*Dicer*^{+/+} and SM-*Dicer*^{-/-} mice (100-120 sections per mouse) were collected on RNase-free and UV-sterilized POL-membrane 0.9 μm FrameSlides (Leica Microsystem, Wetzlar, Germany) and dried at 40°C using Thermostat plus. All the steps were performed in the RNase free condition to preserve RNA integrity. To collect ECs and SMCs, the inner cell monolayer of the artery was considered as the layer which contains ECs and the subsequent layer considered as medial layer containing SMCs (Figure 9). ECs and SMCs were carefully collected in separate tubes contains 50 μl of TM1 buffer (PAXgene RNA isolation kit) using laser microdissection (Leica LMD7000) equipped with an inverted camera (Leica DFC365 FX) to visualize laser-dissected sections as digital images. Total RNA was isolated using the PAXgene RNA MinElute kit (Qiagen).

2.12.1 Human carotid lesion samples

Human atherosclerotic lesion samples were obtained during carotid endarterectomy (kindly provided by Dr. Jochen Grommes, European Vascular Center Aachen-Maastricht, Aachen, Germany) and fixed with 4% paraformaldehyde. Paraffin embedded tissues (see also section 2.11.1) were sectioned (5 μm thick) and incubated with primary antibodies for ARHGEF26 (1:20) and *in situ* PCR for miR-27a-3p combined with α -smooth muscle actin (SMA; 1:200) (Table 2, see also section 2.3.1). Fluorescently conjugated secondary antibodies (FITC, Cy3, Dylight488, or Dylight549) (Table 8, see also section 2.3.2) were used to detect the primary antibodies. The nuclei were counterstained with DAPI (Vector Laboratories). All participants

gave their written informed consent. The study was approved by the Ethics Committee of the Medical Faculty at RWTH Aachen University for the collection of human plaque.

2.13 Cell culture

Human aortic SMCs (HASMCs) (Promocell GmbH, Heidelberg, Germany; passage 2–5) at a density of 1.5×10^5 cells per well were seeded on 6-well plates (Sigma-Aldrich) and grown in smooth muscle cell growth medium 2 (Promocell), which contains growth factors, such as EGF, bFGF, and Insulin. Lipofectamine-2000 was used to transfect HASMCs for 48 h with the following nucleic acids: Locked nucleic acid (LNA)-modified miR-27a-3p inhibitors (CGGAACCTTAGCCACTGTGA) or nontargeting control oligonucleotides (GTGTAACACGTCTATACGCCCA) (50 nM each; Exiqon), miR-27a-3p mimics (UUCACAGUGGCUAAGUCCGC) or nontargeting control oligonucleotides (50 nM each; Thermo Scientific). *ARHGEF26* was silenced using a GapmeR (GTAATGCAAGGATAGA) or control GapmeR (AACACGTCTATACGC) (50 nM each; Exiqon). GapmeRs are single strand (16 nucleotides long) antisense oligonucleotides that were used to study the loss of functions of proteins, mRNA and lncRNAs. They catalyze degradation of complementary RNA targets using RNase H. GapmeRs have the LNA-containing flanking regions which confer nuclease resistance to the antisense oligo while at the same time it increases target binding affinity regardless of the GC content. The central DNA “gap” activates the cleavage of RNase H upon binding. *ARHGEF26* target site blocker (*ARHGEF26*-TSB) (TTCACAGGATTCAAATAG) or control-TSB (GCTCCCTTCAATCCAA) (50 nM miRCURY LNATM miRNA Target Site Blockers; Exiqon) were used to study the functional role of the targeting of *ARHGEF26* by miR-27a-3p. TSB is antisense oligonucleotides that bind to the miRNA target site of an mRNA to prevent miRNA from gaining access to that binding site. HASMCs were stimulated with IL-1 β (5 ng/ml, Thermo Scientific). Total RNA was isolated after 48 h using the RNeasy Mini Kit or mirVana Isolation Kit.

2.14 *In vitro* immunostaining

HASMCs (passage 2–5) were plated on glass coverslips (Neuvitro, Vancouver, WA, USA) in 24-well tissue culture plates (Sigma-Aldrich) for 24 h at a density of 3×10^4 cells per well. HASMCs were fixed in ice-cold methanol-acetone with a 50-50 mixture (v/v) for 5 min.

Immunostaining was performed using a primary antibody against Ki67 (1:1500). Cell nuclei were counterstained with DAPI. The primary antibody was detected with fluorescently labeled anti-rabbit, FITC-conjugated secondary antibodies (1:100, see also sections 2.3.1 and 2.3.2). Images were acquired using a Leica-DM6000B light microscope and the numbers of positive cells in 20 fields from each chamber were counted using ImageJ software.

2.15 MiRNA target identification and quantification system (MirTrap)

HASMCs were co-transfected with miR-27a-3p mimics (50 nM, Thermo Scientific) and the vector called pMirTrap using the transfection reagent XfectTM miRNA which contains Xfect Polymer (all from Clontech, aint-Germain-en-Laye, France). The pMirTrap vector expresses a DYKDDDDK-tagged GW182 protein that enables locking of the mRNA/miRNA complex in the miRISC. HASMCs were collected after 24 h, washed with ice-cold PBS, and incubated in lysis buffer (MirTrap System) supplemented with protease inhibitors (Complete Protease Inhibitor Cocktail Tablets; Roche). The input RNA was isolated from the cell lysates. Anti-DYKDDDDK-conjugated magnetic beads were washed two times with lysis wash buffer containing 0.1 unit/ μ l RNase inhibitor, 1 mM DTT, and protease inhibitors, and blocked for 3 h at 4°C with tRNA solution and BSA. Immunoprecipitation was performed by incubating anti-DYKDDDDK beads with the cell lysate for 2 h at 4°C and centrifugation at 1000 rpm. Total RNA was isolated after 48 h using the RNeasy Mini Kit. The efficiency of transfection was determined by transfection of miR-132 mimics, the empty pMirTrap vector or the pMirTrap positive control vector, which expresses an *Aequorea coerulescens* green fluorescein protein (AcGFP1) that contains the miR-132 target sequence. The fold enrichment of the target mRNAs in the GW182-immunoprecipitates was normalized to GAPDH according to the manufacturer's protocol.

2.16 Luciferase reporter assay

HEK293 cells cultured in complete DMEM (PAA Laboratories GmbH, Cölbe, Germany) were co-transfected with the Gaussia luciferase (GLuc) expressing pEZX-MT05 vector with or without the full length 3'-UTR of the human *ARHGEF26* (500 ng, GeneCopoeia, Vienna, Austria), and miR-27a-3p mimic or control mimic oligonucleotides using Lipofectamine 2000 for 48 h.

The miR-27a-3p binding site was mutated using the QuickChange site-directed mutagenesis kit (Agilent Technologies), *PfuTurbo* DNA polymerase (Thermo Scientific) and a PCR cycler, and using following primers (Sigma-Aldrich): 5'-

GCTAAAAAGCAACTATTTGAATCCGTGTAATTAATTTATAAG-3' and 5'-CTTATAAATTAATTACACGGATTCAAATAGTTGCTTTTTAGC-3'. The product was treated with *Dpn* I endonuclease to digest the parental DNA template and to select for mutation-containing synthesized DNA¹²⁰. The mutated pEZX-MT05 vector was transformed into XL10-Gold Ultra component cells (Agilent Technologies) and the plasmid was isolated using the EndoFree Plasmid Maxi Kit (Qiagen). The GLuc and secreted alkaline phosphatase (SEAP) activities were measured 48 h after the transfection using the Secrete Pair Dual Luminescent Assay (GeneCopoeia) and a microplate reader (Tecan Group Ltd., Männedorf, Switzerland). The signal from GLuc luminescence was normalized to that of SEAP.

2.17 Western blot analysis

HASMCs were transfected with *ARHGEF26*-TSBs or control-TSBs and were lysed after 48 h in RIPA buffer (Sigma-Aldrich) containing protease inhibitors. Cell lysates from each sample were separated on SDS-PAGE gels and transferred to nitrocellulose membranes (Amersham/GE Healthcare, Uppsala, Sweden). The membrane was incubated with primary antibodies against ARHGEF26 (1:150, at 4°C ON) and ACTB (1:1000, at room temperature for 1 h), after blocking nonspecific binding with 5% milk in TBS (see also section 2.4) for 1.5 h at room temperature. To visualize the antigens, a secondary HRP-conjugated antibody (1:1000, at room temperature for 1 h), an enhanced chemiluminescence detection system (ECL Advance, GE Healthcare Life Sciences) and an LAS 3000 Imager (Fuji Photo Film Co., Ltd., Tokyo, Japan) were used. The intensity of the bands was quantified by Multigauge software (Fuji Photo Film). ARHGEF26 band intensities were expressed as a percentage of the ACTB bands.

2.18 Statistics

Quantitative PCR miRNA array data are presented as means, and groups were compared using an unpaired, moderated two-tailed t-test (Statminer 4.2, Integromics). The data represent as means \pm s.e.m. More than 2 groups were compared using 1-way ANOVA followed by Newman-Keuls post-test and two groups were compared using paired, 2-tailed t-test (Prism 5.0; GraphPad and Genespring software). $P < 0.05$ was considered to be statistically significant.

3 Results

3.1 Expression pattern of *Dicer* and miRNAs during neointima formation

MiRNA microarray analysis was performed in carotid arteries of *Apoe*^{-/-} mice before (0 day) and 1, 7, 14, and 28 days after wire-induced injury to study the expression of 611 miRNAs.

Transcripts of 401 miRNAs were detectable, 211 miRNAs of which were differentially expressed during neointima formation ($P \leq 0.05$, $n = 3-4$ mice per group) (Supplemental Table 2 available on <http://link.springer.com/article/10.1007%2Fs00018-016-2349-0#SupplementaryMaterial>) (Figure 10).

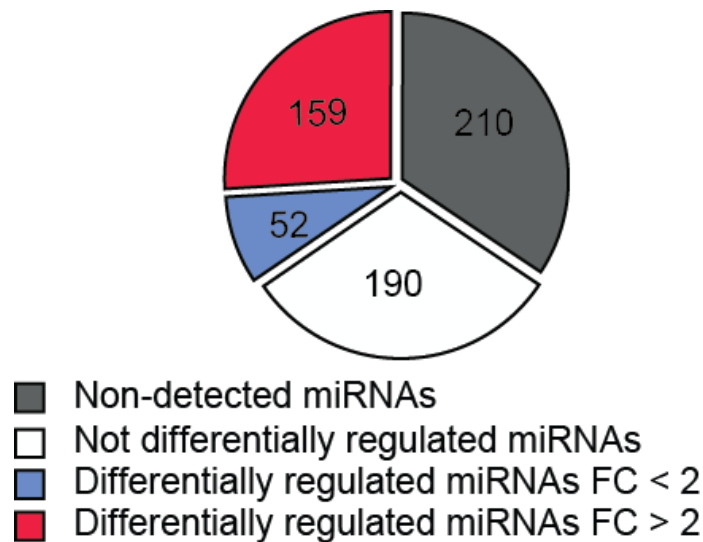


Figure 10. Differential expression of miRNAs during neointima formation. MiRNA microarray analysis was performed in carotid arteries from *Apoe*^{-/-} mice before (0 day) and 1, 7, 14, and 28 days after wire-induced injury ($n = 3-4$ mice per group). The number of differentially ($P \leq 0.05$) and not differentially regulated miRNAs among the detectable miRNAs is shown. FC, fold change.

The expression level of 159 significantly regulated miRNAs changed more than 2-fold. Notably, 21 of the 25 most significantly regulated miRNAs were upregulated at day 7 and 14 after injury (Figures 11A-E) and their expression time course differed mainly at day 1. The expression level of 8 miRNAs peaked at day 1 (e.g., miR-21-3p and miR-16-5p, Figure 11A), whereas the expression of 5 miRNAs increased stepwise between day 1 and 7 (e.g., miR-222-3p; Figure 11B). Moreover, the expression level of 2 miRNAs (e.g., miR-34a-5p; Figure 11C) and 4 miRNAs (e.g., miR-299-3p; Figure 11D) remained unchanged and transiently decreased at day 1, respectively. The expression of two miRNAs, miR-377-3p and miR-299-5p (Figure 11E), peaked

at day 7 and returned to the baseline levels thereafter. By contrast, the expression level of 4 out of 25 most significantly regulated miRNAs were downregulated at day 7, 14, and 28 after vascular injury (Figure 11F-H). However, miR-654-3p was upregulated at day 1 (Figure 11F) but along 3 other miRNAs, such as miR-29c-3p (Figure 11G) and miR-181c-5p (Figure 11H), were downregulated at day 7 and 14 after injury and returned to the baseline level at day 28.

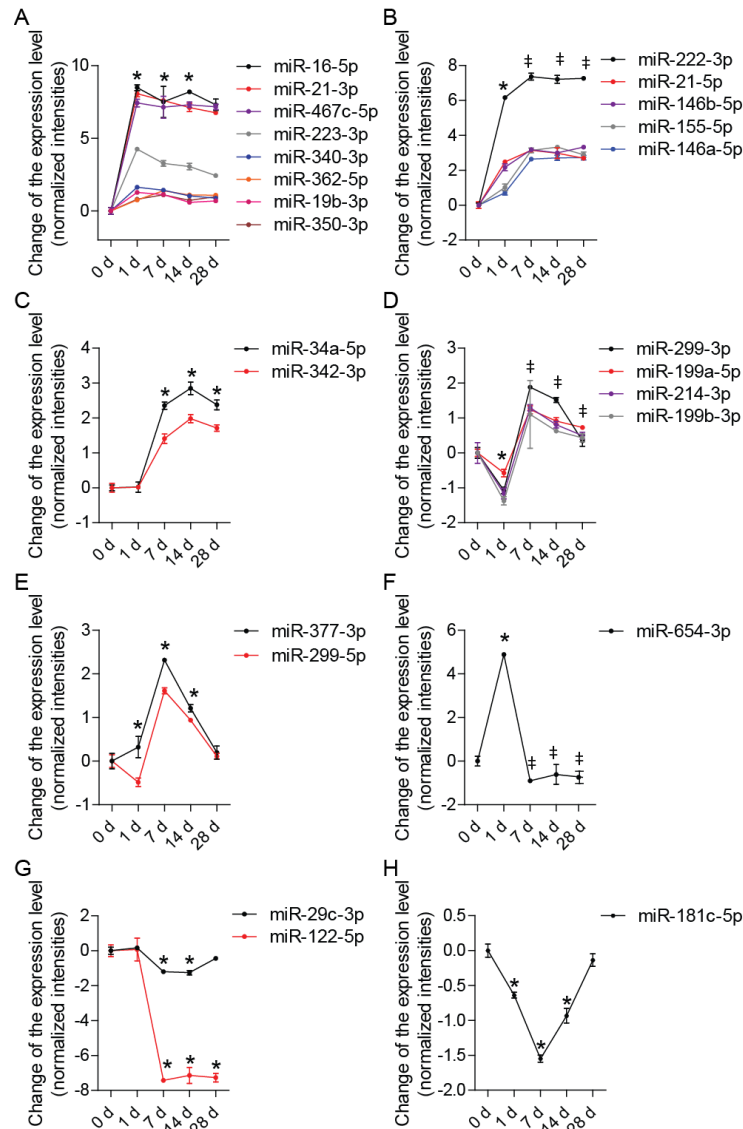


Figure 11. Differential expression of miRNAs in wire-injured carotid arteries from *Apoe*^{-/-} mice. MiRNA microarray analysis was performed in carotid arteries from *Apoe*^{-/-} mice before (0 day) and 1, 7, 14, and 28 days after wire-induced injury (n = 3–4 mice per group). (A–H) Expression patterns of the 25 most significantly regulated miRNAs (FC ≥ 2). (A, B) Upregulated miRNAs at day 1, 7, 14, and 28 after injury. (C, D) Upregulated miRNAs at day 7, 14, and 28 after injury. (E, F) Upregulated miRNAs with a peak at day 1, and 7 and returned to the baseline level thereafter. (G, H) Different expression patterns of miRNAs downregulated during neointima formation. Error bars represent ± s.e.m. **P* < 0.05 compared with 0 day; ‡*P* < 0.05 compared with 1 day.

To study the regulation of *Dicer* expression during neointima formation, carotid injury was induced in HFD-diet fed *Apoe*^{-/-} mice. Expression of *Dicer* in the carotid arteries was quantified at different time points by qRT-PCR. Notably, the expression of *Dicer* mRNA was significantly up-regulated in carotid arteries at day 7 and day 14 after injury compared with uninjured arteries (Figure 12). These data suggest that *Dicer* may contribute to the process of neointima formation.

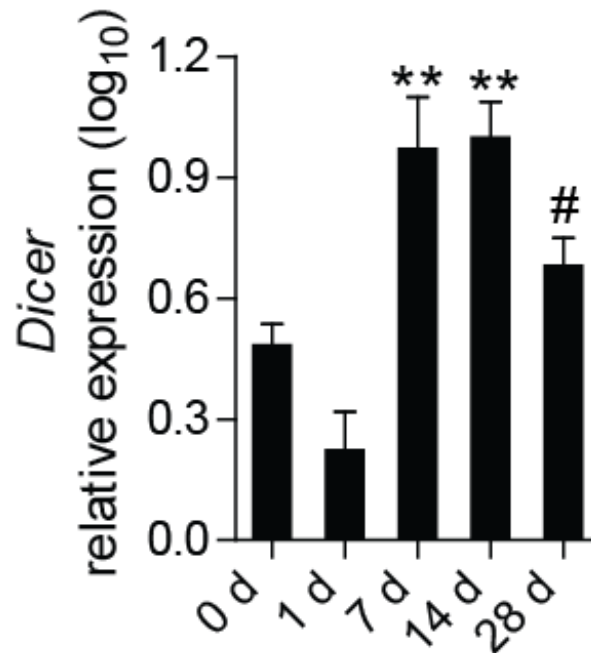


Figure 12. *Dicer* mRNA expression increased during neointima formation. Quantitation of *Dicer* mRNA expression in uninjured (0 day) and injured carotid arteries (1, 7, 14, and 28 days after vascular injury) from *Apoe*^{-/-} mice by qRT-PCR (n = 3–4 mice per group). All data are represented as the means ± s.e.m. of the indicated number (n) of repeats. ***P* < 0.01 compared to 0 day and 1 day and #*P* < 0.05 compared to 1 day. *P* values were obtained by one-way analysis of variance (ANOVA).

3.2 The effect of *Dicer* knockout in SMCs on neointima formation

3.2.1 SMC-specific deletion of *Dicer* in *Apoe*^{-/-} mice

A tamoxifen-inducible transgenic mouse model was used to knockout *Dicer* in SMCs. To study whether tamoxifen injection indeed resulted in SMC-specific *Dicer* knockout in SM-*Dicer*^{-/-} mice *Dicer* expression was quantified in carotid arteries (see section 2.6). Compared with SM-*Dicer*^{+/+} control mice, the expression of *Dicer* was significantly reduced in injured carotid arteries of tamoxifen-injected SM-*Dicer*^{-/-} mice 14 days after injury (Figure 13A).

To investigate whether the knockout of *Dicer* is SMC specific, *Dicer* mRNA expression was quantified in laser-microdissected SMCs and ECs isolated from the uninjured carotid arteries of

SM-*Dicer*^{-/-} and SM-*Dicer*^{+/+} mice 35 days after tamoxifen injection. Whereas *Dicer* expression was similar between SMCs and ECs from SM-*Dicer*^{+/+} mice, *Dicer* mRNA levels were reduced in SMCs compared with ECs in SM-*Dicer*^{-/-} mice (Figure 13B). These data indicate that *Dicer* expression is specifically reduced in vascular SMCs.

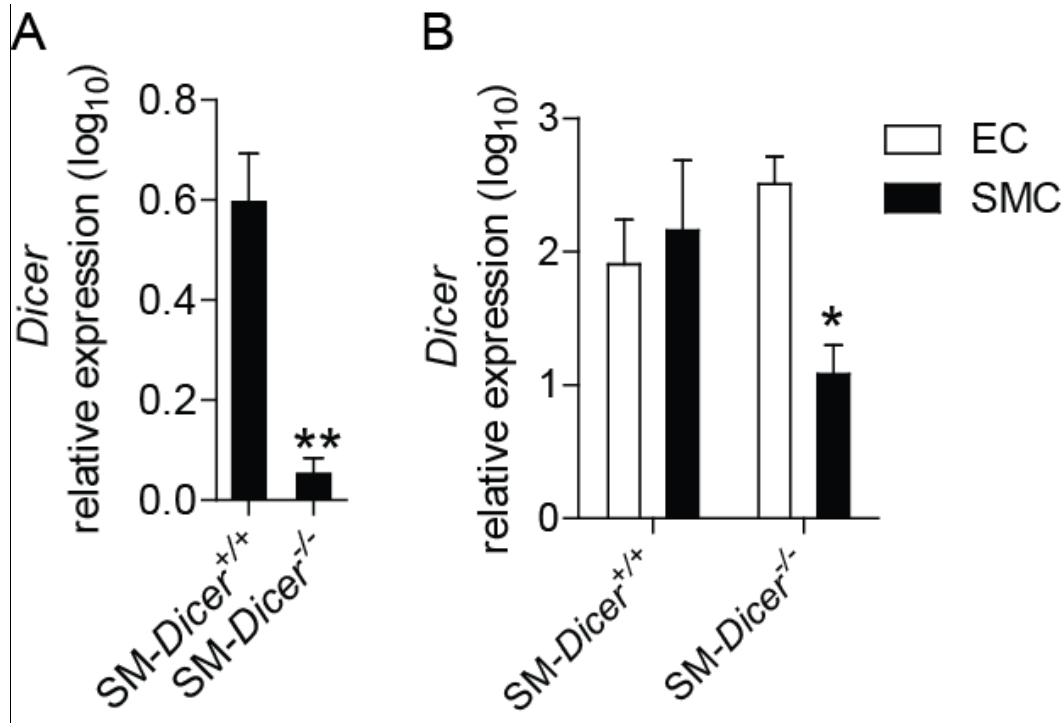


Figure 13. *Dicer* mRNA expression in SM-*Dicer*^{-/-} and SM-*Dicer*^{+/+} mice. (A) Quantification of *Dicer* mRNA expression in injured carotid arteries from SM-*Dicer*^{-/-} mice and SM-*Dicer*^{+/+} mice by qRT-PCR (n = 4 mice per group). (B) Quantification of *Dicer* mRNA expression in SMCs and ECs of uninjured carotid arteries from SM-*Dicer*^{-/-} mice and SM-*Dicer*^{+/+} mice by qRT-PCR (n = 2-3 mice per group). All data are represented as the means \pm s.e.m. of the indicated number (n) of repeats. **P* < 0.05, ***P* < 0.01 compared with SM-*Dicer*^{+/+} mice. *P* values were obtained by Student's *t* test or one-way analysis of variance (ANOVA).

3.2.1 Effect of SMC-specific-*Dicer* knockout on neointima formation

To study the effect of *Dicer* in SMCs on neointimal growth, wire-induced vascular injury was performed in SM-*Dicer*^{-/-} and SM-*Dicer*^{+/+} mice. The left carotid arteries of SM-*Dicer*^{-/-} and SM-*Dicer*^{+/+} mice were harvested 14 days and 28 days after injury. Planimetry of the neointima in histological sections of the carotid arteries showed that loss of *Dicer* expression in SMCs enhanced neointima formation in the carotid artery at 14 days and 28 days after injury, indicating that *Dicer*-dependent miRNA biogenesis limits neointima formation (Figure 14A-C).

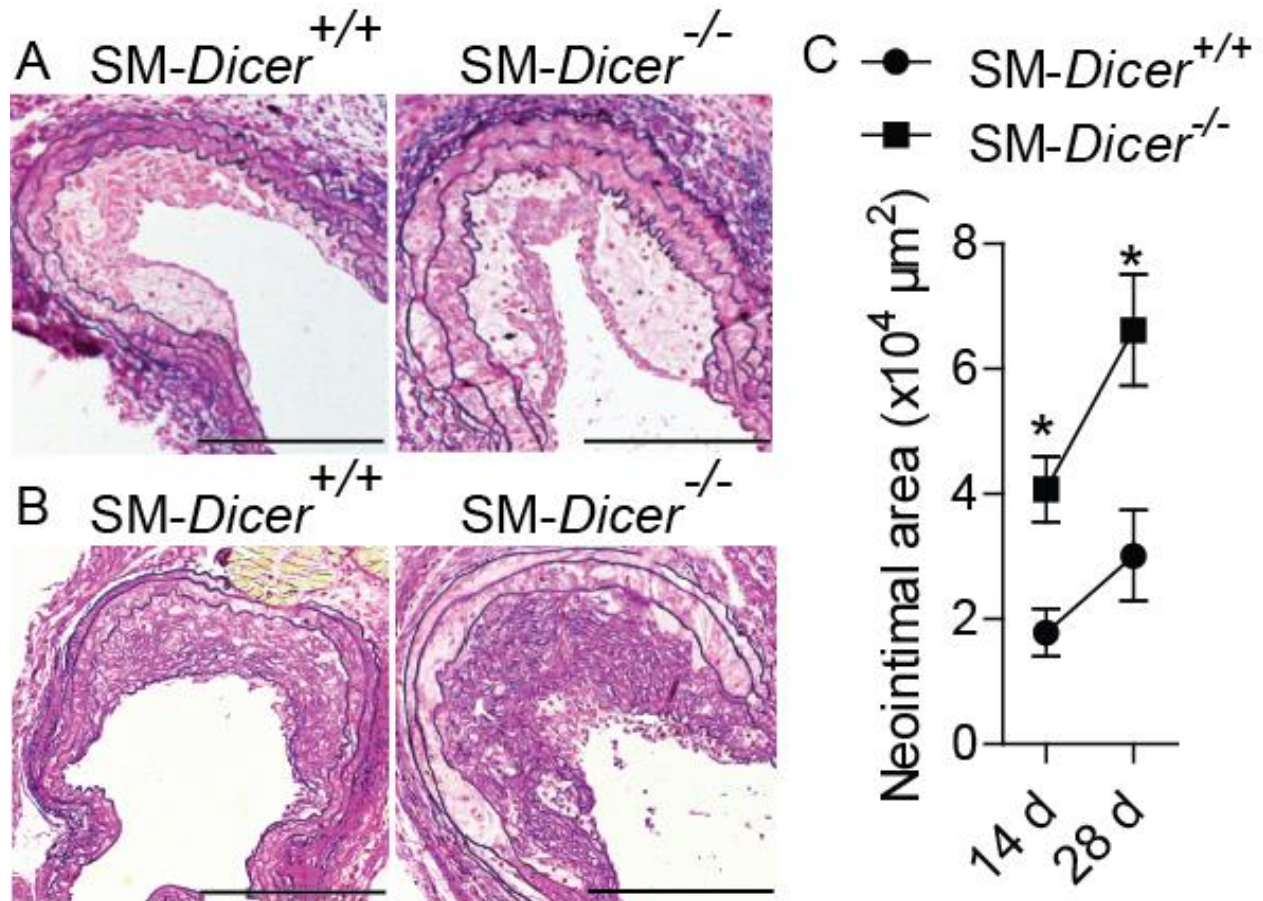


Figure 14. *Dicer* deletion in SMCs increased neointima formation. Lesion areas were quantified in carotid sections of SM-*Dicer*^{-/-} mice and SM-*Dicer*^{+/+} mice at 14 days (A) and 28 days (B) after vascular injury stained with elastic van Gieson stain (representative images are shown). (C) Quantification of neointima formation in injured carotid arteries from SM-*Dicer*^{-/-} mice and SM-*Dicer*^{+/+} mice (n = 5–7 mice per group). Scale bars, 200 μm. All data are represented as the means ± s.e.m. of the indicated number (n) of repeats. **P* < 0.05 compared with SM-*Dicer*^{+/+} mice. *P* values were obtained by Student's *t* test.

To investigate the effect of SMC-specific *Dicer* deletion on the cellular composition of the neointima, the neointimal SMC content was studied in carotid arteries from SM-*Dicer*^{-/-} mice and SM-*Dicer*^{+/+} mice 14 and 28 days after vascular injury by SMA immunostaining (Figure 15A-B).

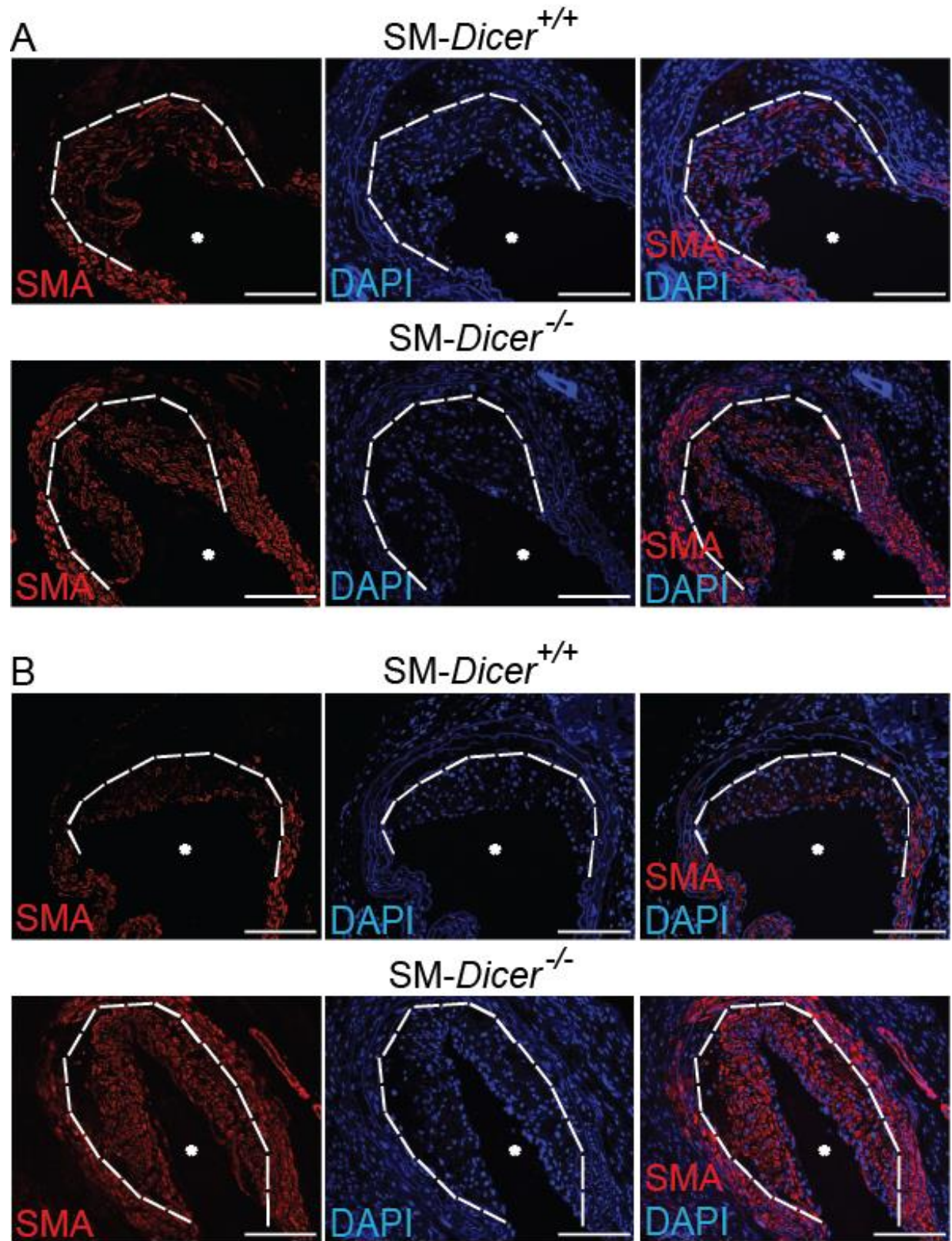


Figure 15. Effect of SMC-specific *Dicer* deletion on neointimal SMC accumulation. Neointimal SMC content determined by SMA immunostaining at 14 days (A) and 28 days (B) after vascular injury (representative images are shown). Nuclei were counterstained with DAPI. The dash lines delineate the neointimal area. The asterisks indicate the lumen area. Scale bars, 100 μ m.

In *SM-Dicer*^{-/-} mice, the neointimal SMA⁺ cell content was increased at 14 and 28 days after injury compared with *SM-Dicer*^{+/+} mice (Figure 16). These data indicate that increased neointima formation in *SM-Dicer*^{-/-} mice is a consequence of enhanced SMC accumulation.

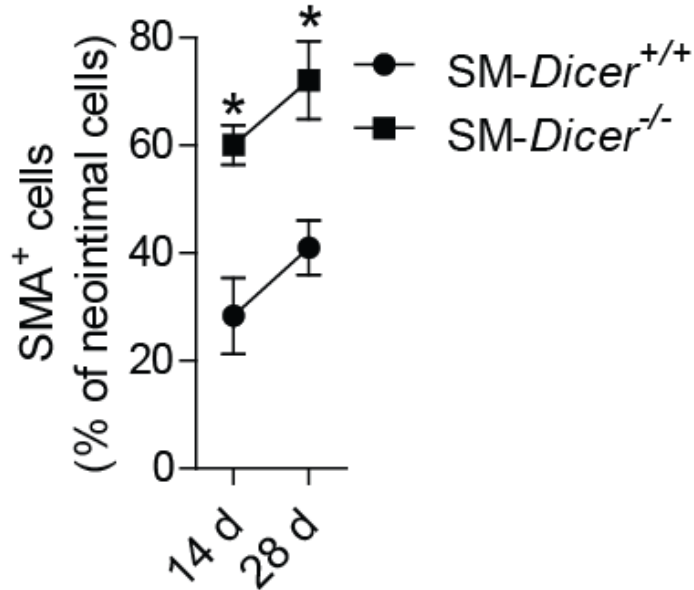


Figure 16. Effect of SMC-specific *Dicer* deletion on neointimal SMC content. Neointimal SMC content determined by SMA immunostaining at 14 days and 28 days after vascular injury (n = 5–7 mice per group). All data are represented as the means ± s.e.m. of the indicated number (n) of repeats. **P* < 0.05 compared with *SM-Dicer*^{+/+} mice. *P* values were obtained by Student's *t* test.

To study whether the effect on the neointimal area was associated with an increased neointimal macrophage content, Mac2 immunostaining was performed in carotid arteries of *SM-Dicer*^{-/-} and *SM-Dicer*^{+/+} mice 14 and 28 days after vascular injury (Figure 17).

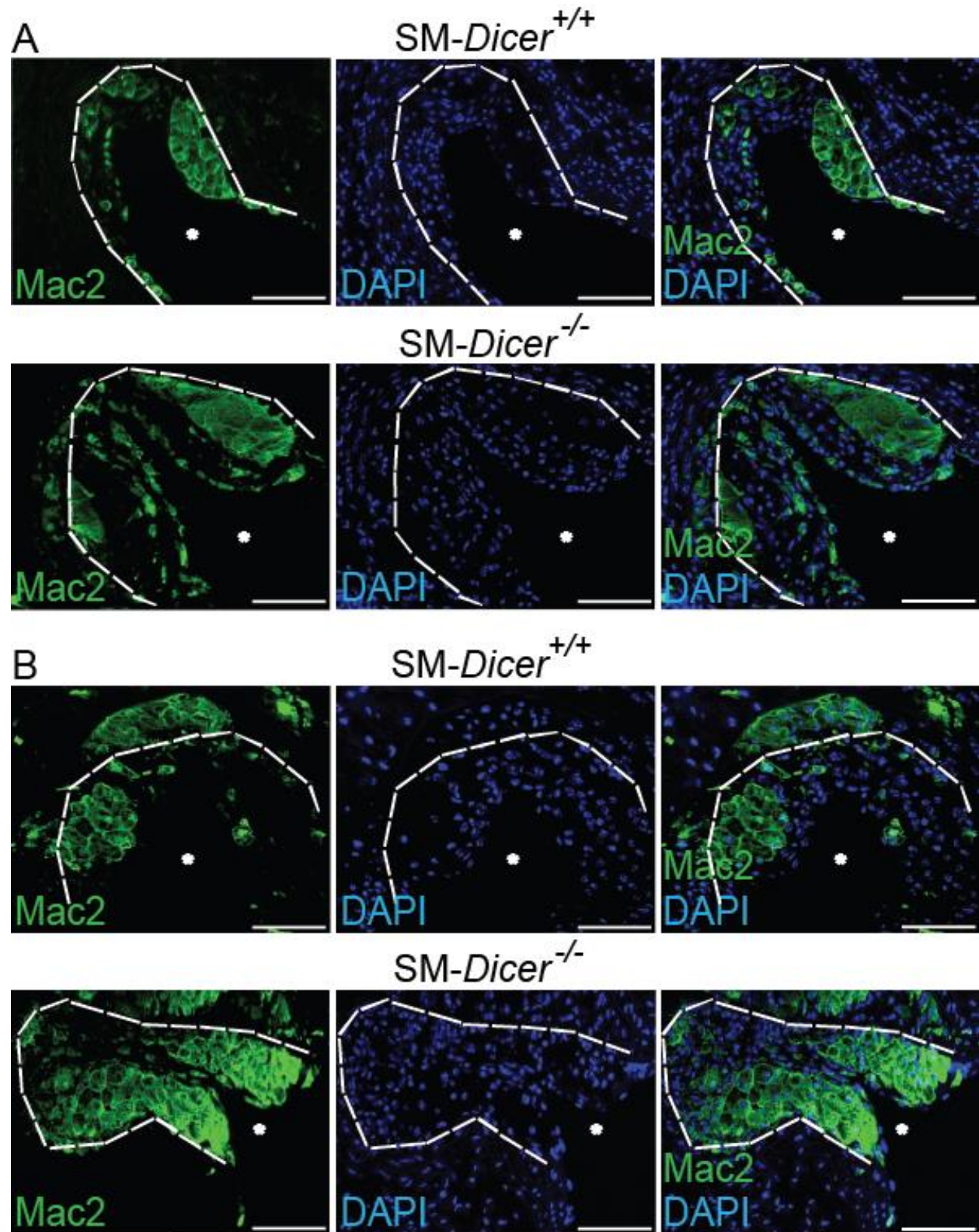


Figure 17. Effect of SMC-specific *Dicer* deletion on lesional macrophages. Neointimal macrophage content after 14 days (**A**) and 28 days (**B**) of vascular injury determined by Mac2 immunostaining (representative images are shown). Nuclei were counterstained with DAPI. The dash lines delineate the neointimal area. The asterisks indicate the lumen area. Scale bars, 100 μ m.

The analysis of the lesional accumulation of Mac2 positive macrophages in the wire injured carotid arteries revealed that the neointimal macrophage content did not differ between both groups (Figure 18). These data indicate that neointimal macrophage accumulation does not contribute to increased neointima formation in SM-*Dicer*^{-/-} mice.

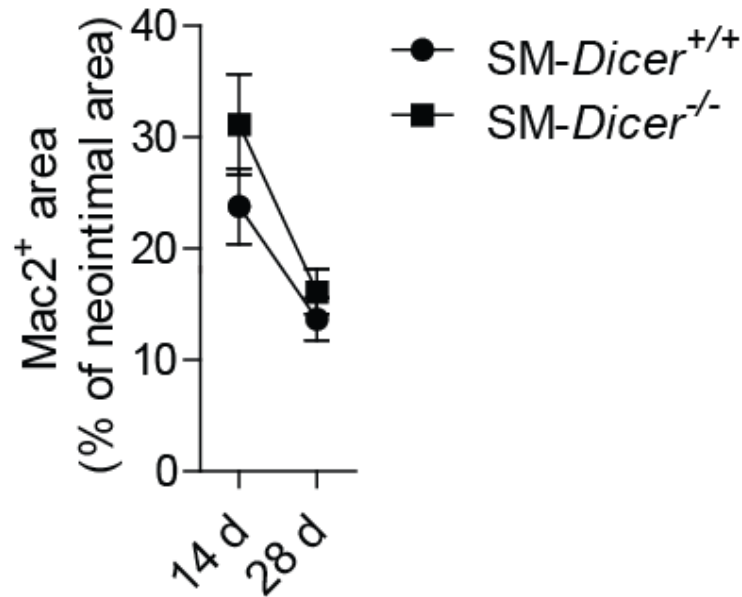


Figure 18. Effect of SMC-specific *Dicer* deletion on the neointimal macrophage content. Neointimal macrophage content after 14 days and 28 days of vascular injury determined by Mac2 immunostaining (n = 5–7 mice per group). All data are represented as the means ± s.e.m. of the indicated number (n) of repeats. *P* values were obtained by Student's *t* test.

3.2.2 Effect of *Dicer* deficiency on neointimal SMC proliferation and apoptosis

To investigate whether SMC proliferation contributes to increased neointima formation in SM-*Dicer*^{-/-} mice, double immunostaining of Ki67 and SMA was performed in carotid arteries from SM-*Dicer*^{-/-} mice and SM-*Dicer*^{+/+} mice 14 and 28 days after vascular injury (Figure 19).

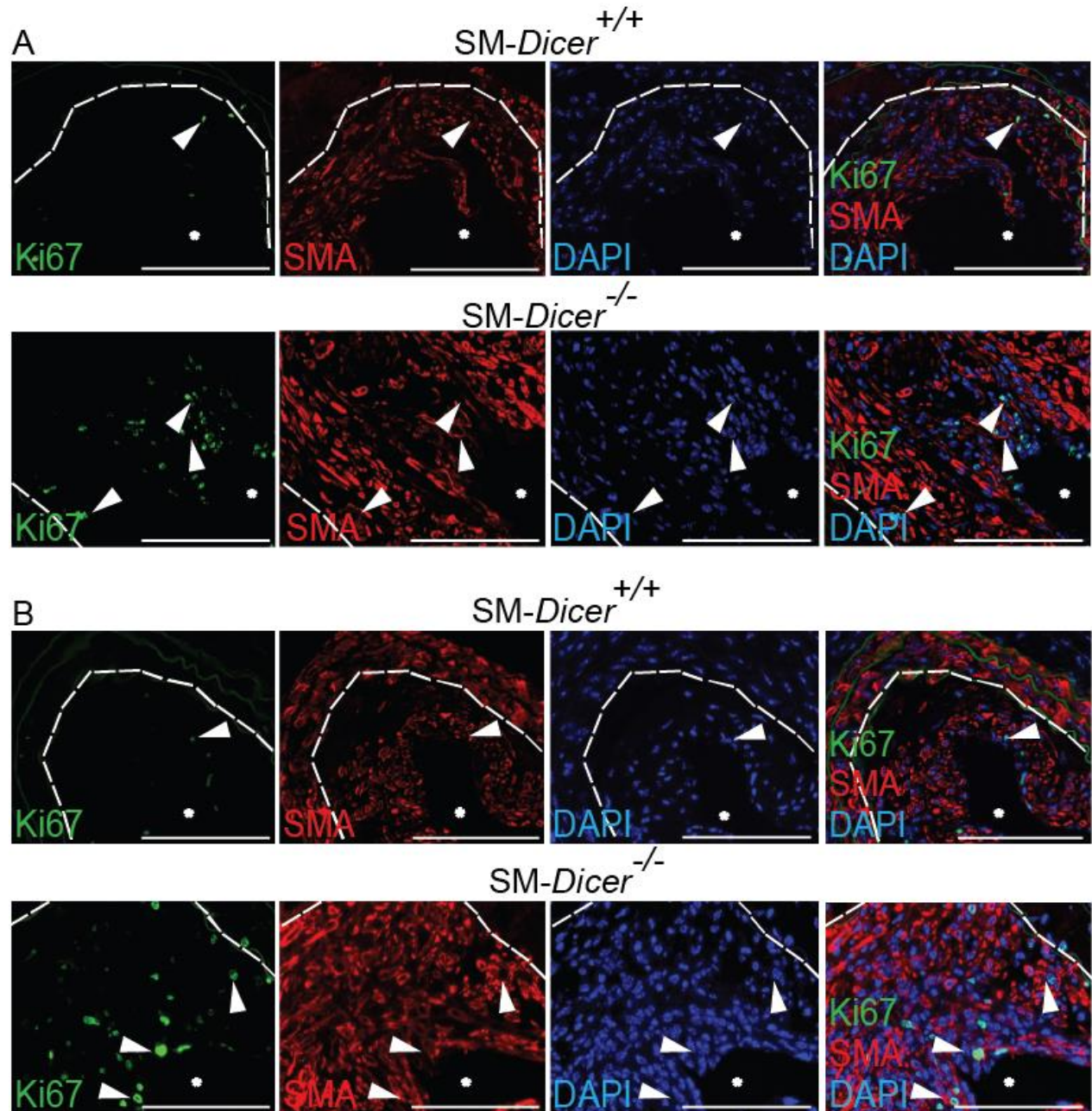


Figure 19. Effect of SMC-specific *Dicer* deletion on SMC proliferation. Neointimal SMC proliferation 14 days (A) and 28 days (B) after vascular injury determined by double immunostaining of SMA and Ki67 (representative images are shown). Nuclei were counterstained with DAPI. The dash lines delineate the neointimal area. The arrow heads indicate Ki67⁺ SMA⁺ cells. The asterisks indicate the lumen. Scale bars, 100 μm.

The number of Ki67⁺ neointimal SMCs was higher in *SM-Dicer*^{-/-} than in *SM-Dicer*^{+/+} mice at 14 and 28 days after vascular injury (Figure 20), indicating that reduced SMC proliferation limits neointima formation in *SM-Dicer*^{+/+} mice.

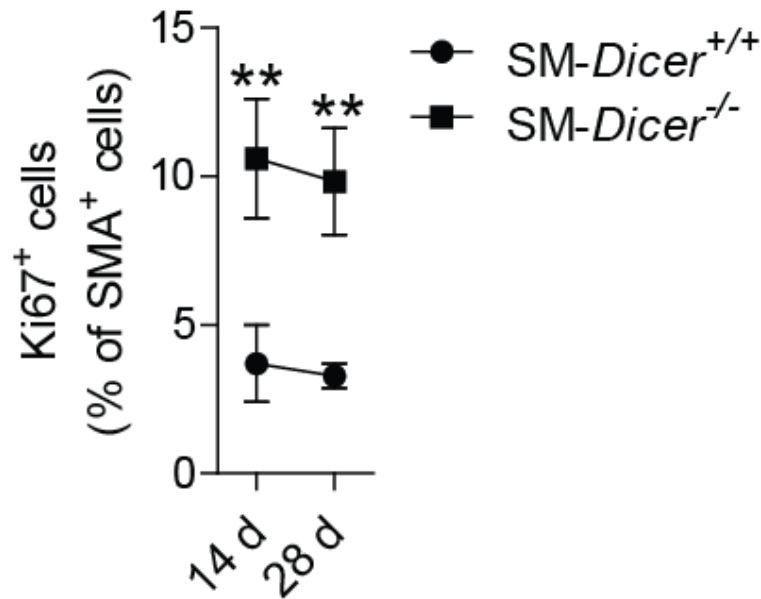


Figure 20. Effect of SMC-specific *Dicer* deletion on proliferation of neointimal SMC. Neointimal SMC proliferation after 14 days and 28 days of vascular injury determined by double immunostaining for Ki67 and SMA (n = 5–7 mice per group). All data are represented as the means \pm s.e.m. of the indicated number (n) of repeats. ** $P < 0.01$ compared with SM-Dicer^{+/+} mice. P values were obtained by Student's t test.

SMCs apoptosis induced by vascular injury triggers the healing response that may lead to neointimal hyperplasia¹²¹. To test whether *Dicer* affects SMC apoptosis during neointima formation immunostaining of activated caspase 3 and SMA was performed in carotid arteries from SM-Dicer^{-/-} mice and SM-Dicer^{+/+} mice 14 and 28 days after vascular injury (Figure 21A). The percentage of apoptotic SMCs in the neointima was not different between SM-Dicer^{-/-} mice and SM-Dicer^{+/+} mice (Figure 21B). These data suggest that SMC-specific *Dicer* deletion does not alter SMC apoptosis following vascular injury.

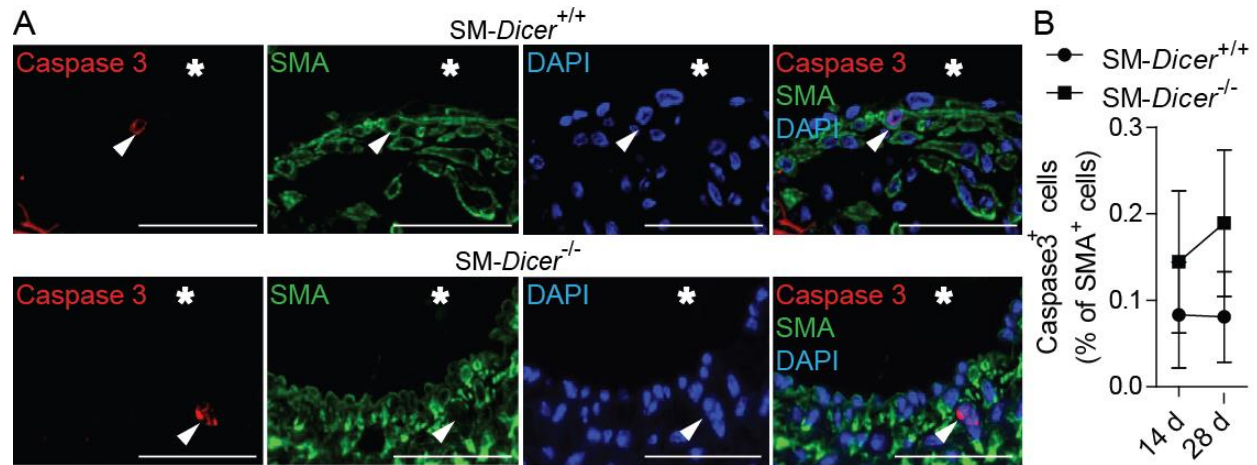
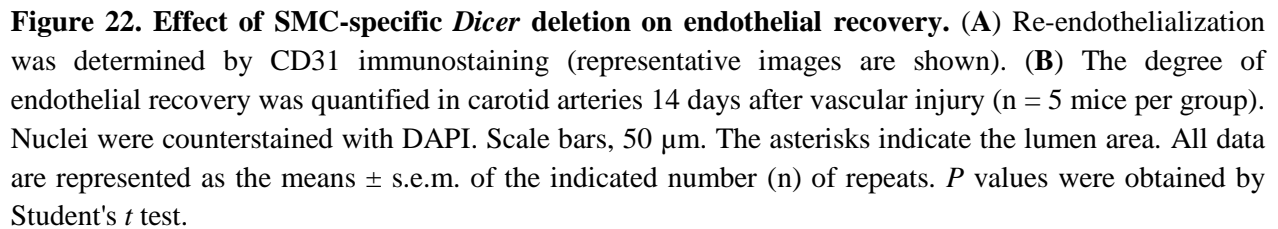


Figure 21. Effect of SMC-specific *Dicer* deletion on SMC apoptosis. (A) Neointimal SMC apoptosis was detected using double immunostaining of activated caspase 3 and SMA (representative images are shown). (B) SMC apoptosis was quantified at 14 and 28 days after injury ($n = 5-7$ mice per group). Nuclei were counterstained with DAPI. Representative overlays of caspase 3 and DAPI positive SMA immunostainings are shown. Scale bars, 100 μm . The asterisks indicate the lumen area. The arrowheads indicate caspase 3⁺/SMA⁺ cells. All data are represented as the means \pm s.e.m. of the indicated number (n) of repeats. P values were obtained by Student's t test.

3.2.3 **Effect of SM-*Dicer* deficiency on endothelial recovery**

Re-endothelialization after arterial injury is associated with the termination of SMC proliferation and neointimal growth, and reduces thrombosis²¹. To study whether SMC-specific *Dicer* knockout affects endothelial recovery, the endothelial luminal lining was studied in SM-*Dicer*^{+/+} and SM-*Dicer*^{-/-} mice at 14 days after vascular injury by CD31 immunostaining. Endothelial-specific staining of CD31 showed that the absence of *Dicer* in SMCs did not affect the endothelial coverage at 14 days after vascular injury (Figure 22A-B). These data suggest that changes in re-endothelialization do not contribute to neointima formation in SM-*Dicer*^{-/-} mice.



3.2.4 Fully differentiated SMC deletion inhibits SMC differentiation

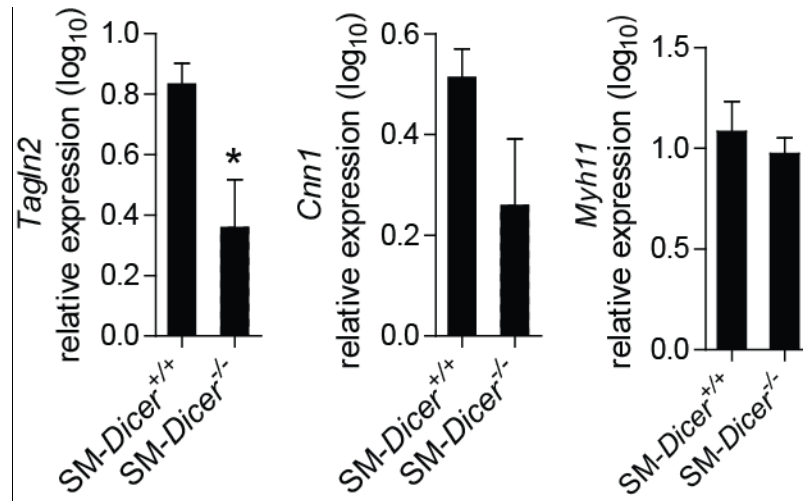


Figure 23. Effect of *Dicer* deletion on SMC markers expression. The mRNA expression levels of the SMC contractile markers *Tagln2*, *Cnn1*, and *Myh11* were determined 28 days after vascular injury by qPCR (n = 7 mice per group). The data are represented as the means \pm s.e.m. of the indicated number (n) of repeats. * $P < 0.05$. P values were obtained by Student's t test.

3.3 Effect of SM-*Dicer* deficiency on the miRNA expression profiles

To determine miRNAs regulated by *Dicer* in SMCs during neointima formation, the miRNA expression profile in carotid arteries was compared between SM-*Dicer*^{-/-} mice and SM-*Dicer*^{+/+} mice 14 days after injury by qPCR array analysis. Among 678 miRNAs studied, 497 miRNAs were detected of which 92 of them were significantly downregulated after deletion of *Dicer* in SMC (Supplemental Table 3 available on <http://link.springer.com/article/10.1007%2Fs00018-016-2349-0#SupplementaryMaterial>). Notably, no miRNAs were upregulated after SMC-specific *Dicer* deletion. The expression levels of miR-147-3p, miR-143-3p, miR-100-5p, miR-99a-5p, and miR-27a-3p were most significantly reduced among the 92 downregulated miRNAs in SM-*Dicer*^{-/-} mice compared to SM-*Dicer*^{+/+} mice (Figure 24 and Table 13). SMC-specific miRNAs, such as miR-143-3p and miR-145-5p, were among the significantly downregulated miRNAs after SMC-specific *Dicer* deletion, whereas the expression of endothelial miR-126-5p was not different between SM-*Dicer*^{-/-} mice and SM-*Dicer*^{+/+} mice (Figure 24). Among the miRNAs downregulated in SM-*Dicer*^{-/-} mice, 31 miRNAs, including miR-143-3p, miR-9-5p, miR-27a-3p, and miR-27b-3p, were previously reported in other studies to inhibit SMC proliferation *in vitro*^{95, 103} (Table 13).

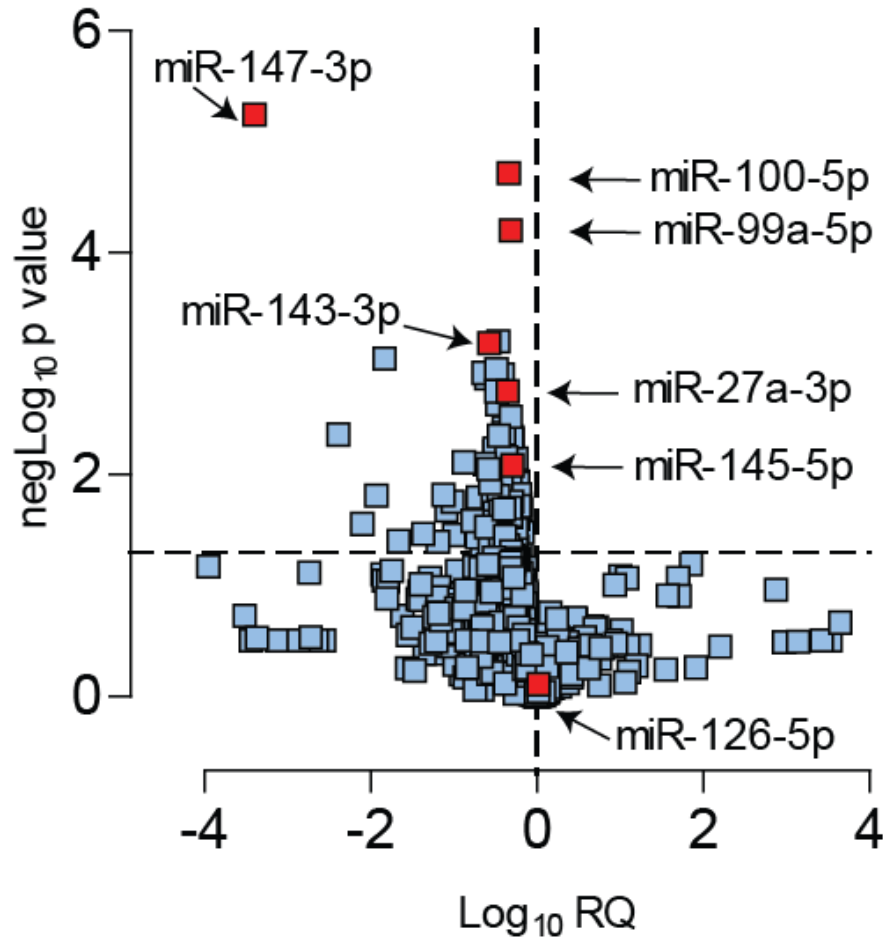


Figure 24. MiRNA expression profile in injured arteries following SMC-specific *Dicer* deletion. Expression profile of miRNAs in carotid lesions from SM-*Dicer*^{-/-} mice compared to that from SM-*Dicer*^{+/+} mice 14 days after vascular injury (n = 3-4 mice per group). X axis represents fold change. Y axis represents *P* value. Left upper quadrant: significantly downregulated miRNAs. Right upper quadrant: significantly upregulated miRNAs. Left lower quadrant: downregulated miRNAs. Right lower quadrant: upregulated miRNAs. RQ, relative quantification.

Table 13. MiRNAs downregulated in the carotid arteries from SM-*Dicer*^{-/-} mice compared with SM-*Dicer*^{+/+} mice 14 days after vascular injury (n = 3-4 mice per group).

miRNA	Log ₁₀ RQ	negLog ₁₀ <i>P</i> value	Effect on SMC proliferation	References
miR-147-3p	-3.39	5.24	∅	103
miR-100-5p	-0.34	4.02	∅	103
miR-99a-5p	-0.31	3.80	↓	103
miR-652-3p	-0.46	3.20		
miR-143-3p	-0.57	3.18	↓	95

miR-669m-3p	-1.83	3.04		
miR-301a-3p	-0.48	2.95	Ø	95, 103
miR-224-5p	-0.64	2.92		
miR-210-3p	-0.41	2.90	Ø	103
miR-185-5p	-0.60	2.87		
miR-9-5p	-0.48	2.75	↓	103
miR-27a-3p	-0.35	2.75	↓	103
miR-301b-3p	-0.47	2.63		
miR-497-5p	-0.31	2.52		
miR-27b-3p	-0.39	2.42	↓	103
miR-365-3p	-0.39	2.37	↓	122
miR-154-5p	-2.38	2.36		
let-7a-3p	-0.45	2.35		
miR-152-5p	-0.29	2.34		
let-7a-5p	-0.29	2.32		
miR-145-5p	-0.50	2.23	↓	98, 122
miR-140-5p	-0.50	2.21	↓	98, 103
miR-28-5p	-0.36	2.15	↓	103
let-7g-5p	-0.25	2.14	Ø	103
miR-1930-5p	-0.87	2.11		
let-7d-5p	-0.29	2.08		
let-7i-5p	-0.31	2.06		
miR-696-3p	-0.57	2.05		
miR-132-3p	-0.40	2.03	↓	103, 123
miR-148a-3p	-0.32	1.94		
let-7e-5p	-0.22	1.93		
miR-1198-5p	-0.56	1.92		

miR-127-3p	-0.22	1.92	↓	103, 123
miR-376a-3p	-0.42	1.91	↓	103
miR-331-3p	-0.20	1.82	Ø	103
miR-130b-5p	-1.121	1.82		
miR-467a-5p	-0.53	1.81		
miR-130a-3p	-0.25	1.81		
miR-207-3p	-1.93	1.81		
miR-140-3p	-0.46	1.80	↓	103
miR-125a-3p	-0.71	1.79	Ø	103
miR-29b-3p	-0.32	1.76		
miR-26a-5p	-0.22	1.76	↑	124
miR-547-3p	-0.29	1.75		
miR-24-3p	-0.21	1.73	↓	124, 125
miR-195-5p	-0.19	1.73	↓	125, 126
miR-30b-5p	-0.20	1.73	Ø	103, 126
miR-376c-3p	-0.20	1.71		
miR-139-5p	-0.40	1.70		
miR-30e-3p	-0.32	1.70	Ø	103
miR-26b-5p	-0.19	1.69	Ø	103
miR-24-5p	-0.39	1.69		
miR-30c-5p	-0.24	1.68		
miR-187-3p	-1.08	1.68	↓	103
miR-1839-3p	-0.43	1.67		
miR-206-3p	-0.50	1.65	↓	103
miR-30a-3p	-0.30	1.63	↓	103
miR-192-5p	-0.21	1.63	Ø	103
miR-99b-5p	-0.30	1.62	↓	103

miR-29c-3p	-0.22	1.60	↓	103
miR-103-3p	-0.36	1.60		
miR-125b-5p	-0.20	1.59	Ø	103
miR-15a-3p	-0.77	1.58		
miR-27b-5p	-0.57	1.57		
miR-130b-3p	-0.41	1.57	Ø	103
miR-297a-5p	-2.10	1.55		
miR-23b-3p	-0.22	1.55	↓	127
miR-1949-3p	-0.60	1.53		
miR-423-3p	-0.42	1.52		
miR-484-3p	-0.24	1.51	Ø	103, 127
miR-495-3p	-0.43	1.49		
miR-29a-3p	-0.17	1.47	↓	125
miR-99b-3p	-1.36	1.47	↓	103, 125
miR-148b-3p	-0.32	1.47	↓	103
miR-181c-5p	-0.27	1.46		
miR-431-5p	-0.99	1.46	↓	103
miR-193b-3p	-0.48	1.45		
miR-1839-5p	-0.43	1.45		
miR-485-3p	-0.38	1.44	↓	103
miR-30d-5p	-0.33	1.44	Ø	103
miR-29a-5p	-0.72	1.43		
miR-221-3p	-0.37	1.42	↓	103
miR-503-5p	-1.66	1.40	Ø	103
let-7f-5p	-0.30	1.40	Ø	103
miR-509-3p	-1.18	1.39		
miR-125a-5p	-0.19	1.36	Ø	103

miR-421-3p	-0.34	1.36	Ø	103
miR-30e-5p	-0.23	1.35	↓	103
miR-425-3p	-0.56	1.33	↓	103
miR-93-3p	-0.24	1.32	↓	103
miR-455-5p	-0.40	1.31	↓	103
miR-872-3p	-0.30	1.30		

3.4 Effect of SM-*Dicer* deficiency on the mRNA expression profiles

To determine mRNAs regulated by *Dicer* in SMCs during neointima formation, global gene expression analysis in carotid arteries from SM-*Dicer*^{-/-} mice and SM-*Dicer*^{+/+} mice 14 days after injury was performed using microarrays. Genome-wide mRNA expression analysis showed that 484 annotated genes were upregulated and 294 genes were downregulated in the injured carotid arteries from SM-*Dicer*^{-/-} mice (fold change ≥ 1.5 , $p \leq 0.05$, $n = 3$ mice per group; Figure 25A) (Supplementary Table 4 available on <http://link.springer.com/article/10.1007%2Fs00018-016-2349-0#SupplementaryMaterial>). *Dicer* deficiency in SMCs increased the expression level of *Igfbp3*, *Chst1*, *Sh3bgrl2*, *Arhgef26*, *Sh2d5*, and *Dll4* as determined by qRT-PCR (Figure 25B). To study the effect of SMC miRNAs on signaling pathways during neointima formation, differentially regulated genes in SM-*Dicer*^{-/-} mice compared with SM-*Dicer*^{+/+} mice were analyzed by IPA software to identify upstream regulators. This analysis indicated activation of pro-proliferative signaling pathways like AKT, ERK1/2, PDGF-BB, and EGF, and of pro-inflammatory signaling through NF- κ B and IL-1 in SM-*Dicer*^{-/-} mice (Figure 25C). Moreover, inhibition of anti-proliferative upstream regulators such as retinoblastom-protein 1 and cyclin-dependent kinase 1 was found after *Dicer* deficiency. These data indicate that concomitant activation of inflammatory and growth factor signaling pathways causes neointimal SMC proliferation after *Dicer* deletion in SMCs.

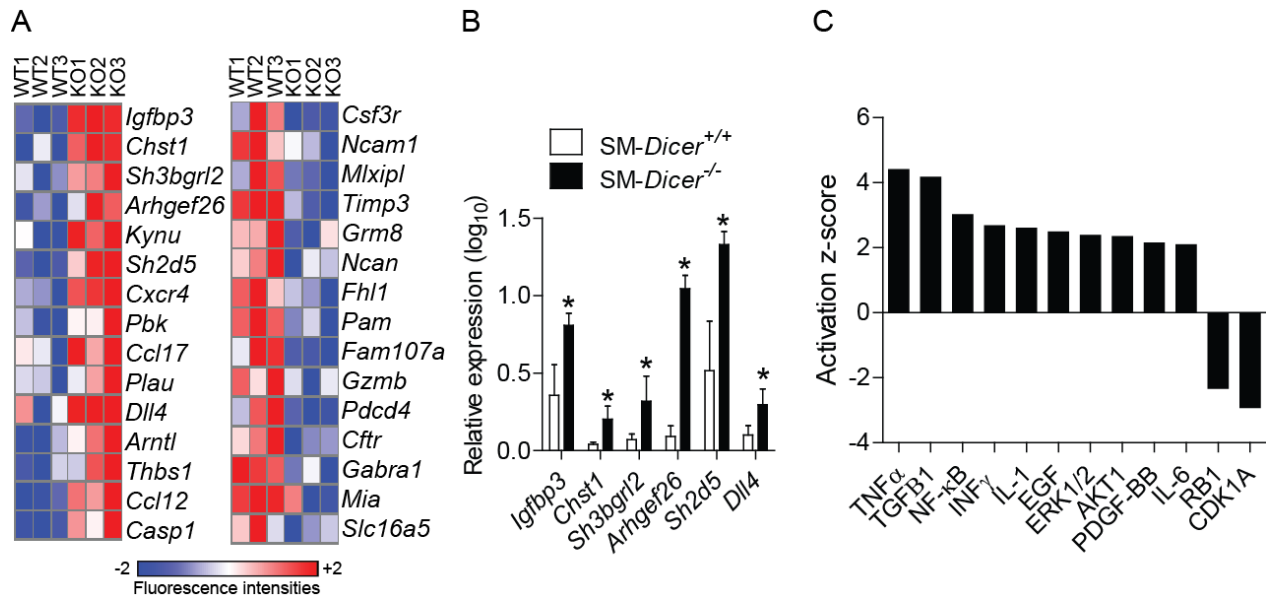


Figure 25. mRNA expression profile in injured arteries following *Dicer* deletion in SMCs. (A) Heat map of a subset of differentially expressed mRNAs in the injured carotid artery of SM-*Dicer*^{-/-} mice compared with SM-*Dicer*^{+/+} mice after 14 days of vascular injury as determined by microarrays (n = 3 mice per group; *P* < 0.05; fold change cutoff = 1.5). (B) Quantification of *Igfbp3*, *Chst1*, *Sh3bgrl2*, *Arhgef26*, *Sh2d5*, and *Dll4* expression in injured carotid arteries from SM-*Dicer*^{+/+} and SM-*Dicer*^{-/-} mice 14 days after vascular injury by qPCR (n = 4–6 mice per group). (C) Predicted inhibition and activation of signaling pathways that regulate the differentially expressed genes in injured carotid arteries from SM-*Dicer*^{+/+} and SM-*Dicer*^{-/-} mice 14 days after vascular injury determined by IPA software. **P* < 0.05 compared with SM-*Dicer*^{+/+} mice. *P* values were obtained by Student's *t* test.

3.4.1 MiRNA-mRNA interactions involved in neointima formation

To identify SMC-specific miRNA-mRNA interactions that regulate neointima formation, integrative target prediction analysis was performed using the web tool Magia². Five-hundred twenty-one interactions between 51 miRNAs downregulated and 126 mRNAs upregulated in SM-*Dicer*^{-/-} mice were predicted (Supplemental Table 5 available on <http://link.springer.com/article/10.1007%2Fs00018-016-2349-0#SupplementaryMaterial>).

Among the 70 most significant interactions (between 26 miRNAs and 47 mRNAs), the highest number of targets was predicted for miR-27a-3p (12 mRNAs), miR-154-5p (9 mRNAs), miR-140-3p (6 mRNAs), and miR-497-5p (6 mRNAs) (Figure 26). Moreover, the miR-27a-3p binding sites of *Arhgef26*, *Chst1*, *Dll4*, and *Oit3* were conserved between mouse and humans (Figure 26). These data suggest that miR-27a-3p might play a central role in neointima formation.

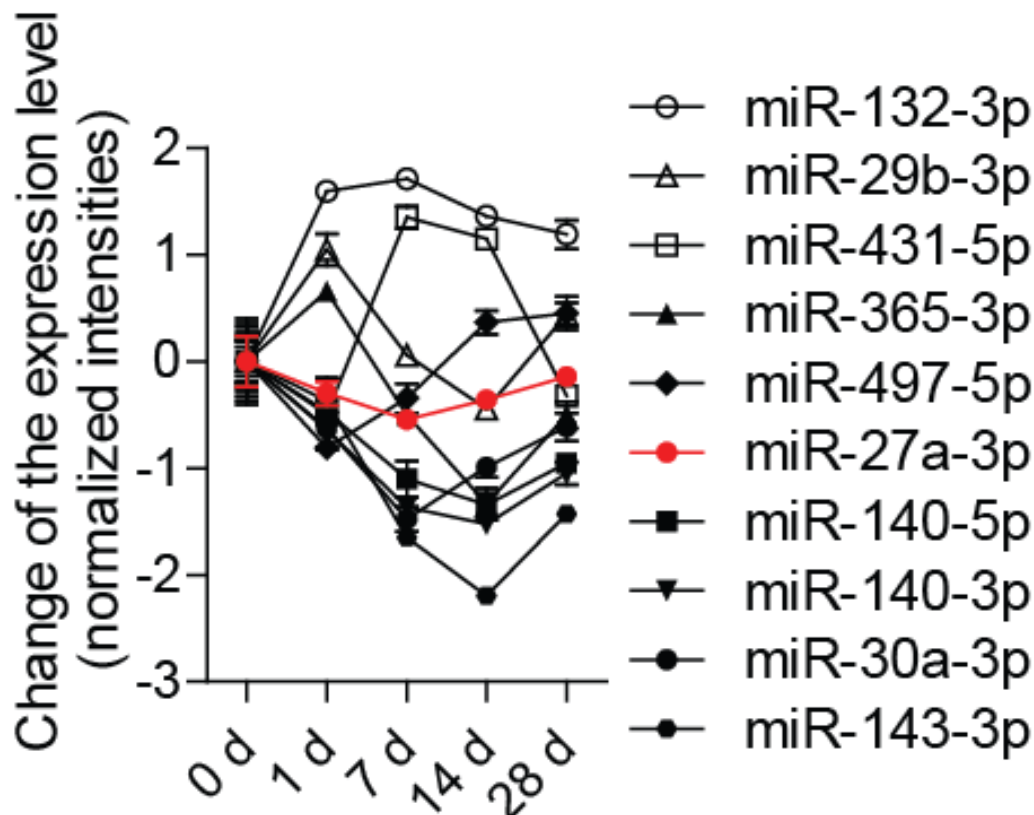


Figure 27. MiRNA expression profile in wire-injured carotid arteries from *Apoe*^{-/-} mice. Expression time course of miRNAs, which are predicted to target mRNAs during neointima formation, in injured carotid arteries of *Apoe*^{-/-} mice (n = 3-4 mice per group). Black line = *P* < 0.05; red line = *P* > 0.05; Error bars represent ± s.e.m.

3.5 Expression of miR-27a-3p in medial and neointimal SMCs

MiR-27a-3p was one of the most strongly downregulated miRNAs in SM-*Dicer*^{-/-} mice (Figure 24). To study whether *Dicer* affects miR-27a-3p expression in vascular SMCs, *in situ* PCR for miR-27a-3p combined with SMA immunostaining was performed. MiR-27a-3p was highly expressed in medial SMCs of uninjured carotid arteries from SM-*Dicer*^{+/+} mice (Figure 28A). Moreover, miR-27a-3p was expressed in neointimal SMCs of SM-*Dicer*^{+/+} mice at 14 days after vascular injury (Figure 28B). By contrast, miR-27a-3p was not detectable in the medial or neointimal SMCs of SM-*Dicer*^{-/-} mice. Therefore, miR-27a-3p is expressed in both medial and neointimal SMCs in the presence of *Dicer*.

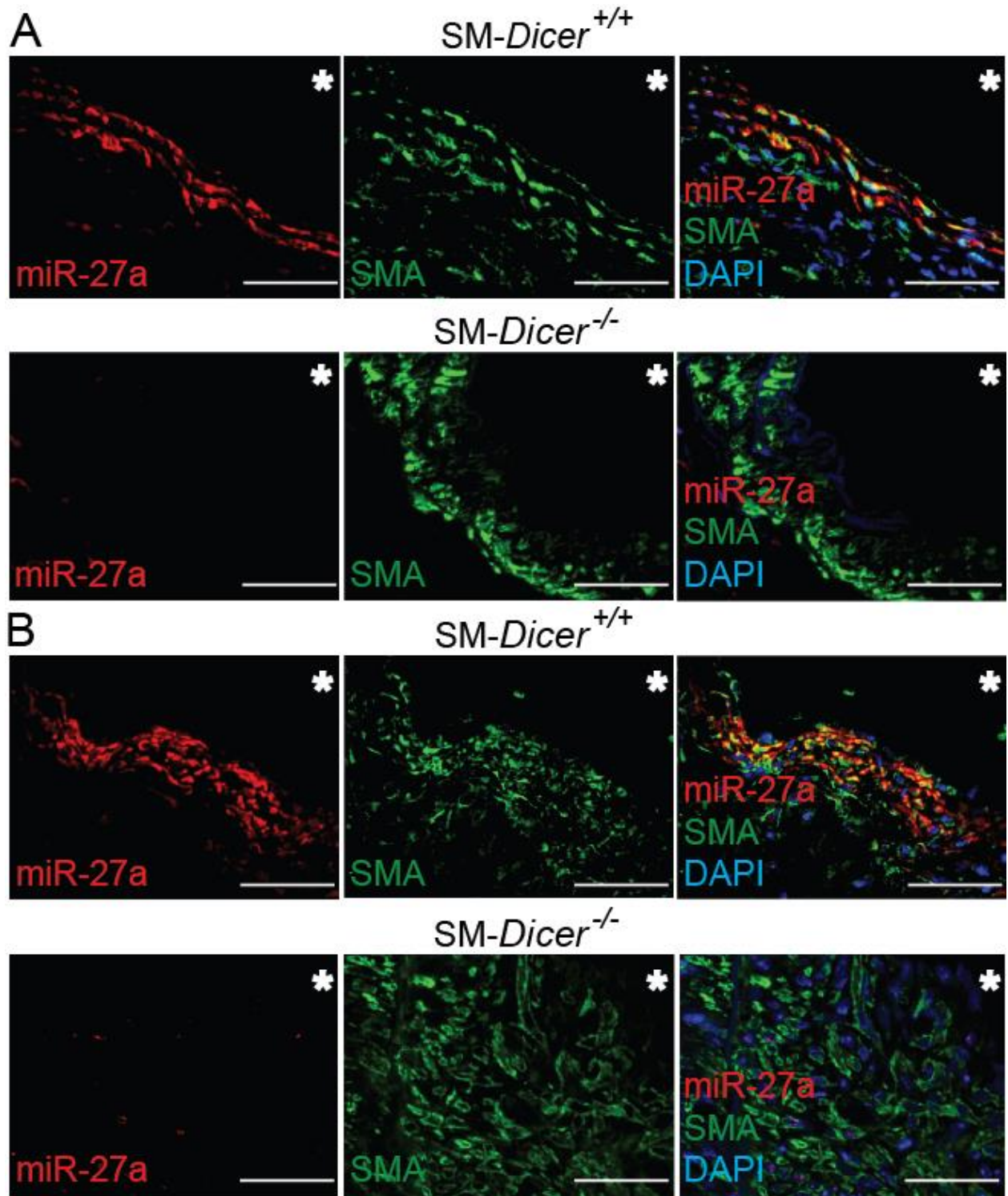


Figure 28. Expression of miR-27a-3p in vascular SMCs of *SM-Dicer*^{+/+} and *SM-Dicer*^{-/-} mice. *In situ* PCR for miR-27a-3p and SMA immunostaining in medial SMCs of uninjured carotid arteries (**A**) and neointimal SMCs of injured carotid arteries (**B**) from *SM-Dicer*^{+/+} and *SM-Dicer*^{-/-} mice 14 days after vascular injury (representative images are shown). Overlays show the cellular co-localization of miR-27a-3p and SMA in neointimal and medial cells. Nuclei were counterstained with DAPI. The asterisks indicate the lumen. Scale bars, 50 μ m.

3.6 Identification of miR-27a-3p targets in SMCs

MiR-27a-3p was predicted to target four mRNAs upregulated in injured carotid arteries of SM-*Dicer*^{-/-} mice via conserved binding sites (Figure 26). To study whether miR-27a-3p regulates these four target genes in SMCs, gain-and-loss-of-function experiments were performed in HASMCs. Silencing of miR-27a-3p expression in HASMCs using LNA inhibitors (Figure 29A) increased the expression of *ARHGEF26* and reduced the expression of *DLL4* and *OIT3* (Figure 29B). Moreover, overexpression of miR-27a-3p in HASMCs (Figure 29C) reduced the expression of *ARHGEF26*, but did not alter the expression level of *DLL4*, *CHST1*, and *OIT3* (Figure 29D). These data indicate miR-27a-3p targets *ARHGEF26* in SMCs.

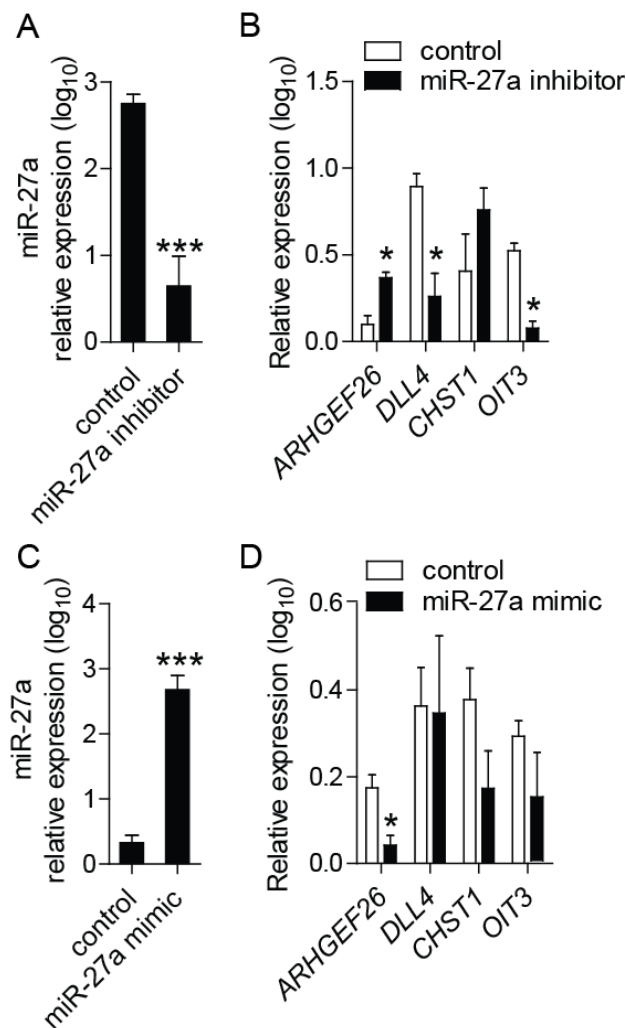


Figure 29. Effect of miR-27a-3p on expression of four conserved target genes in SMCs. The expression levels of miR-27a-3p, *ARHGEF26*, *DLL4*, *CHST1*, and *OIT3* were quantified in HASMCs following miR-27a-3p inhibitors treatment (A, B) or miR-27a-3p mimics treatment (C, D) (n = 3). **P* < 0.05 and ****P* < 0.001. *P* values were obtained by Student's *t* test.

To identify direct targets of miR-27a-3p in SMCs, MYC-tagged trinucleotide repeat containing 6A (TNRC6A, known as GW182), a component of the miRISC, was overexpressed in HASMCs. Immunoprecipitation of GW182 showed that treatment with miR-27a-3p-mimics resulted in a 15-3.6 fold enrichment of *ARHGEF26* mRNA in the miRISC. By contrast, *DLL4*, *CHST1*, and *OIT3* mRNAs were not enriched in the miRISC after miR-27a-3p mimic treatment (Figure 30). These data indicate miR-27a-3p targets *ARHGEF26* but not *DLL4*, *CHST1*, and *OIT3* in SMCs is directly repressed by miR-27a-3p.

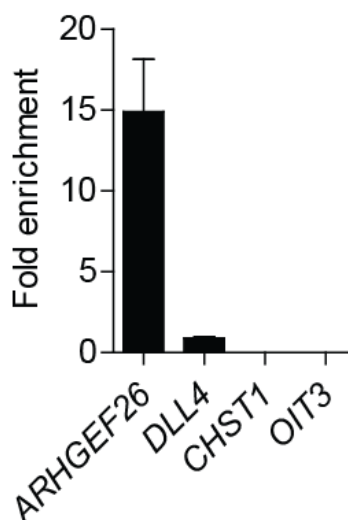


Figure 30. Effect of miR-27a-3p on target gene enrichment in the miRISC. Effect of miR-27a-3p mimic treatment on the enrichment of its potential targets in the miRISC of HASMCs overexpressing a MYC-tagged GW182 protein determined by GW182 immunoprecipitation and qPCR (n = 2). Results are expressed as target enrichment in miR-27a-3p mimic-treated over control mimic-treated HASMCs.

3.6.3 Binding site of miR-27a-3p in the *ARHGEF26* 3'-UTR

Three predicted binding sites for miR-27a-3p were detected in the 3'-UTR of human *ARHGEF26* by in silico analysis. One of those binding sites was highly conserved between different species including mouse and human. To confirm the miR-27a-3p binding site in the *ARHGEF26* mRNA, luciferase reporter assays were performed using the full length of *ARHGEF26* 3'-UTR and the *ARHGEF26* 3'-UTR that contained a mutation of the miR-27a-3p binding site (Figure 31A). The luciferase activity of the wild type *ARHGEF26* 3'-UTR was significantly reduced by miR-27a-3p mimic treatment (Figure 31B). The reduction of the luciferase activity by miR-27a-3p was not observed using the mutated *ARHGEF26* 3'-UTR (Figure 31B). These finding clearly show that miR-27a-3p directly targets *ARHGEF26* through binding to one of the predicted binding sites in its 3'-UTR.

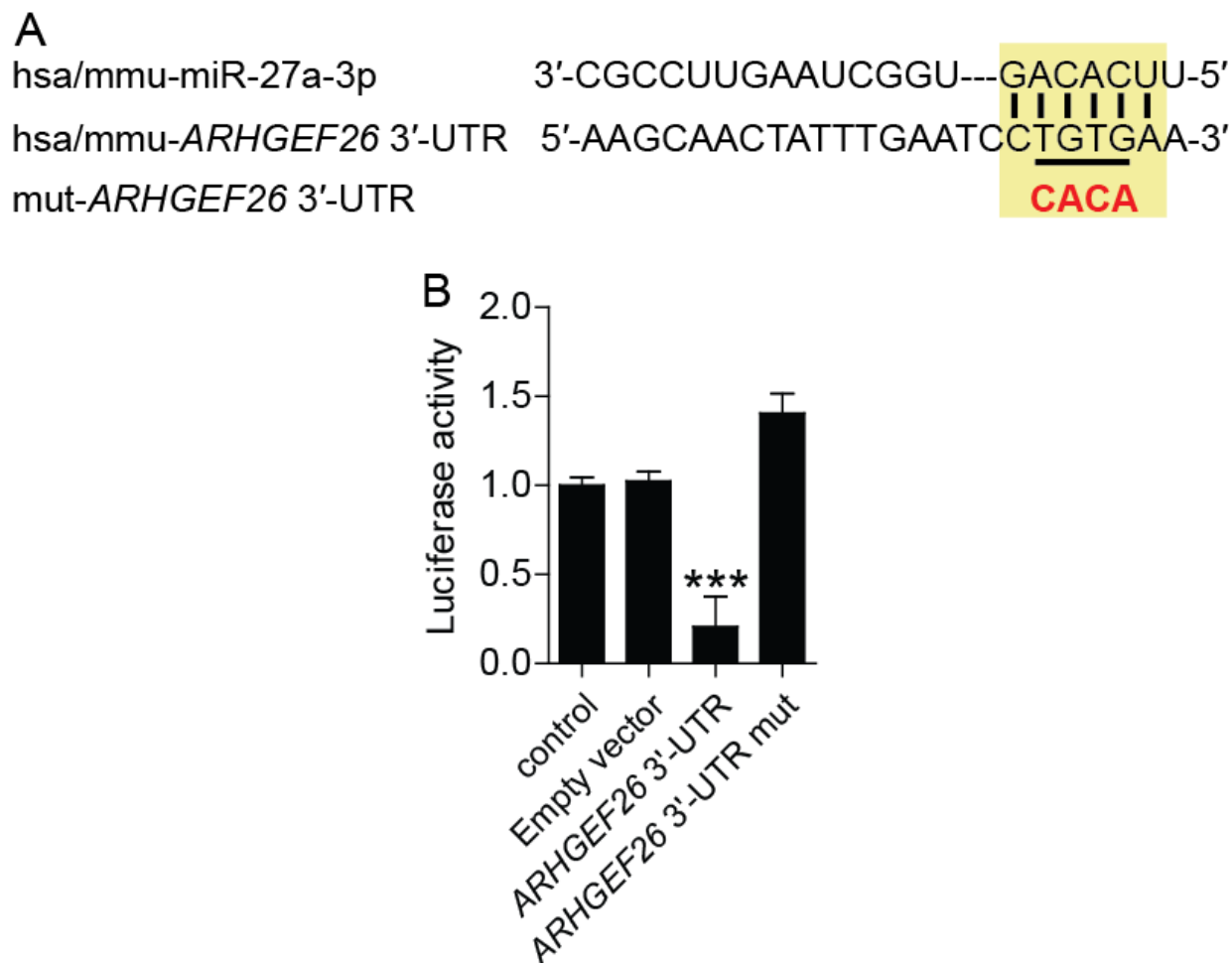


Figure 31. Binding site of miR-27a-3p in the *ARHGEF26* 3'-UTR. (A) Potential target site for miR-27a-3p in the *ARHGEF26* 3'-UTR, predicted by the miRanda prediction algorithm. The miR-27a-3p target (yellow) site was mutated (indicated in red) in the binding site. The seed sequence of miR-27a-3p is highlighted in yellow. (B) Luciferase reporter assays performed in HEK293 cells treated with miR-27a-3p mimics or control mimics (control) using the pEZX-MT05 vector without *ARHGEF26* 3'-UTR (empty vector), pEZX-MT05 vector containing the *ARHGEF26* 3'-UTR or the *ARHGEF26* 3'-UTR with mutations in the predicted miR-27a-3p binding site (n = 3). All data are represented as the means \pm s.e.m. of the indicated number (n) of repeats. *** $P < 0.001$. P values were obtained by one-way analysis of variance (ANOVA).

3.7 Effect of miR-27a-3p targeting *ARHGEF26* on SMC proliferation

To study the role of miR-27a-3p and its target *ARHGEF26* in SMC proliferation, expression of miR-27a-3p and *ARHGEF26* was silenced. Treatment with *ARHGEF26* GapmeRs reduced the expression of *ARHGEF26* in HASMCs (Figure 32A). Treatment with miR-27a-3p inhibitors increased SMC proliferation, whereas silencing of *ARHGEF26* prevented this effect of miR-27a-3p inhibition on SMC proliferation (Figure 32B). These data indicate that the effect of miR-27a-3p on SMC proliferation is mediated by targeting *ARHGEF26*.

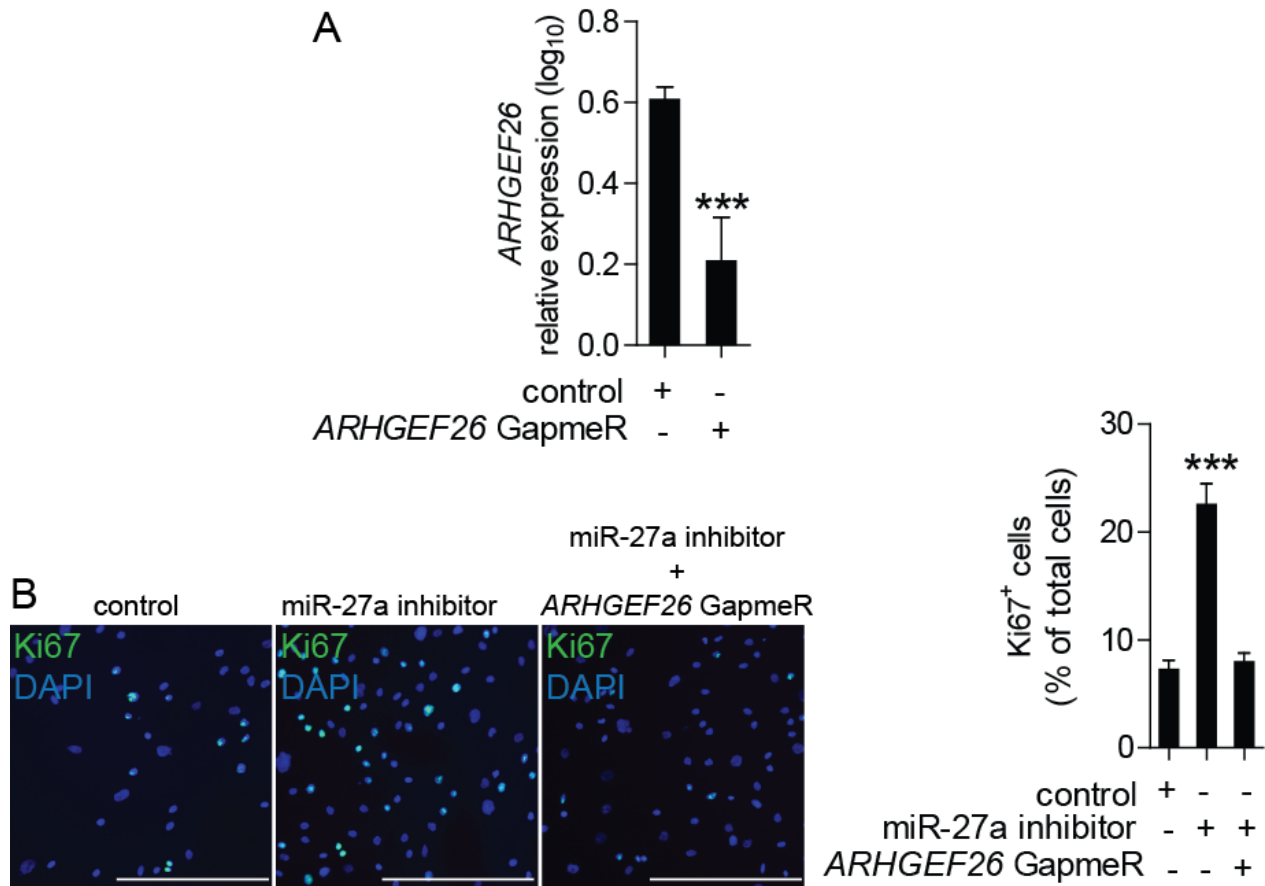


Figure 32. Effect of miR-27a-3p and *ARHGEF26* on SMC proliferation. (A) Quantification of *ARHGEF26* mRNA in HASMCs treated with *ARHGEF26* GapmeRs or control GapmeRs (n = 3). (B) Proliferation of HASMCs was determined by Ki67 immunostaining after treatment with miR-27a-3p inhibitors and *ARHGEF26* GapmeRs. Nuclei were counterstained with DAPI (n = 3). Scale bars, 250 μ m. *** $P < 0.001$. P values were obtained by Student's t test or one-way analysis of variance (ANOVA).

In addition, the interaction between miR-27a-3p and its binding site on the *ARHGEF26* 3'-UTR was blocked using LNA-modified target site blockers (TSBs) (Figure 33A). Treatment with TSBs upregulated *ARHGEF26* expression at the mRNA (Figure 33B) and protein levels (Figure 33C) compared to the treatment with control oligonucleotide.

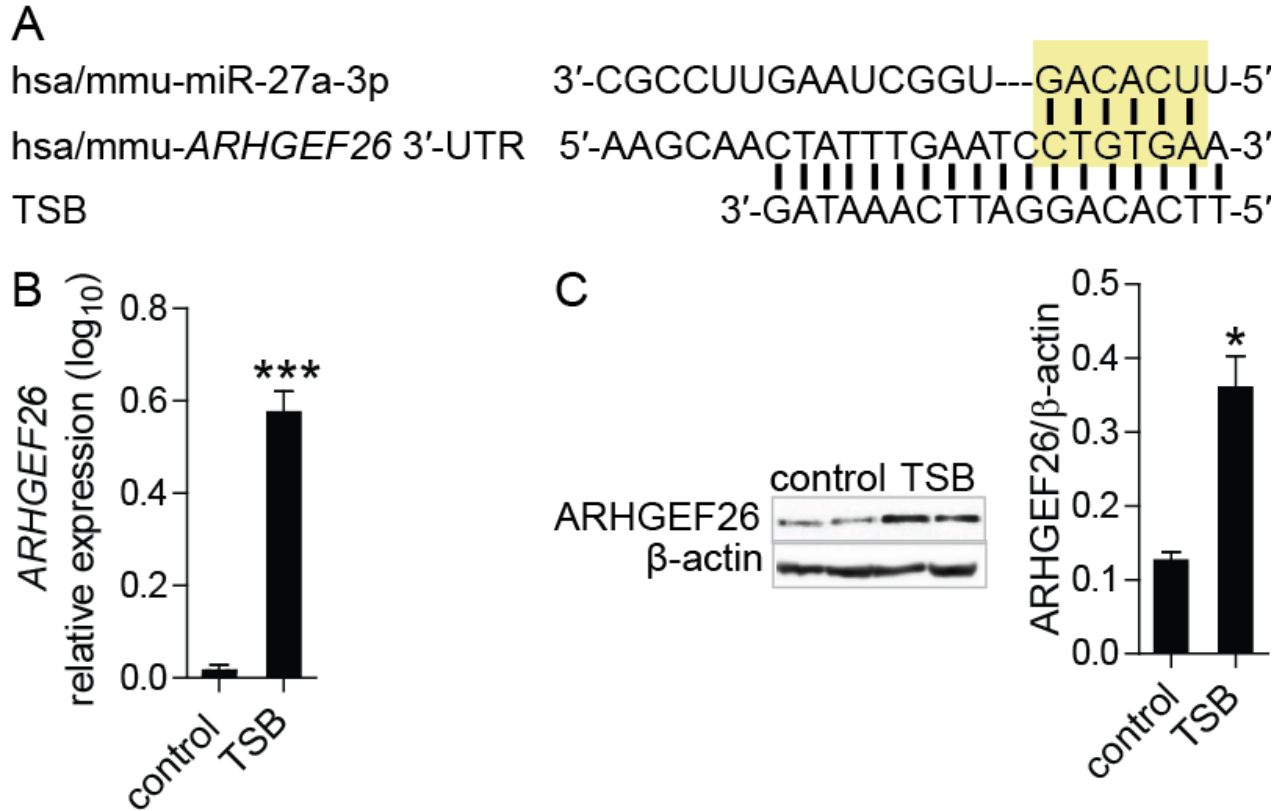


Figure 33. Effect of blocking the interaction between miR-27a-3p and *ARHGEF26*. (A) Sequence of the *ARHGEF26*-target site blockers (TSBs), an LNA-modified oligonucleotide that blocks the target site of miR-27a-3p in the *ARHGEF26* 3'-UTR. Quantification of *ARHGEF26* mRNA levels (B) and protein levels (C), determined by qPCR and Western blot, respectively, in HASMCs treated with TSBs or control-TSBs (n = 3). All data are represented as the means \pm s.e.m. of the indicated number (n) of repeats. * $P < 0.05$ or *** $P < 0.001$. P values were obtained by Student's t test.

Moreover, blocking the interaction between miR-27a-3p and *ARHGEF26* increased SMC proliferation (Figure 34A), and suppressed the expression of cell cycle inhibitors such as *CDKN1A* and *CDKN1B* (Figure 34B) and SMC contractile markers such as *TAGLN* and *MYH11* (Figure 34C). Taken together, these results indicate that miR-27a-3p inhibits SMC proliferation by interacting with a conserved binding site in the *ARHGEF26* 3'-UTR.

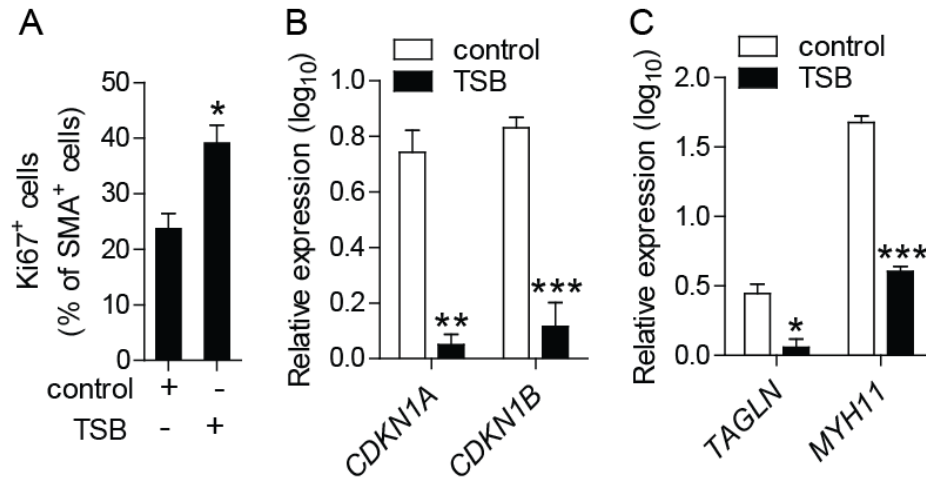


Figure 34. Effect of blocking the interaction of miR-27a-3p with the 3'-UTR *ARHGEF26* on SMC proliferation and differentiation. Cell proliferation ($n = 4$) (A), the expression levels of the cell cycle inhibitors *CDKN1A* and *CDKN1B* ($n = 3$) (B), and the expression levels of the contractile markers *TAGLN* and *MYH11* ($n = 3$) (C) were determined in HASMCs treated with TSBs or control-TSBs. The data are represented as the means \pm s.e.m. of the indicated number (n) of repeats. * $P < 0.05$, ** $P < 0.01$, *** $P < 0.001$. P values were obtained by Student's t test.

3.8 Effect of IL-1 β on the expression of miR-27a-3p and *ARHGEF26*

The inflammatory cytokine interleukin-1 β (IL-1 β) has recently been shown to repress expression of multiple SMC differentiation marker genes in cultured SMCs¹²⁸. In order to study the effect of IL-1 β on miR-27a-3p and *ARHGEF26* expression, *in vitro* experiments were performed on HASMCs. Inflammatory activation of HASMCs by IL-1 β increased the expression of *ARHGEF26* and reduce miR-27a-3p expression (Figure 35).

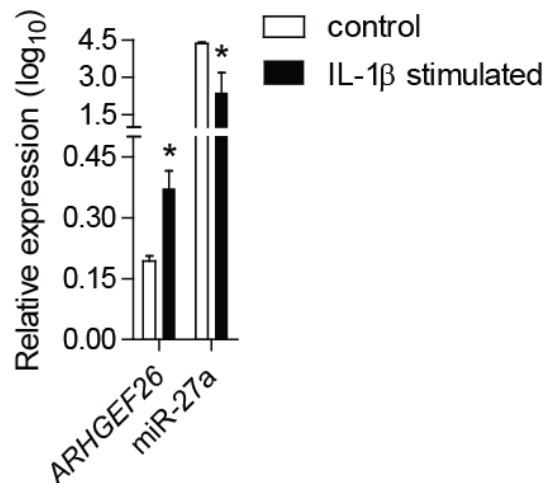


Figure 35. Effect of IL-1 β on miR-27a-3p and *ARHGEF26* expression. The *ARHGEF26* and miR-27a-3p expression level after stimulation of HASMCs with IL-1 β ($n = 6$). Error bars represent \pm s.e.m. * $P < 0.05$. P values were obtained by Student's t test.

3.9 MiR-27a-3p and ARHGEF26 expression in SMCs of mouse and human lesions

To study Arhgef26 expression in neointimal SMCs at the protein level, combined Arhgef26 and SMA immunostaining was performed in injured carotid arteries from SM-*Dicer*^{-/-} and SM-*Dicer*^{+/+} mice. In line with the results obtained at the RNA level, the number of neointimal SMCs expressing Arhgef26 was substantially increased in SM-*Dicer*^{-/-} mice compared with that in SM-*Dicer*^{+/+} mice (Figure 36A-B). These data show that Dicer deficiency increases Arhgef26 expression in SMCs during neointima formation.

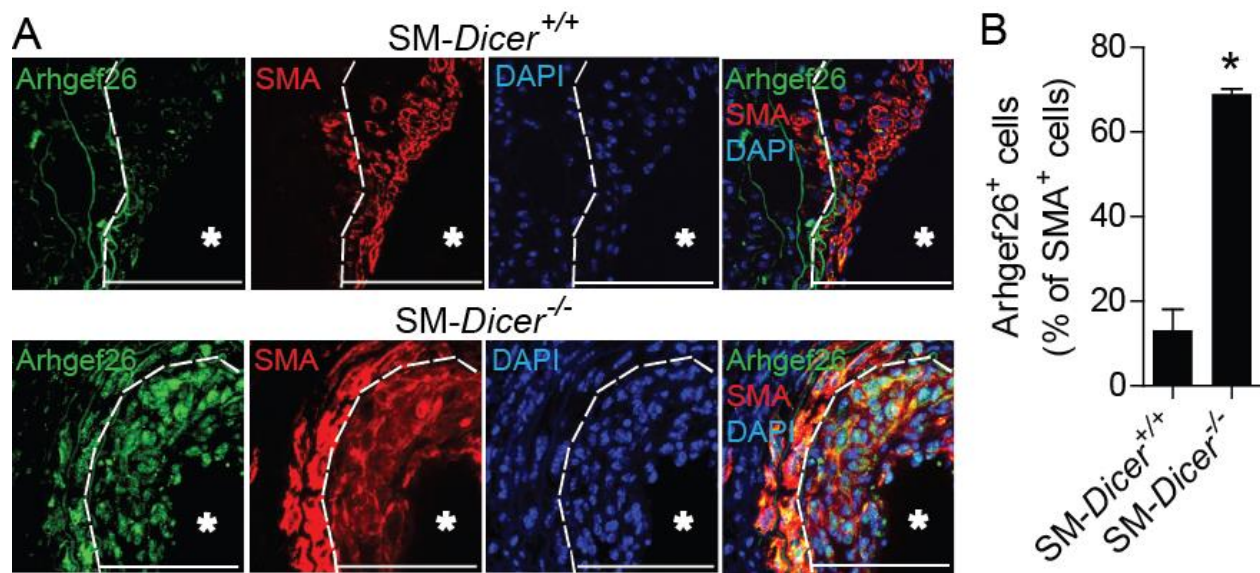


Figure 36. Expression of Arhgef26 in mouse carotid lesions. (A) Arhgef26 in neointimal SMCs was determined by double immunostaining of Arhgef26 and SMA in injured carotid arteries of SM-*Dicer*^{+/+} and SM-*Dicer*^{-/-} mice 14 days after vascular injury (representative images are shown). (B) Quantification of Arhgef26 expressing SMCs in the neointima of SM-*Dicer*^{+/+} and SM-*Dicer*^{-/-} mice 14 days after vascular injury (n = 5 mice per group). Nuclei were counterstained with DAPI. The dash lines delineate the neointimal area. The asterisks indicate the lumen area. Scale bars, 50 μm. **P* < 0.05 compared with SM-*Dicer*^{+/+}. *P* values were obtained by Student's *t* test.

3.9.2 MiR-27a-3p and ARHGEF26 expression in human atherosclerotic lesions

To identify miR-27a-3p and ARHGEF26 in human atherosclerotic lesions, *in situ* PCR of miR-27a-3p or immunostaining of ARHGEF26 was performed in combination with immunostaining for SMA. MiR-27a-3p and ARHGEF26 was detected in SMCs of human atherosclerotic lesions (Figure 37A-B). Therefore, miR-27a and ARHGEF26 are both expressed in SMCs from human atherosclerotic plaque.

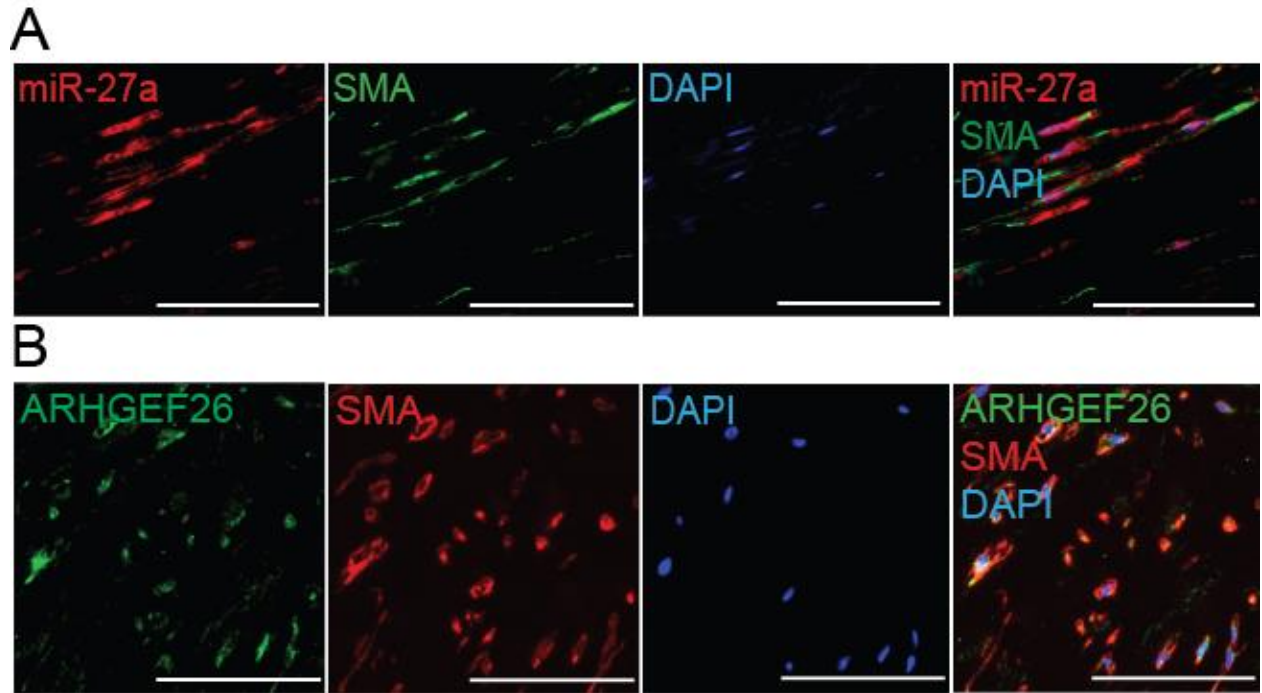


Figure 37. MiR-27a-3p and ARHGEF26 expression in human atherosclerotic lesions. Localization of miR-27a-3p and the expression of ARHGEF26 in human atherosclerotic lesions was determined by *in situ* PCR for miR-27a-3p (A) or immunostaining of ARHGEF26 (B) combined with immunostaining for SMA (representative images were shown). Nuclei were counterstained with DAPI. Scale bars, 50 μm.

4 Discussion

4.1 MiRNAs are differentially expressed after vascular injury

MiRNAs are differentially expressed in the vessel wall in response to the endogenous or exogenous stimuli, which suggests that they could modulate the vascular response to injuries^{100, 129}. Ji et al. showed that miRNAs are differentially expressed following balloon injury in rat carotid artery¹⁰⁰. Similarly, the current study showed that approximately half of the miRNAs detected in mouse carotid arteries were differentially expressed following wire-induced injuries. In line with the findings of Ji et al. in rats¹⁰⁰, among the 25 most significantly differentially expressed miRNAs, the expression of 21 miRNAs, including miR-21-3p, -16-5p, and -223-3p, was increased and the expression of 4 miRNAs, such as miR-29c-3p and -122-5p, was downregulated during neointima formation. These data indicates that a specific set of miRNAs is involved in the regulation of the vascular response to injury. Although the majority of differentially regulated miRNAs was upregulated in injured arteries, *Dicer* deletion in SMCs predominantly reduced the expression of miRNAs that were not upregulated after vascular injury. This result suggests that many miRNAs upregulated during neointima formation are not increased in SMCs but rather are upregulated in other cell types, such as leukocytes. For instance, the level of miR-155 and miR-223, which are high in hematopoietic cells, did not change in injured arteries by SMC-specific *Dicer* knockout in injured arteries, although it was greatly increased after vascular injury^{130, 131}. MiR-21 expression is increased in rat and mouse after balloon injury and its deletion reduces neointima formation¹⁰⁰. In the present study, miR-21 was unaltered in carotid arteries after *Dicer* deletion in SMCs, suggesting that non SMC-derived miR-21 promotes neointimal growth. In fact, *Dicer* in SMCs appears to limit the injury-induced downregulation of miRNAs.

4.2 *Dicer* limits neointima formation by reducing SMC proliferation

Up-regulation of a large number of miRNAs in injured arteries suggests that those miRNAs may enhance neointima formation and their suppression for instance by *Dicer* deletion may protect against neointima formation. However, the current study showed that post-natal deletion of *Dicer* in SMCs increased neointimal growth following wire-induced injury. This effect of *Dicer* deletion in SMCs was associated with increased accumulation and proliferation of neointimal

SMCs, whereas the neointimal macrophage content and endothelial recovery were not altered. These data indicate that Dicer and miRNAs biogenesis in SMCs limits neointima formation.

In contrast to the finding of the current study, Dicer increases SMC proliferation during development⁸⁹, indicating that Dicer plays different roles in SMCs during arterial repair and development. This difference may be because of distinction in the mechanisms of these two conditions in SMC proliferation. Notably, activation of both inflammatory signaling and growth factor which causes neointimal SMC proliferation is specific to arterial repair^{132, 133}. For instance, activation of TNF and PDGF signaling pathways contribute to SMC proliferation and migration that leads to neointimal hyperplasia¹³²⁻¹³⁵.

Growth factors modulate vascular cell survival and growth by activating signaling pathways such as PI3K/Akt/mTOR and Ras/RAF/MEK/ERK1/2¹³³. ERK1/2 belongs to a sub family of MAPKs that regulate cellular processes such as transcription and proliferation^{31, 32}. Phosphorylation activates ERK kinase activity and may mediate its translocation to the nucleus, where it regulates transcription by activating several transcription factors, especially of genes such as cyclin E and cyclin D1, leading to cell cycle progression¹³⁶⁻¹³⁸. In vascular SMCs, ERK activation increases proliferation and is involved in the development of restenosis¹³⁶. The MAPK inhibitor PD0185625 abrogates p44/p42 MAPK activation *in vivo*, which results in reduced SMC proliferation and neointimal formation after vascular injury^{31, 139}.

In addition, inhibition of mTOR by using rapamycin affects PI3K/Akt/mTOR signaling pathway and promotes SMC contractile phenotype^{36, 37, 140}. Moreover, cytokines such as IL-1 β and tumor necrosis factor α (TNF α) activate pro-inflammatory NF- κ B signaling in neointimal SMCs that involves in cross-talk with mitogenic pathways and increases the SMC proliferative response during neointima formation^{38, 39, 140}. Multipotential mediator in inflammatory reaction, TNF α , contributes to stability of atherosclerotic plaque and lesion development through regulating SMC proliferation and apoptosis^{133, 141}. NF- κ B pathway is activated in the SMCs of human atherosclerotic lesions and in vascular SMCs after balloon induced-injury in rat carotid arteries^{141, 142}. Our findings indicate that miRNAs biogenesis by RNase Dicer in SMCs after arterial injury reduces SMC proliferation by inhibiting growth factor and inflammatory signaling such as AKT, ERK1/2, PDGF-BB, EGF, NF- κ B and IL-1.

Although vascular SMCs rarely proliferate after birth, the combined effect of growth factors, such as PDGF and EGF, and inflammatory signaling pathways, such as NF- κ B, following vascular injury induces a phenotypic switch of SMCs characterized by increased proliferative

activity^{133, 143}. Our results indicated that *Dicer* in SMCs suppressed growth factor and inflammatory cytokine signaling after vascular injury, and thereby limit neointimal growth and the proliferation of neointimal SMCs.

In addition to proliferation, *Dicer* promotes a contractile SMC phenotype in uninjured arteries by regulating the contractile proteins expression such as actin, alpha 2, smooth muscle, aorta (ACTA2), *Cnn1*, potassium calcium-activated channel subfamily M regulatory beta subunit 1, *Myh11*, and *Myocd*⁸⁹. However, the current study showed that *Dicer* regulated the expression of the contractile protein transgelin 2 (*Tagln2*) but not that of *Myh11* and *Cnn1*. These data suggest that *Dicer* mainly regulated the SMC proliferation following vascular injury rather than contractile phenotype SMC.

4.3 *Dicer* generates anti-proliferative miRNAs in SMCs

The knockout of *Dicer* in SMCs reduced the neointimal expression of 92 miRNAs, including miR-24, miR-27a/b, miR-143/145, and miR-29a^{95, 103}. Thirty-one of 92 miRNAs downregulated in injured arteries after SMC-specific *Dicer* deletion, such as miR-143/145, miR-365-3p, miR-132-3p, miR-24-3p, miR-29-3p, in induced arteries, have been shown to inhibit SMC proliferation *in vitro* (Figure 38)¹⁰³.

The expression of the miR-143/145 cluster is enhanced in SMCs and mediates the maintenance of a contractile SMC phenotype^{94, 95}. MiR-365-3p, another miRNA downregulated after SMC specific *Dicer* deletion, decreases PDGF-induced SMC proliferation by targeting the 3'-UTR of cyclin D1 in rat carotid arteries after balloon injury¹²². Moreover, miR-132-3p inhibits vascular SMC proliferation by targeting LRR binding FLII interacting protein 1¹²³. *Myoc* as a regulator of SMC migration induces the expression of miR-24-3p and miR-29a-3p, which target the PDGF receptor β and thus reduce neointima formation by inhibiting SMC migration and proliferation¹²⁵. MiR-195-5p is an abundant miRNAs in vascular SMCs that reduces SMC migration and proliferation, and decreases the synthesis of proinflammatory cytokines such as IL-1 β , IL-8, and IL-6¹²⁶. MiR-23b-3p expressed in a cluster together with miR-27b and miR-24-1 is involved in angiogenesis, cardiac ischemia, and retinal vascular development^{125, 144, 145}. MiR-23b-3p inhibits vascular SMC proliferation and migration by targeting transcription factor forkhead box O4, which partially represses SMC contractile genes such as, ACTA2 and MYH11^{127, 144, 145}.

By contrast, 19 of the 92 miRNAs downregulated after SMC-specific *Dicer* deletion in injured arteries, including miR-147-3p and miR-210-3p, do not affect SMC proliferation *in vitro*¹⁰³. MiR-

147-3p, the most significantly downregulated miRNA, does not affect SMC proliferation, but was reported to suppress inflammatory activation in macrophages^{103, 146}. MiR-210-3p is expressed in ECs and overexpression of this miRNA increases ECs migration, but has no effect on SMCs proliferation^{103, 147}. MiR-26a-5p increases SMC proliferation and migration, and inhibits apoptosis, possibly through a mechanism that targets TGF- β /BMP signaling^{147, 148}. Taking together, the results of the current study showed that Dicer deletion in SMC predominantly suppresses the expression of miRNAs that limit SMC proliferation, indicating that Dicer inhibits neointima formation by generating anti-proliferative miRNAs after vascular injury.

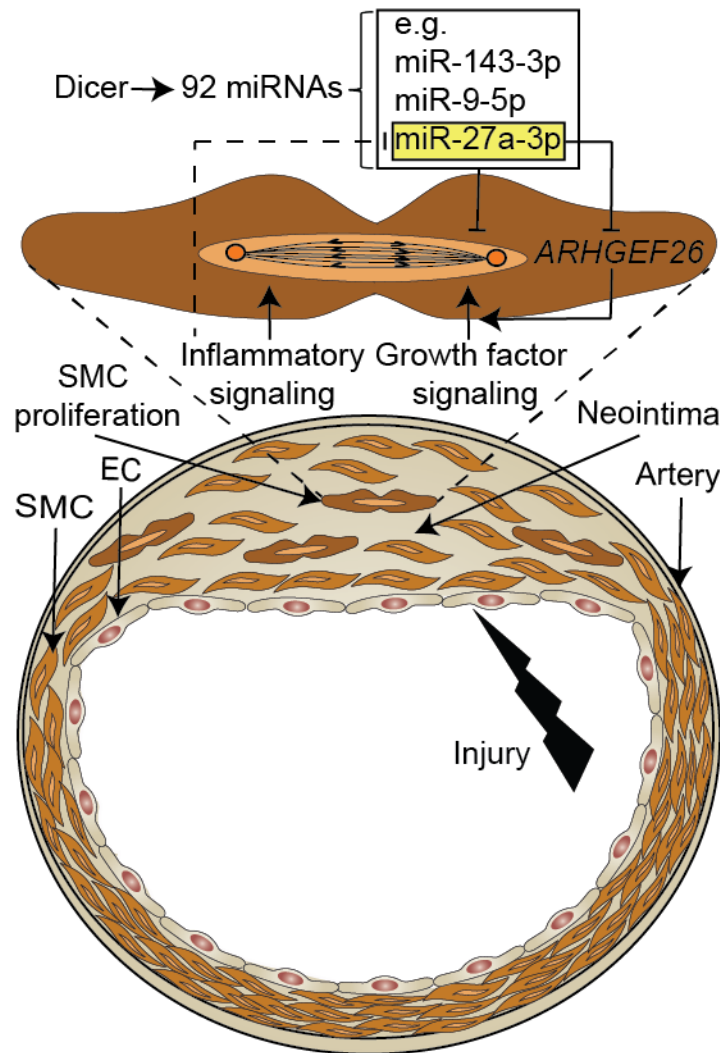


Figure 38. Proposed mechanism of Dicer in SMCs during neointima formation. Dicer generates anti-proliferative miRNAs, like miR-27-3p, which leads to reduced neointima formation by inhibiting SMC proliferation. In the predicted miRNA-mRNA interactome, miR-27a-3p can reduce inflammation-induced SMC proliferation by targeting *AERHGEF26*¹⁴⁹.

4.4 MiR-27a-3p reduced SMC proliferation

MiR-27a-3p was one of the most strongly downregulated miRNAs in injured carotid arteries after *Dicer* deletion in SMCs and inhibits SMC proliferation *in vitro*¹⁰³. Moreover, the highest number of miRNA-mRNA interactions was predicted between miR-27a-3p and 12 mRNAs upregulated in *SM-Dicer*^{-/-} mice, including 4 potential targets that are conserved between human and mouse. By contrast, among the 9 predicted interactions of miR-154-5p and the 6 interactions of miR-140-3p, none were conserved between mouse and human. These data indicate that miR-27a-3p played a central role in *Dicer*-mediated effects on neointima formation although it was not differentially expressed during neointima formation in *Apoe*^{-/-} mice. In addition, miR-27a-3p was highly expressed in medial SMCs of uninjured carotid arteries, which suggests that under normal conditions the presence of this miRNA in the vessel wall maintain the contractile SMC phenotype.

The highly conserved miR-27a-3p is expressed together with miR-23a and miR-24-2 in a polycistronic transcript from an intergenic region^{144, 145}. Accordingly, all three mature miRNAs of the miR-27a-3p/23a/24-2 cluster are downregulated after deletion of *Dicer* in SMCs. Moreover, SRF also upregulates the expression of the pri-miR-27a-3p/23a/24-2 through direct interaction with a transcriptional binding site, suggesting that miR-27a-3p, miR-23a, and miR-24 promote a contractile SMC phenotype¹⁵⁰. In addition, Myoc reduces SMC proliferation and limits neointima formation probably by upregulating miR-24, which targets the PDGF receptor β and thereby inhibits SMC migration¹⁵⁰. Moreover, gain-and-loss-of-function experiments showed that miR-27a-3p inhibited proliferation of human SMCs and the IL-1 β -induced downregulation of miR-27a-3p may mediate the proliferative effect of this inflammatory signaling pathway on SMC. However, the underlying mechanism by which IL-1 β regulates miR-27a-3p expression is unclear.

4.5 MiR-27a-3p inhibits SMC proliferation by targeting *ARHGEF26*

Several genes upregulated in *SM-Dicer*^{-/-} mice contained conserved miR-27a-3p binding sites in their 3'-UTR, but only targeting of the *ARHGEF26* mRNA by miR-27a-3p was experimentally confirmed. Different cell types, such as leukocytes and ECs are involved in neointima formation thus, many upregulated mRNAs predicted to have binding sites for miR-27a-3p may come not only from SMCs but also from other cell types. The 3'-UTR of the human *ARHGEF26* mRNA contained three predicted miR-27a-3p target sites, but only one of those sites is conserved between mouse and humans. According to the classification by Bartel¹⁵¹, this conserved binding

site is a canonical 7-merA1 site consisting of six Watson-Crick base pairings with the nucleotides 2-7 of the miR-27a-3p seed sequence and an adenine in opposite to nucleotide 1 of the miRNA.

Rho-GTPase plays complex roles in SMC proliferation and neointima formation through different mechanisms. Several experimental and clinical studies indicate that part of SMC proliferation and migration following in-stent restenosis is associated with Rho-GTPase activity¹⁵²⁻¹⁵⁴. In addition Rho-GTPase also plays central roles in SMC contractility, and differentiation¹⁵⁵. In the current study, silencing *ARHGEF26* rescued the effect of miR-27a-3p inhibition on SMC proliferation and blocking the interaction between miR-27a-3p and *ARHGEF26* increased SMC proliferation, demonstrating that the effect of miR-27a-3p on SMC differentiation was mediated through targeting of *ARHGEF26*. *ARHGEF26* as a potential target of miR-27a-3p activates the Rho GTPase RhoG by GTP loading and thereby enhances downstream signaling through Rac1 activation, which has been implicated in neointima formation^{156, 157}. Moreover, *ARHGEF26* is overexpressed during prostate cancer and therefore contributes to cancer development and progression through activation of growth factor signaling pathways, such as Akt and ERK1/2 pathways independent of its guanine nucleotide exchange factor function, and increases proliferation of cancer cells^{152, 158, 159}. Notably, both EGF signaling and ERK1/2 activation promote neointima formation by inducing SMC proliferation^{32, 152, 159-161}. Moreover, downregulation of miR-27a-3p in SMCs by inflammatory stimuli plays an important role in inflammation which induces SMC proliferation during neointima formation by mediating NF-κB-induced upregulation of *ARHGEF26*. Therefore, miR-27a-mediated targeting of *ARHGEF26* may play a crucial role in promoting inflammation-induced SMC proliferation during neointima formation.

Genetic deletion of *ARHGEF26* in *Apoe*^{-/-} mice reduces docking structure formation that contributes to decreased atherosclerosis in these mice¹⁵⁴. This protective effect of *Arhgef26* deletion has been attributed to decrease intercellular adhesion molecule 1-mediated formation of docking structures around adherent leukocytes¹⁵⁴. Moreover, in the current study we showed that SMC-specific Dicer deletion increased expression of *Arhgef26* in wire-injured carotid arteries. MiR-27a-3p and *ARHGEF26* were expressed in SMCs from human atherosclerotic lesions, suggesting that the miR-27a-3p/*ARHGEF26* axis in SMCs may also play a role in human atherosclerosis.

Taken together, we showed that Dicer activity controls neointimal hyperplasia by reducing SMC proliferation after vascular injury. In addition to other anti-proliferative miRNAs, miR-27a-3p-

mediated targeting of *Arhgef26* may contribute to the effect of Dicer in SMCs on neointima formation by reducing inflammation-induced growth factor signaling. Hence, local treatment with miR-27a-3p is a promising therapeutic strategy for restenosis. Taking into account that the miRNA-based therapeutics may regulate entire protein or gene networks as compared with the classical pharmacological approach¹⁶². However, due to the increased risk of lentiviral or adenoviral delivery of antisense oligonucleotides, new therapeutic strategies, such as miRNA-mimics or miRNA-inhibitor, are a promising strategy¹⁶³. This miRNA-based eluting stent could be optimized by considering the effective dose of the local administration of miRNA or by using several miRNAs on a single stent. In addition, long-term efficiency of using miRNA in preventing restenosis needs to be still investigated.

5 Summary

The main cause for restenosis following coronary intervention is neointimal hyperplasia due to smooth muscle cell (SMC) accumulation with an immature and synthetic phenotype. Small, non-coding microRNAs (miRNAs) generated by the RNase Dicer play an important role in SMCs during differentiation and development. Following vascular injury, several miRNAs, such as miR-221 and miR-21, are upregulated and promote neointima formation by increasing SMC proliferation. However, the role of Dicer in SMCs during neointima formation is unclear.

To study the effect of Dicer in SMCs during neointima formation in atherosclerosis-prone mice, SMMHC-Cre/*Dicer*^{+/+}*apolipoprotein E* (*Apoe*)^{-/-} (smooth muscle [SM]-*Dicer*^{+/+}) and SMMHC-Cre/*Dicer*^{flox/flox}*Apoe*^{-/-} (SM-*Dicer*^{-/-}) mice were treated with tamoxifen to induce *Dicer* deletion in SMCs and fed a high fat diet, and subjected to vascular injury of the left carotid artery. Following wire injury in carotid arteries of *Apoe*^{-/-} mice, miRNA microarray analysis revealed that most of the significantly regulated miRNAs, such as miR-21-3p and miR-222-3p, were upregulated. Moreover, conditional deletion of Dicer in SMCs increased neointima formation, the neointimal SMC content and proliferation in SM-*Dicer*^{-/-} mice after 14 and 28 days compared to SM-*Dicer*^{+/+} mice as quantified by Elastic van Gieson stain and Ki67/SMA immunostaining.

To identify miRNA-mRNA interactions in SMCs that regulate neointima formation, miRNA expression and genome-wide gene expression profiles in carotid arteries were compared between SM-*Dicer*^{-/-} mice and SM-*Dicer*^{+/+} mice at 14 days after vascular injury. Among the 92 miRNAs downregulated in SM-*Dicer*^{-/-} mice 31 miRNAs, including miR-9-5p, miR-27a-3p, miR-143-3p and miR-27b-3p, were previously shown to inhibit SMC proliferation *in vitro*¹⁰³. Genome-wide gene expression profiles in SM-*Dicer*^{-/-} mice also showed that SMC-specific *Dicer* deletion mostly reduced expression of miRNAs that were not upregulated in *Apoe*^{-/-} mice after wire-induced injury. Dicer in SMCs reduced SMC proliferation and neointima formation by limiting the downregulation of miRNAs and maintaining the expression levels of miRNAs. Therefore, these data indicate that many miRNAs are not upregulated in SMCs, but in other cell types such as leukocytes.

Integrative target prediction analysis predicted 521 interactions between 126 mRNAs and 51 miRNAs that were upregulated and downregulated in SM-*Dicer*^{-/-} mice, respectively, and predicted binding sites in 12 genes for miR-27a-3p, including conserved binding sites in the *ARHGEF26*, *CHST1*, *OIT3* and *DLL4* mRNAs. Notably, 11 of the 31 anti-proliferative miRNAs

reduce neointima formation^{95, 103}, including miR-132-3p. Moreover, miR-27a-3p suppressed *ARHGEF26* but not *CHST1*, *DLL4* and *OIT3* mRNA expression in human SMCs by targeting the predicted binding site in the *ARHGEF26* 3'-UTR as demonstrated by GW182 immunoprecipitation (MirTrap) and luciferase 3'-UTR reporter assays. Combined *in situ* PCR and SMA immunostaining revealed that miR-27a-3p was expressed in neointimal and medial SMCs in SM-*Dicer*^{+/+} mice and SM-*Dicer*^{-/-} mice. The number of neointimal SMCs expressing ARHGEF26 protein was significantly increased in SM-*Dicer*^{-/-} mice as detected by ARHGEF26/SMA immunostaining. Inhibition of miR-27a-3p or the miR-27a-3p binding site in the *ARHGEF26* 3'-UTR using LNA-inhibitors increased the proliferation of human SMCs as determined by Ki67 immunostaining. Moreover, treating HASMCs with IL-1 β reduced the expression of miR-27a-3p and increased the expression of *ARHGEF26*. Our data suggest that downregulation of miR-27a-3p in SMCs by inflammatory stimuli plays an important role in inflammation-induced SMC proliferation during neointima formation by mediating NF- κ B-induced upregulation of *ARHGEF26* due to suppression of miR-27a-3p expression¹⁶⁴.

In conclusion, biogenesis of miRNA by Dicer in SMCs limits neointima formation by suppressing SMC proliferation. This effect of Dicer is partly due to the expression of miR-27a-3p, which inhibits SMC proliferation by targeting *ARHGEF26*, a guanine exchange factor that promotes growth factor signaling. Thus, an increasing Dicer activity in SMCs represents a potential approach to prevent restenosis due to neointimal hyperplasia.

6 Zusammenfassung

Die Restenose nach koronarer Intervention entwickelt sich als neointimale Hyperplasie infolge der Akkumulation glatter Muskelzellen (SMC), die unreife synthetische Eigenschaften aufweisen. Kleine, nichtkodierende microRNAs (miRNAs), gebildet durch die RNase Dicer, spielen eine wichtige Rolle bei der Entwicklung und Differenzierung von SMC. Die Expression einiger miRNAs, wie miR-221 und miR-21, ist erhöht nach Gefäßverletzung und führt zur Neointimabildung durch die verstärkte SMC Proliferation. Allerdings ist die Rolle von Dicer in SMC im Rahmen der Neointimabildung nicht klar.

Um den Einfluss von Dicer in SMCs auf die Neointimabildung in atheroskleroseanfälligen Mäusen zu untersuchen, wurden SMMHC-Cre/*Dicer*^{+/+}*apolipoprotein E* (*Apoe*)^{-/-} (glatte Muskelzellen [SM]-*Dicer*^{+/+}) und SMMHC-Cre/*Dicer*^{flox/flox}*Apoe*^{-/-} (SM-*Dicer*^{-/-}) Mäuse mit Tamoxifen behandelt, um die Dicer Deletion in SMC zu induzieren und anschließend auf High-Fat Diät gesetzt.

Die Analyse des miRNA Microarray nach Gefäßverletzung der linken Arteria carotis communis (A. communis) von *Apoe*^{-/-} Mäusen zeigte, dass die Expression der signifikant regulierten miRNAs, wie miR-21-3p und miR-222-3p, erhöht war. Ferner führte die konditionelle SMC Dicer Gendeletion (SM-*Dicer*^{-/-}) zur verstärkten Neointimabildung, erhöhtem neointimalen SMC Anteil und gesteigerter SMC Proliferation nach 14 und 28 Tagen im Vergleich zu den SM-*Dicer*^{+/+} Mäusen, gemessen mittels Elastic van Gieson Färbung und Ki67/SMA Immunfärbung.

Um die miRNA-mRNA Interaktionen in SMC zu untersuchen, die Neointimabildung regulieren, wurden die miRNA- und die genomweite Genexpressionsprofile in A. communis 14 Tage nach Gefäßverletzung gemessen und zwischen SM-*Dicer*^{-/-} und SM-*Dicer*^{+/+} Mäusen verglichen. Unter den 92 herunterregulierten miRNAs in SM-*Dicer*^{-/-} Mäusen können 31 miRNAs, inkl. miR-9-5p, miR-27a-3p, miR-143-3p und miR-27b-3p die SMC Proliferation in vitro inhibieren¹⁰³. Die Untersuchung der genomweiten Expressionsprofile in SM-*Dicer*^{-/-} Mäusen hat auch gezeigt, dass die SMC-spezifische Dicer Deletion hauptsächlich die Expression der miRNAs reduzierte, die in den *Apoe*^{-/-} Mäusen nach Gefäßverletzung nicht erhöht waren. Dicer in SMC reduziert die SMC Proliferation und die Neointimabildung durch eine Begrenzung der Reduktion von miRNAs und eine Erhaltung der Expressionsniveaus von miRNAs. Diese Ergebnisse deuten darauf hin, dass viele miRNAs nicht in SMC, sondern in anderen Zelltypen wie Leukozyten vermehrt exprimiert sind.

Mit Hilfe eines integrativen Vorhersageprogramms wurden 521 Interaktionen zwischen den

erhöhten 126 mRNAs und den verringerten 51 miRNAs in SM-*Dicer*^{-/-} Mäusen vorausberechnet. Ferner wurden Bindungsstellen in 12 Genen für miR-27a-3p, inkl. konservierter Bindungsstellen in den *ARHGEF26*, *CHST1*, *OIT3* und *DLL4* mRNAs prognostiziert. Wichtig erscheint es, dass 11 von 31 anti-proliferativen miRNAs, einschließlich miR-132-3p, die Neointimabildung verringern können^{95, 103}. Außerdem konnte miR-27a-3p in humanen SMC die Expression von *ARHGEF26*, aber nicht von *CHST1*, *DLL4* und *OIT3* mRNAs mittels vorhergesagten Bindungsstellen in den *ARHGEF26* 3'-UTR supprimieren, wie mithilfe von GW182 Immunpräzipitation (MirTrap) und Luziferase 3'-UTR Reporter-Assays detektiert werden konnte. Eine Kombination von *in situ* PCR und SMA Immunfärbung konnte zeigen, dass miR-27a-3p in den neointimalen und medialen SMC in SM-*Dicer*^{+/+} und SM-*Dicer*^{-/-} Mäusen exprimiert wird. Die Anzahl von neointimalen SMC, die das ARHGEF26 Protein exprimieren, war deutlich angestiegen in den SM-*Dicer*^{-/-} Mäusen, gemessen mittels ARHGEF26/SMA Immunfärbung. Die Suppression von miR-27a-3p oder der Bindungsstelle in der *ARHGEF26* 3'-UTR mittels LNA-Inhibitoren führte zu einer Erhöhung der Proliferation humaner SMC, detektiert mithilfe von Ki67 Immunfärbung. Ferner reduzierte die Behandlung von HASMCs mit IL-1 β die miR-27a-3p Expression und erhöhte die *ARHGEF26* Expression. Unsere Ergebnisse deuten darauf hin, dass die reduzierte Expression von miR-27a-3p in SMC eine wichtige Rolle in der SMC Proliferation unter inflammatorischen Bedingungen während der Neointimabildung spielt. Dies kann über die NF- κ B-induzierte Erhöhung von *ARHGEF26* aufgrund der miR-27a-3p Suppression vermittelt werden¹⁶⁴.

Zusammenfassend lässt sich sagen, dass die Dicer-vermittelte Biogenese von miRNAs in SMC die Neointimabildung, durch die Suppression der SMC Proliferation, inhibiert. Dieser Effekt von Dicer ist auch auf die miR-27a-3p zurückzuführen, die die SMC Proliferation via Bindung an *ARHGEF26* inhibiert. *ARHGEF26* begünstigt als Guanine-Austauschfaktor das Wachstumsfaktoren-Signaling. In diesem Zusammenhang kann eine erhöhte Dicer Aktivität in SMCs einen potentiellen Ansatz zur Bekämpfung von Restenose durch eine verminderte Neointimabildung darstellen.

7 References

1. Pagidipati NJ and Gaziano TA. Estimating Deaths From Cardiovascular Disease: A Review of Global Methodologies of Mortality Measurement. *Circulation*. 2013;127:749-756.
2. Hansson GK and Hermansson A. The immune system in atherosclerosis. *Nat Immunol*. 2011;12:204-12.
3. Weintraub W. The Pathophysiology and Burden of Restenosis. *The American Journal of Cardiology*. 2007;100:S3-S9.
4. Welt FG and Rogers C. Inflammation and restenosis in the stent era. *Arterioscler Thromb Vasc Biol*. 2002;22:1769-76.
5. Alfonso F, Byrne RA, Rivero F and Kastrati A. Current treatment of in-stent restenosis. *J Am Coll Cardiol*. 2014;63:2659-73.
6. Marx SO, Totary-Jain H and Marks AR. Vascular smooth muscle cell proliferation in restenosis. *Circ Cardiovasc Interv*. 2011;4:104-11.
7. Weintraub WS. The pathophysiology and burden of restenosis. *Am J Cardiol*. 2007;100:3k-9k.
8. Cassese S, Byrne RA, Tada T, Pinieck S, Joner M, Ibrahim T, King LA, Fusaro M, Laugwitz KL and Kastrati A. Incidence and predictors of restenosis after coronary stenting in 10 004 patients with surveillance angiography. *Heart*. 2014;100:153-9.
9. Garratt KN, Edwards WD, Kaufmann UP, Vlietstra RE and Holmes DR, Jr. Differential histopathology of primary atherosclerotic and restenotic lesions in coronary arteries and saphenous vein bypass grafts: analysis of tissue obtained from 73 patients by directional atherectomy. *J Am Coll Cardiol*. 1991;17:442-8.
10. Hoylaerts MF. Platelet-vessel wall interactions in thrombosis and restenosis role of von Willebrand factor. *Verhandelingen - Koninklijke Academie voor Geneeskunde van België*. 1997;59:161-83.
11. Chandrasekar B and Tanguay JF. Platelets and restenosis. *J Am Coll Cardiol*. 2000;35:555-62.
12. Smyth SS, Reis ED, Zhang W, Fallon JT, Gordon RE and Collier BS. Beta(3)-integrin-deficient mice but not P-selectin-deficient mice develop intimal hyperplasia after vascular injury: correlation with leukocyte recruitment to adherent platelets 1 hour after injury. *Circulation*. 2001;103:2501-7.
13. McEver RP and Cummings RD. Role of PSGL-1 binding to selectins in leukocyte recruitment. *J Clin Invest*. 1997;100:S97-103.
14. Springer TA. Traffic signals for lymphocyte recirculation and leukocyte emigration: the multistep paradigm. *Cell*. 1994;76:301-14.
15. Clarke MC, Talib S, Figg NL and Bennett MR. Vascular smooth muscle cell apoptosis induces interleukin-1-directed inflammation: effects of hyperlipidemia-mediated inhibition of phagocytosis. *Circ Res*. 2010;106:363-72.
16. Crowley ST, Ray CJ, Nawaz D, Majack RA and Horwitz LD. Multiple growth factors are released from mechanically injured vascular smooth muscle cells. *Am J Physiol*. 1995;269:H1641-7.
17. Jovinge S, Hultgardh-Nilsson A, Regnstrom J and Nilsson J. Tumor necrosis factor-alpha activates smooth muscle cell migration in culture and is expressed in the balloon-injured rat aorta. *Arterioscler Thromb Vasc Biol*. 1997;17:490-7.
18. Ferns GA and Avades TY. The mechanisms of coronary restenosis: insights from experimental models. *Int J Exp Pathol*. 2000;81:63-88.
19. Schwartz SM, deBlois D and O'Brien ER. The intima. Soil for atherosclerosis and restenosis. *Circ Res*. 1995;77:445-65.
20. Lindner V, Fingerle J and Reidy MA. Mouse model of arterial injury. *Circ Res*. 1993;73:792-6.
21. Welt FGP and Rogers C. Inflammation and Restenosis in the Stent Era. *Arteriosclerosis, Thrombosis, and Vascular Biology*. 2002;22:1769-1776.
22. Wall VZ and Bornfeldt KE. Arterial smooth muscle. *Arterioscler Thromb Vasc Biol*. 2014;34:2175-9.
23. Owens GK. Regulation of differentiation of vascular smooth muscle cells. *Physiol Rev*. 1995;75:487-517.

24. Stegemann JP, Hong H and Nerem RM. Mechanical, biochemical, and extracellular matrix effects on vascular smooth muscle cell phenotype. *J Appl Physiol* (1985). 2005;98:2321-7.
25. Beamish JA, He P, Kottke-Marchant K and Marchant RE. Molecular Regulation of Contractile Smooth Muscle Cell Phenotype: Implications for Vascular Tissue Engineering. *Tissue Engineering Part B, Reviews*. 2010;16:467-491.
26. Rensen S, Doevendans P and van Eys G. Regulation and characteristics of vascular smooth muscle cell phenotypic diversity. *Neth Heart J*. 2007;15:100-8.
27. Hao H, Gabbiani G and Bochaton-Piallat ML. Arterial smooth muscle cell heterogeneity: implications for atherosclerosis and restenosis development. *Arterioscler Thromb Vasc Biol*. 2003;23:1510-20.
28. Chamley-Campbell J, Campbell GR and Ross R. The smooth muscle cell in culture. *Physiol Rev*. 1979;59:1-61.
29. Ottlinger ME, Pukac LA and Karnovsky MJ. Heparin inhibits mitogen-activated protein kinase activation in intact rat vascular smooth muscle cells. *J Biol Chem*. 1993;268:19173-6.
30. Hayashi K, Shibata K, Morita T, Iwasaki K, Watanabe M and Sobue K. Insulin receptor substrate-1/SHP-2 interaction, a phenotype-dependent switching machinery of insulin-like growth factor-I signaling in vascular smooth muscle cells. *J Biol Chem*. 2004;279:40807-18.
31. Gennaro G, Menard C, Michaud SE, Deblois D and Rivard A. Inhibition of vascular smooth muscle cell proliferation and neointimal formation in injured arteries by a novel, oral mitogen-activated protein kinase/extracellular signal-regulated kinase inhibitor. *Circulation*. 2004;110:3367-71.
32. Liu B, Fisher M and Groves P. Down-regulation of the ERK1 and ERK2 mitogen-activated protein kinases using antisense oligonucleotides inhibits intimal hyperplasia in a porcine model of coronary balloon angioplasty. *Cardiovasc Res*. 2002;54:640-8.
33. Chan AK, Kalmes A, Hawkins S, Daum G and Clowes AW. Blockade of the epidermal growth factor receptor decreases intimal hyperplasia in balloon-injured rat carotid artery. *J Vasc Surg*. 2003;37:644-9.
34. Stabile E, Zhou YF, Saji M, Castagna M, Shou M, Kinnaird TD, Baffour R, Ringel MD, Epstein SE and Fuchs S. Akt controls vascular smooth muscle cell proliferation in vitro and in vivo by delaying G1/S exit. *Circ Res*. 2003;93:1059-65.
35. Dong LH, Wen JK, Liu G, McNutt MA, Miao SB, Gao R, Zheng B, Zhang H and Han M. Blockade of the Ras-extracellular signal-regulated kinase 1/2 pathway is involved in smooth muscle 22 alpha-mediated suppression of vascular smooth muscle cell proliferation and neointima hyperplasia. *Arterioscler Thromb Vasc Biol*. 2010;30:683-91.
36. Johnson SC, Rabinovitch PS and Kaeberlein M. mTOR is a key modulator of ageing and age-related disease. *Nature*. 2013;493:338-345.
37. Giordano A and Romano A. Inhibition of human in-stent restenosis: a molecular view. *Curr Opin Pharmacol*. 2011;11:372-7.
38. Furgeson SB, Simpson PA, Park I, Vanputten V, Horita H, Kontos CD, Nemenoff RA and Weiser-Evans MC. Inactivation of the tumour suppressor, PTEN, in smooth muscle promotes a pro-inflammatory phenotype and enhances neointima formation. *Cardiovascular Research*. 2010;86:274-82.
39. Romashkova JA and Makarov SS. NF-kappaB is a target of AKT in anti-apoptotic PDGF signaling. *Nature*. 1999;401:86-90.
40. Ambros V. The evolution of our thinking about microRNAs. *Nat Med*. 2008;14:1036-40.
41. Lee RC, Feinbaum RL and Ambros V. The *C. elegans* heterochronic gene *lin-4* encodes small RNAs with antisense complementarity to *lin-14*. *Cell*. 1993;75:843-54.
42. Huntzinger E and Izaurralde E. Gene silencing by microRNAs: contributions of translational repression and mRNA decay. *Nature Reviews Genetics*. 2011;12:99-110.
43. Polimeni A, De Rosa S and Indolfi C. Vascular miRNAs after balloon angioplasty. *Trends Cardiovasc Med*. 2013;23:9-14.
44. Stellos K and Dimmeler S. Vascular MicroRNAs. *From Disease Mechanisms to Therapeutic Targets*. 2014;114:3-4.

45. Iaconetti C, Gareri C, Polimeni A and Indolfi C. Non-coding RNAs: the "dark matter" of cardiovascular pathophysiology. *Int J Mol Sci.* 2013;14:19987-20018.
46. Davies MJ and Thomas A. Thrombosis and acute coronary-artery lesions in sudden cardiac ischemic death. *N Engl J Med.* 1984;310:1137-40.
47. Nazari-Jahantigh M, Wei Y and Schober A. The role of microRNAs in arterial remodelling. *Thromb Haemost.* 2012;107:611-8.
48. Urbich C, Kuehbacher A and Dimmeler S. Role of microRNAs in vascular diseases, inflammation, and angiogenesis. *Cardiovascular Research.* 2008;79:581-8.
49. Krol J, Loedige I and Filipowicz W. The widespread regulation of microRNA biogenesis, function and decay. *Nat Rev Genet.* 2010;11:597-610.
50. Ha M and Kim VN. Regulation of microRNA biogenesis. *Nat Rev Mol Cell Biol.* 2014;15:509-524.
51. Bentwich I, Avniel A, Karov Y, Aharonov R, Gilad S, Barad O, Barzilai A, Einat P, Einav U, Meiri E, Sharon E, Spector Y and Bentwich Z. Identification of hundreds of conserved and nonconserved human microRNAs. *Nat Genet.* 2005;37:766-70.
52. Graves P and Zeng Y. Biogenesis of mammalian microRNAs: a global view. *Genomics Proteomics Bioinformatics.* 2012;10:239-45.
53. Kim VN. MicroRNA biogenesis: coordinated cropping and dicing. *Nature Reviews Molecular Cell Biology.* 2005;6:376-385.
54. Kim VN, Han J and Siomi MC. Biogenesis of small RNAs in animals. *Nature Reviews Molecular Cell Biology.* 2009;10:126-139.
55. Bohnsack MT, Czaplinski K and Gorlich D. Exportin 5 is a RanGTP-dependent dsRNA-binding protein that mediates nuclear export of pre-miRNAs. *RNA.* 2004;10:185-91.
56. Yi R, Qin Y, Macara IG and Cullen BR. Exportin-5 mediates the nuclear export of pre-microRNAs and short hairpin RNAs. *Genes Dev.* 2003;17:3011-6.
57. Lamontagne B, Larose S, Boulanger J and Elela SA. The RNase III family: a conserved structure and expanding functions in eukaryotic dsRNA metabolism. *Curr Issues Mol Biol.* 2001;3:71-8.
58. Heyam A, Lagos D and Plevin M. Dissecting the roles of TRBP and PACT in double-stranded RNA recognition and processing of noncoding RNAs. *Wiley Interdiscip Rev RNA.* 2015;6:271-89.
59. Ma JB, Ye K and Patel DJ. Structural basis for overhang-specific small interfering RNA recognition by the PAZ domain. *Nature.* 2004;429:318-22.
60. Tsutsumi A, Kawamata T, Izumi N, Seitz H and Tomari Y. Recognition of the pre-miRNA structure by Drosophila Dicer-1. *Nat Struct Mol Biol.* 2011;18:1153-8.
61. Park JE, Heo I, Tian Y, Simanshu DK, Chang H, Jee D, Patel DJ and Kim VN. Dicer recognizes the 5' end of RNA for efficient and accurate processing. *Nature.* 2011;475:201-5.
62. Ji X. The mechanism of RNase III action: how dicer dices. *Curr Top Microbiol Immunol.* 2008;320:99-116.
63. Kurzynska-Kokorniak A, Pokornowska M, Koralewska N, Hoffmann W, Bienkowska-Szewczyk K and Figlerowicz M. Revealing a new activity of the human Dicer DUF283 domain in vitro. *Scientific Reports.* 2016;6:23989.
64. Welker NC, Maity TS, Ye X, Aruscavage PJ, Krauchuk AA, Liu Q and Bass BL. Dicer's helicase domain discriminates dsRNA termini to promote an altered reaction mode. *Mol Cell.* 2011;41:589-99.
65. Macrae IJ, Zhou K, Li F, Repic A, Brooks AN, Cande WZ, Adams PD and Doudna JA. Structural basis for double-stranded RNA processing by Dicer. *Science.* 2006;311:195-8.
66. Rakheja D, Chen KS, Liu Y, Shukla AA, Schmid V, Chang TC, Khokhar S, Wickiser JE, Karandikar NJ, Malter JS, Mendell JT and Amatruda JF. Somatic mutations in DROSHA and DICER1 impair microRNA biogenesis through distinct mechanisms in Wilms tumours. *Nat Commun.* 2014;2:4802.
67. Martello G, Rosato A, Ferrari F, Manfrin A, Cordenonsi M, Dupont S, Enzo E, Guzzardo V, Rondina M, Spruce T, Parenti AR, Daidone MG, Bicciato S and Piccolo S. A MicroRNA targeting dicer for metastasis control. *Cell.* 2010;141:1195-207.
68. Gurtan AM, Lu V, Bhutkar A and Sharp PA. In vivo structure-function analysis of human Dicer reveals directional processing of precursor miRNAs. *RNA.* 2012;18:1116-22.

69. Lau PW, Guiley KZ, De N, Potter CS, Carragher B and MacRae IJ. The molecular architecture of human Dicer. *Nat Struct Mol Biol.* 2012;19:436-40.
70. Kwak PB and Tomari Y. The N domain of Argonaute drives duplex unwinding during RISC assembly. *Nat Struct Mol Biol.* 2012;19:145-51.
71. Ameres SL, Martinez J and Schroeder R. Molecular basis for target RNA recognition and cleavage by human RISC. *Cell.* 2007;130:101-12.
72. Shivdasani RA. MicroRNAs: regulators of gene expression and cell differentiation. *Blood.* 2006;108:3646-53.
73. Winter J, Jung S, Keller S, Gregory RI and Diederichs S. Many roads to maturity: microRNA biogenesis pathways and their regulation. *Nature cell biology.* 2009;11:228-34.
74. Schirle NT, Sheu-Gruttadauria J and MacRae IJ. Structural basis for microRNA targeting. *Science.* 2014;346:608-13.
75. Patel DJ. RNA. Complete pairing not needed. *Science.* 2014;346:542-3.
76. Sawh AN and Duchaine TF. Turning Dicer on its head. *Nat Struct Mol Biol.* 2012;19:365-366.
77. Bartel DP. MicroRNAs: genomics, biogenesis, mechanism, and function. *Cell.* 2004;116:281-97.
78. Lewis BP, Burge CB and Bartel DP. Conserved seed pairing, often flanked by adenosines, indicates that thousands of human genes are microRNA targets. *Cell.* 2005;120:15-20.
79. Hinkal GW, Grelier G, Puisieux A and Moyret-Lalle C. Complexity in the regulation of Dicer expression: Dicer variant proteins are differentially expressed in epithelial and mesenchymal breast cancer cells and decreased during EMT. *Br J Cancer.* 2011;104:387-8.
80. Jafarnejad SM, Ardekani GS, Ghaffari M, Martinka M and Li G. Sox4-mediated Dicer expression is critical for suppression of melanoma cell invasion. *Oncogene.* 2013;32:2131-9.
81. Levy C, Khaled M, Robinson KC, Veguilla RA, Chen PH, Yokoyama S, Makino E, Lu J, Larue L, Beermann F, Chin L, Bosenberg M, Song JS and Fisher DE. Lineage-specific transcriptional regulation of DICER by MITF in melanocytes. *Cell.* 2010;141:994-1005.
82. Grelier G, Voirin N, Ay AS, Cox DG, Chabaud S, Treilleux I, Leon-Goddard S, Rimokh R, Mikaelian I, Venoux C, Puisieux A, Lasset C and Moyret-Lalle C. Prognostic value of Dicer expression in human breast cancers and association with the mesenchymal phenotype. *Br J Cancer.* 2009;101:673-83.
83. Albinsson S, Suarez Y, Skoura A, Offermanns S, Miano JM and Sessa WC. MicroRNAs are necessary for vascular smooth muscle growth, differentiation, and function. *Arterioscler Thromb Vasc Biol.* 2010;30:1118-26.
84. Suarez Y, Fernandez-Hernando C, Pober JS and Sessa WC. Dicer dependent microRNAs regulate gene expression and functions in human endothelial cells. *Circulation Research.* 2007;100:1164-73.
85. Suarez Y, Fernandez-Hernando C, Yu J, Gerber SA, Harrison KD, Pober JS, Iruela-Arispe ML, Merkenschlager M and Sessa WC. Dicer-dependent endothelial microRNAs are necessary for postnatal angiogenesis. *Proc Natl Acad Sci U S A.* 2008;105:14082-7.
86. Cobb BS, Hertweck A, Smith J, O'Connor E, Graf D, Cook T, Smale ST, Sakaguchi S, Livesey FJ, Fisher AG and Merkenschlager M. A role for Dicer in immune regulation. *J Exp Med.* 2006;203:2519-27.
87. Cobb BS, Nesterova TB, Thompson E, Hertweck A, O'Connor E, Godwin J, Wilson CB, Brockdorff N, Fisher AG, Smale ST and Merkenschlager M. T cell lineage choice and differentiation in the absence of the RNase III enzyme Dicer. *J Exp Med.* 2005;201:1367-73.
88. Mudhasani R, Zhu Z, Hutvagner G, Eischen CM, Lyle S, Hall LL, Lawrence JB, Imbalzano AN and Jones SN. Loss of miRNA biogenesis induces p19Arf-p53 signaling and senescence in primary cells. *J Cell Biol.* 2008;181:1055-63.
89. Albinsson S, Skoura A, Yu J, DiLorenzo A, Fernandez-Hernando C, Offermanns S, Miano JM and Sessa WC. Smooth muscle miRNAs are critical for post-natal regulation of blood pressure and vascular function. *PLoS One.* 2011;6:e18869.
90. Schober A, Thum T and Zerneck A. MicroRNAs in vascular biology - metabolism and atherosclerosis. *Thrombosis and Haemostasis.* 2012;107:603-604.
91. Ntarelli L and Schober A. MicroRNAs and the response to injury in atherosclerosis. *Hamostaseologie.* 2015;35:142-150.

92. Nazari-Jahantigh M, Egea V, Schober A and Weber C. MicroRNA-specific regulatory mechanisms in atherosclerosis. *J Mol Cell Cardiol.* 2014.
93. Small EM and Olson EN. Pervasive roles of microRNAs in cardiovascular biology. *Nature.* 2011;469:336-342.
94. Rangrez AY, Massy ZA, Metzinger-Le Meuth V and Metzinger L. miR-143 and miR-145: molecular keys to switch the phenotype of vascular smooth muscle cells. *Circ Cardiovasc Genet.* 2011;4:197-205.
95. Cordes KR, Sheehy NT, White MP, Berry EC, Morton SU, Muth AN, Lee TH, Miano JM, Ivey KN and Srivastava D. miR-145 and miR-143 regulate smooth muscle cell fate and plasticity. *Nature.* 2009;460:705-10.
96. Xin M, Small EM, Sutherland LB, Qi X, McAnally J, Plato CF, Richardson JA, Bassel-Duby R and Olson EN. MicroRNAs miR-143 and miR-145 modulate cytoskeletal dynamics and responsiveness of smooth muscle cells to injury. *Genes Dev.* 2009;23:2166-78.
97. Zheng X-L. Myocardin and smooth muscle differentiation. *Archives of Biochemistry and Biophysics.* 2014;543:48-56.
98. Cheng Y, Liu X, Yang J, Lin Y, Xu DZ, Lu Q, Deitch EA, Huo Y, Delphin ES and Zhang C. MicroRNA-145, a novel smooth muscle cell phenotypic marker and modulator, controls vascular neointimal lesion formation. *Circ Res.* 2009;105:158-66.
99. Liu X, Cheng Y, Zhang S, Lin Y, Yang J and Zhang C. A necessary role of miR-221 and miR-222 in vascular smooth muscle cell proliferation and neointimal hyperplasia. *Circ Res.* 2009;104:476-87.
100. Ji R, Cheng Y, Yue J, Yang J, Liu X, Chen H, Dean DB and Zhang C. MicroRNA expression signature and antisense-mediated depletion reveal an essential role of MicroRNA in vascular neointimal lesion formation. *Circ Res.* 2007;100:1579-88.
101. Wang D, Deuse T, Stubbendorff M, Chernogubova E, Erben RG, Eken SM, Jin H, Li Y, Busch A, Heeger CH, Behnisch B, Reichenspurner H, Robbins RC, Spin JM, Tsao PS, Schrepfer S and Maegdefessel L. Local MicroRNA Modulation Using a Novel Anti-miR-21-Eluting Stent Effectively Prevents Experimental In-Stent Restenosis. *Arterioscler Thromb Vasc Biol.* 2015;35:1945-53.
102. Abizaid A. Sirolimus-eluting coronary stents: a review. *Vascular Health and Risk Management.* 2007;3:191-201.
103. Fiedler J, Stohr A, Gupta SK, Hartmann D, Holzmann A, Just A, Hansen A, Hilfiker-Kleiner D, Eschenhagen T and Thum T. Functional microRNA library screening identifies the hypoxamir miR-24 as a potent regulator of smooth muscle cell proliferation and vascularization. *Antioxid Redox Signal.* 2014;21:1167-76.
104. Costa MA and Simon DI. Molecular basis of restenosis and drug-eluting stents. *Circulation.* 2005;111:2257-73.
105. Hoffmann R, Mintz GS, Dussaillant GR, Popma JJ, Pichard AD, Satler LF, Kent KM, Griffin J and Leon MB. Patterns and mechanisms of in-stent restenosis. A serial intravascular ultrasound study. *Circulation.* 1996;94:1247-54.
106. Bernstein E, Kim SY, Carmell MA, Murchison EP, Alcorn H, Li MZ, Mills AA, Elledge SJ, Anderson KV and Hannon GJ. Dicer is essential for mouse development. *Nat Genet.* 2003;35:215-7.
107. Siciliano V, Garzilli I, Fracassi C, Criscuolo S, Ventre S and di Bernardo D. MiRNAs confer phenotypic robustness to gene networks by suppressing biological noise. *Nat Commun.* 2013;4:2364.
108. Ebert MS and Sharp PA. Roles for MicroRNAs in conferring robustness to biological processes. *Cell.* 2012;149:515-524.
109. McDonald RA, Hata A, MacLean MR, Morrell NW and Baker AH. MicroRNA and vascular remodelling in acute vascular injury and pulmonary vascular remodelling. *Cardiovasc Res.* 2012;93:594-604.
110. Clark PM, Loher P, Quann K, Brody J, Londin ER and Rigoutsos I. Argonaute CLIP-Seq reveals miRNA targetome diversity across tissue types. *Sci Rep.* 2014;4:5947.
111. Chi SW, Zang JB, Mele A and Darnell RB. Argonaute HITS-CLIP decodes microRNA-mRNA interaction maps. *Nature.* 2009;460:479-86.

112. Chen WJ, Yin K, Zhao GJ, Fu YC and Tang CK. The magic and mystery of microRNA-27 in atherosclerosis. *Atherosclerosis*. 2012;222:314-23.
113. Harfe BD, McManus MT, Mansfield JH, Hornstein E and Tabin CJ. The RNaseIII enzyme Dicer is required for morphogenesis but not patterning of the vertebrate limb. *Proc Natl Acad Sci U S A*. 2005;102:10898-903.
114. Wirth A, Benyo Z, Lukasova M, Leutgeb B, Wettschureck N, Gorbey S, Orsy P, Horvath B, Maser-Gluth C, Greiner E, Lemmer B, Schutz G, Gutkind JS and Offermanns S. G12-G13-LARG-mediated signaling in vascular smooth muscle is required for salt-induced hypertension. *Nat Med*. 2008;14:64-8.
115. Schober A, Knarren S, Lietz M, Lin EA and Weber C. Crucial role of stromal cell-derived factor-1alpha in neointima formation after vascular injury in apolipoprotein E-deficient mice. *Circulation*. 2003;108:2491-7.
116. Bisognin A, Sales G, Coppe A, Bortoluzzi S and Romualdi C. MAGIA2: from miRNA and genes expression data integrative analysis to microRNA-transcription factor mixed regulatory circuits (2012 update). *Nucleic acids research*. 2012.
117. Vandesompele J, De Preter K, Pattyn F, Poppe B, Van Roy N, De Paepe A and Speleman F. Accurate normalization of real-time quantitative RT-PCR data by geometric averaging of multiple internal control genes. *Genome Biol*. 2002;3:RESEARCH0034.
118. Nuovo G, Lee EJ, Lawler S, Godlewski J and Schmittgen T. In situ detection of mature microRNAs by labeled extension on ultramer templates. *Biotechniques*. 2009;46:115-26.
119. Nuovo GJ, Elton TS, Nana-Sinkam P, Volinia S, Croce CM and Schmittgen TD. A methodology for the combined in situ analyses of the precursor and mature forms of microRNAs and correlation with their putative targets. *Nat Protoc*. 2009;4:107-15.
120. Nelson M and McClelland M. Use of DNA Methyltransferase Endonuclease Enzyme Combinations for Megabase Mapping of Chromosomes. *Methods in Enzymology*. 1992;216:279-303.
121. Yu H, Clarke MC, Figg N, Littlewood TD and Bennett MR. Smooth muscle cell apoptosis promotes vessel remodeling and repair via activation of cell migration, proliferation, and collagen synthesis. *Arterioscler Thromb Vasc Biol*. 2011;31:2402-9.
122. Kim MH, Ham O, Lee SY, Choi E, Lee CY, Park JH, Lee J, Seo HH, Seung M, Choi E, Min PK and Hwang KC. MicroRNA-365 inhibits the proliferation of vascular smooth muscle cells by targeting cyclin D1. *J Cell Biochem*. 2014;115:1752-61.
123. Choe N, Kwon JS, Kim JR, Eom GH, Kim Y, Nam KI, Ahn Y, Kee HJ and Kook H. The microRNA miR-132 targets Lrrfip1 to block vascular smooth muscle cell proliferation and neointimal hyperplasia. *Atherosclerosis*. 2013;229:348-55.
124. Leeper NJ, Raiesdana A, Kojima Y, Chun HJ, Azuma J, Maegdefessel L, Kundu RK, Quertermous T, Tsao PS and Spin JM. MicroRNA-26a is a novel regulator of vascular smooth muscle cell function. *J Cell Physiol*. 2011;226:1035-43.
125. Talasila A, Yu H, Ackers-Johnson M, Bot M, van Berkel T, Bennett MR, Bot I and Sinha S. Myocardin regulates vascular response to injury through miR-24/-29a and platelet-derived growth factor receptor-beta. *Arterioscler Thromb Vasc Biol*. 2013;33:2355-65.
126. Wang YS, Wang HY, Liao YC, Tsai PC, Chen KC, Cheng HY, Lin RT and Juo SH. MicroRNA-195 regulates vascular smooth muscle cell phenotype and prevents neointimal formation. *Cardiovasc Res*. 2012;95:517-26.
127. Iaconetti C, De Rosa S, Polimeni A, Sorrentino S, Gareri C, Carino A, Sabatino J, Colangelo M, Curcio A and Indolfi C. Down-regulation of miR-23b induces phenotypic switching of vascular smooth muscle cells in vitro and in vivo. *Cardiovascular research*. 2015;107:522-33.
128. Eun SY, Ko YS, Park SW, Chang KC and Kim HJ. IL-1beta enhances vascular smooth muscle cell proliferation and migration via P2Y2 receptor-mediated RAGE expression and HMGB1 release. *Vascul Pharmacol*. 2015;72:108-17.
129. Raitoharju E, Lyytikainen LP, Levula M, Oksala N, Mennander A, Tarkka M, Klopp N, Illig T, Kahonen M, Karhunen PJ, Laaksonen R and Lehtimäki T. miR-21, miR-210, miR-34a, and miR-146a/b

- are up-regulated in human atherosclerotic plaques in the Tampere Vascular Study. *Atherosclerosis*. 2011;219:211-7.
130. Sun W, Shen W, Yang S, Hu F, Li H and Zhu TH. miR-223 and miR-142 attenuate hematopoietic cell proliferation, and miR-223 positively regulates miR-142 through LMO2 isoforms and CEBP-beta. *Cell Res*. 2010;20:1158-69.
 131. Rodriguez A, Vigorito E, Clare S, Warren MV, Couttet P, Soond DR, van Dongen S, Grocock RJ, Das PP, Miska EA, Vetrie D, Okkenhaug K, Enright AJ, Dougan G, Turner M and Bradley A. Requirement of bic/microRNA-155 for normal immune function. *Science*. 2007;316:608-11.
 132. Yoshida T, Yamashita M, Horimai C and Hayashi M. Smooth muscle-selective inhibition of nuclear factor-kappaB attenuates smooth muscle phenotypic switching and neointima formation following vascular injury. *J Am Heart Assoc*. 2013;2:e000230.
 133. Peppel K, Zhang L, Orman ES, Hagen PO, Amalfitano A, Brian L and Freedman NJ. Activation of vascular smooth muscle cells by TNF and PDGF: overlapping and complementary signal transduction mechanisms. *Cardiovasc Res*. 2005;65:674-82.
 134. Cook CL, Weiser MC, Schwartz PE, Jones CL and Majack RA. Developmentally timed expression of an embryonic growth phenotype in vascular smooth muscle cells. *Circ Res*. 1994;74:189-96.
 135. Chen CN, Li YS, Yeh YT, Lee PL, Usami S, Chien S and Chiu JJ. Synergistic roles of platelet-derived growth factor-BB and interleukin-1beta in phenotypic modulation of human aortic smooth muscle cells. *Proc Natl Acad Sci U S A*. 2006;103:2665-70.
 136. Karki R, Ho OM and Kim DW. Magnolol attenuates neointima formation by inducing cell cycle arrest via inhibition of ERK1/2 and NF-kappaB activation in vascular smooth muscle cells. *Biochim Biophys Acta*. 2013;1830:2619-28.
 137. Mebratu Y and Tesfaigzi Y. How ERK1/2 activation controls cell proliferation and cell death: Is subcellular localization the answer? *Cell Cycle*. 2009;8:1168-75.
 138. Lefloch R, Pouyssegur J and Lenormand P. Total ERK1/2 activity regulates cell proliferation. *Cell Cycle*. 2009;8:705-11.
 139. Izumi Y, Kim S, Namba M, Yasumoto H, Miyazaki H, Hoshiga M, Kaneda Y, Morishita R, Zhan Y and Iwao H. Gene transfer of dominant-negative mutants of extracellular signal-regulated kinase and c-Jun NH2-terminal kinase prevents neointimal formation in balloon-injured rat artery. *Circulation research*. 2001;88:1120-6.
 140. Hegner B, Lange M, Kusch A, Essin K, Sezer O, Schulze-Lohoff E, Luft FC, Gollasch M and Dragun D. mTOR regulates vascular smooth muscle cell differentiation from human bone marrow-derived mesenchymal progenitors. *Arterioscler Thromb Vasc Biol*. 2009;29:232-8.
 141. Wang Z, Rao PJ, Castresana MR and Newman WH. TNF-alpha induces proliferation or apoptosis in human saphenous vein smooth muscle cells depending on phenotype. *Am J Physiol Heart Circ Physiol*. 2005;288:H293-301.
 142. Raines EW, Garton KJ and Ferri N. Beyond the Endothelium. *NF-kB Regulation of Smooth Muscle Function*. 2004;94:706-708.
 143. Brand K, Page S, Rogler G, Bartsch A, Brandl R, Knuechel R, Page M, Kaltschmidt C, Baeuerle PA and Neumeier D. Activated transcription factor nuclear factor-kappa B is present in the atherosclerotic lesion. *Journal of Clinical Investigation*. 1996;97:1715-1722.
 144. Zhou Q, Gallagher R, Ufret-Vincenty R, Li X, Olson EN and Wang S. Regulation of angiogenesis and choroidal neovascularization by members of microRNA-23~27~24 clusters. *Proc Natl Acad Sci U S A*. 2011;108:8287-92.
 145. Bang C, Fiedler J and Thum T. Cardiovascular importance of the microRNA-23/27/24 family. *Microcirculation*. 2012;19:208-14.
 146. Liu G, Friggeri A, Yang Y, Park YJ, Tsuruta Y and Abraham E. miR-147, a microRNA that is induced upon Toll-like receptor stimulation, regulates murine macrophage inflammatory responses. *Proc Natl Acad Sci U S A*. 2009;106:15819-24.
 147. Fasanaro P, D'Alessandra Y, Di Stefano V, Melchionna R, Romani S, Pompilio G, Capogrossi MC and Martelli F. MicroRNA-210 modulates endothelial cell response to hypoxia and inhibits the receptor tyrosine kinase ligand Ephrin-A3. *J Biol Chem*. 2008;283:15878-83.

148. Leeper NJ, Raiesdana A, Kojima Y, Chun HJ, Azuma J, Maegdefessel L, Kundu RK, Quertermous T, Tsao PS and Spin JM. MicroRNA-26a Is a Novel Regulator of Vascular Smooth Muscle Cell Function. *Journal of cellular physiology*. 2011;226:1035-1043.
149. Zahedi F, Nazari-Jahantigh M, Zhou Z, Subramanian P, Wei Y, Grommes J, Offermanns S, Steffens S, Weber C and Schober A. Dicer generates a regulatory microRNA network in smooth muscle cells that limits neointima formation during vascular repair. *Cell Mol Life Sci*. 2016.
150. Hernandez-Torres F, Aranega AE and Franco D. Identification of regulatory elements directing miR-23a-miR-27a-miR-24-2 transcriptional regulation in response to muscle hypertrophic stimuli. *Biochim Biophys Acta*. 2014;1839:885-97.
151. Bartel DP. MicroRNAs: target recognition and regulatory functions. *Cell*. 2009;136:215-33.
152. Ellerbroek SM, Wennerberg K, Arthur WT, Dunty JM, Bowman DR, DeMali KA, Der C and Burridge K. SGEF, a RhoG guanine nucleotide exchange factor that stimulates macropinocytosis. *Mol Biol Cell*. 2004;15:3309-3319.
153. Patel JC and Galan JE. Differential activation and function of Rho GTPases during Salmonella-host cell interactions. *J Cell Biol*. 2006;175:453-63.
154. Samson T, van Buul JD, Kroon J, Welch C, Bakker EN, Matlung HL, van den Berg TK, Sharek L, Doerschuk C, Hahn K and Burridge K. The guanine-nucleotide exchange factor SGEF plays a crucial role in the formation of atherosclerosis. *PLoS One*. 2013;8:e55202.
155. Cai A, Zhou Y and Li L. Rho-GTPase and Atherosclerosis: Pleiotropic Effects of Statins. *J Am Heart Assoc*. 2015;4.
156. Uehata M, Ishizaki T, Satoh H, Ono T, Kawahara T, Morishita T, Tamakawa H, Yamagami K, Inui J, Maekawa M and Narumiya S. Calcium sensitization of smooth muscle mediated by a Rho-associated protein kinase in hypertension. *Nature*. 1997;389:990-4.
157. Liu HW, Halayko AJ, Fernandes DJ, Harmon GS, McCauley JA, Kocieniewski P, McConville J, Fu Y, Forsythe SM, Kogut P, Bellam S, Dowell M, Churchill J, Lesso H, Kassiri K, Mitchell RW, Hershenson MB, Camoretti-Mercado B and Solway J. The RhoA/Rho kinase pathway regulates nuclear localization of serum response factor. *Am J Respir Cell Mol Biol*. 2003;29:39-47.
158. Wang H, Wu R, Yu L, Wu F, Li S, Zhao Y, Li H, Luo G, Wang J and Zhou J. SGEF is overexpressed in prostate cancer and contributes to prostate cancer progression. *Oncol Rep*. 2012;28:1468-74.
159. Wang H, Li S, Li H, Wang P, Huang F, Zhao Y, Yu L, Luo G, Zhang X, Wang J and Zhou J. Grb2 interacts with SGEF and antagonizes the ability of SGEF to enhance EGF-induced ERK1/2 activation. *Mol Cell Biochem*. 2014;389:239-47.
160. Pastore CJ, Isner JM, Bacha PA, Kearney M and Pickering JG. Epidermal growth factor receptor-targeted cytotoxin inhibits neointimal hyperplasia in vivo. Results of local versus systemic administration. *Circ Res*. 1995;77:519-29.
161. Gennaro G, Menard C, Michaud SE, Deblois D and Rivard A. Inhibition of vascular smooth muscle cell proliferation and neointimal formation in injured arteries by a novel, oral mitogen-activated protein kinase/extracellular signal-regulated kinase inhibitor. *Circ*. 2004;110:3367-71.
162. Small EM, Frost RJA and Olson EN. MicroRNAs Add a New Dimension to Cardiovascular Disease. *Circulation*. 2010;121:1022-1032.
163. Mishra PK, Tyagi N, Kumar M and Tyagi SC. MicroRNAs as a therapeutic target for cardiovascular diseases. *J Cell Mol Med*. 2009;13:778-89.
164. Tang RH, Zheng XL, Callis TE, Stansfield WE, He J, Baldwin AS, Wang DZ and Selzman CH. Myocardin inhibits cellular proliferation by inhibiting NF-kappaB(p65)-dependent cell cycle progression. *Proc Natl Acad Sci U S A*. 2008;105:3362-7.

8 Acknowledgment

I would like to express my gratitude to everyone who has supported me throughout the process of this work. First, I would like to thank my supervisor, Prof. Dr. Andreas Schober for giving me the opportunity to work in this institute on an interesting topic. This thesis would not have been possible without his support, advice and the good discussions.

I would like to thank my colleagues for providing a pleasant environment in the lab. I want to express my gratitude to my family for their constant love and support.

9 Curriculum vitae

Personal data:

Name: Ms. Farima Zahedi

Date of birth: 07.07.1981

Place of birth: Tehran, Iran

Nationality: Iranian

Education:

2013-2016: PhD student in Biology (Molecular Cardiology), Ludwig-Maximilians University, Department of Biology, Institute for Cardiovascular Prevention (IPEK), Munich, Germany.

2010 – 2013: Lecturer, Parand Azad University, Parand, Iran

2007 – 2010: M.Sc in Cellular and Developmental Biology, Damghan Azad University, Damghan, Iran.

2001 – 2005: B.Sc. in Microbiology, Zanzan Azad University, Zanzan, Iran.

1995 – 1999: High school education, Zahra high school, Tehran, Iran.

Publications:

Zahedi F*, Nazari-Jahantigh M*, Zhou Z, Subramanian P, Wei Y, Grommes J, Offermanns S, Steffens S, Weber C, and Schober A. Dicer generates a regulatory microRNA network in smooth muscle cells that limits neointima formation during vascular repair. *Cell Mol Life Sci.* 2016; doi:10.1007/s00018-016-2349-0, 1-14. *Equal contribution.

Oral presentation:

Smooth muscle cell-specific deletion of *Dicer* increases neointima formation in *Apolipoprotein E*-deficient mice. Farima Zahedi, Maliheh Nazari-Jahantigh, Andreas Schober. European Society of Cardiology (ESC). 29. August-02. September, 2015, London, United Kingdom.

Poster presentation:

Farima Zahedi, Maliheh Nazari-Jahantigh, Christian Weber, Andreas Schober. The role of microRNA biogenesis in smooth muscle cells during neointima formation. Cardiac regeneration and vascular biology, 11-14 June, 2015, Venice, Italy.

Farima Zahedi, Maliheh Nazari-Jahantigh, Christian Weber, Andreas Schober. The role of microRNA biogenesis in smooth muscle cells during neointima formation. Munich Heart Alliance (MHA), Munich, Germany, 11 February, 2015.

Eidesstattliche Versicherung

Farima Zahedi

Name, Vorname

Ich erkläre hiermit an Eides statt,

dass ich die vorliegende Dissertation mit dem Thema

Role of Dicer in Smooth muscle
Cells during neointima formation

selbständig verfasst, mich außer der angegebenen keiner weiteren Hilfsmittel bedient und alle Erkenntnisse, die aus dem Schrifttum ganz oder annähernd übernommen sind, als solche kenntlich gemacht und nach ihrer Herkunft unter Bezeichnung der Fundstelle einzeln nachgewiesen habe.

Ich erkläre des Weiteren, dass die hier vorgelegte Dissertation nicht in gleicher oder in ähnlicher Form bei einer anderen Stelle zur Erlangung eines akademischen Grades eingereicht wurde.

Munich, 07.11.2016

Ort, Datum

Farima Zahedi

Unterschrift Doktorandin/Doktorand

